REPORT No. 460

THE CHARACTERISTICS OF 78 RELATED AIRFOIL SECTIONS FROM TESTS IN THE VARIABLE-DENSITY WIND TUNNEL

By Eastman N. Jacobs, Kenneth E. Ward, and Robert M. Pinkerton

SUMMARY

An investigation of a large group of related airfoils was made in the N.A.C.A. variable-density wind tunnel at a large value of the Reynolds Number. The tests were made to provide data that may be directly employed for a rational choice of the most suitable airfoil section for a given application. The variation of the aerodynamic characteristics with variations in thickness and mean-line form were therefore systematically studied.

The related airfoil profiles for this investigation were developed by combining certain profile thickness forms, obtained by varying the maximum thickness of a basic distribution, with certain mean lines, obtained by varying the length and the position of the maximum mean-line ordinate. A number of values of these shape variables were used to derive a family of airfoils. For the purposes of this investigation the construction and tests were limited to 68 airfoils of this family. In addition to these, several supplementary airfoils have been included in order to study the effects of certain other changes in the form of the mean line and in the thickness distribution.

The results are presented in the standard graphic form representing the airfoil characteristics for infinite aspect ratio and for aspect ratio 6. A table is also given by means of which the important characteristics of all the airfoils may be conveniently compared. The variation of the aerodynamic characteristics with changes in shape is shown by additional curves and tables. A comparison is made, where possible, with thin-airfoil theory, a summary of which is presented in an appendix.

INTRODUCTION

The forms of the airfoil sections that are in common use today are, directly or indirectly, the result of investigations made at Göttingen of a large number of airfoils. Previously, airfoils such as the R.A.F. 15 and the U.S.A. 27, developed from airfoil profiles investigated in England, were widely used. All these investigations, however, were made at low values of the Reynolds Number; therefore, the airfoils developed may not be the optimum ones for full-scale application. More recently a number of airfoils have been tested in the variable-density wind tunnel at values of the Reynolds Number approaching those of flight (reference 1) but, with the exception of the M-series and a series of propeller sections, the airfoils have not been systematically derived in such a way that the results could be satisfactorily correlated.

The design of an efficient airplane entails the careful balancing of many conflicting requirements. This statement is particularly true of the choice of the wing. Without a knowledge of the variations of the aerodynamic characteristics of the airfoil sections with the variations of shape that affect the weight of the structure, the designer cannot reach a satisfactory balance between the many conflicting requirements.

The purpose of the investigation reported herein was to obtain the characteristics at a large value of the Reynolds Number of a wide variety of related airfoils. The benefits of such a systematic investigation are evident. The results will greatly facilitate the choice of the most satisfactory airfoil for a given application and should eliminate much routine airfoil testing. Finally, because the results may be correlated to indicate the trends of the aerodynamic characteristics with changes of shape, they may point the way to the design of new shapes having better characteristics.

Airfoil profiles may be considered as made up of certain profile-thickness forms disposed about certain mean lines. The major shape variables then become two, the thickness form and the mean-line form. The thickness form is of particular importance from a structural standpoint. On the other hand, the form of the mean line determines almost independently some of the most important aerodynamic properties of the airfoil section, e.g., the angle of zero lift and the pitching-moment characteristics.

The related airfoil profiles for this investigation were derived by changing systematically these shape variables. The symmetrical profiles were defined in terms of a basic thickness variation, symmetrical airfoils of varying thickness being obtained by the application of factors to the basic ordinates. The cambered profiles were then developed by combining these thickness forms with various mean lines. The mean lines were obtained by varying the camber and by varying the shape of the mean line to alter the position of the maximum mean-line ordinate. *The maximum ordinate*

of the mean line is referred to throughout this report as the camber of the airfoil and the position of the maximum ordinate of the mean line as the position of the camber. An airfoil, produced as described above, is designated by a number of four digits: the first indicates the camber in percent of the chord; the second, the position of the camber in tenths of the chord from the leading edge; and the last two, the maximum thickness in percent of the chord. Thus the N.A.C.A. 2315 airfoil has a maximum camber of 2 percent of the chord at a position 0.3 of the chord from the leading edge, and a maximum thickness of 15 percent of the chord; the N.A.C.A. 0012 airfoil is a symmetrical airfoil having a maximum thickness of 12 percent of the chord.

In addition to the systematic series of airfoils, several supplementary airfoils have been included in order to study the effects of a few changes in the form of the mean line and in the thickness distribution.

Preliminary results which have been published include those for 12 symmetrical N.A.C.A. airfoils, the 00 series (reference 2) and other sections having different nose shapes (reference 3); and those for 42 cambered airfoils, the 43 and 63 series (reference 4), the 45 and 65 series (reference 5), the 44 and 64 series (reference 6), and the 24 series (reference 7).

If the chord is taken along the x axis from 0 to 1, the ordinates y are given by an equation of the form

$$\pm y = a_0\sqrt{x} + a_1 x + a_2 x^2 + a_3 x^3 + a_4 x^4$$

The equation was adjusted to give the desired shape by imposing the following conditions to determine the constants:

(1) Maximum ordinate 0.1 at 0.3 chord

$$x = 0.3 \qquad y = 0.1$$
$$dy/dx = 0$$

(2) Ordinate at trailing edge

$$x = 1 \qquad y = 0.002$$

(3) Trailing-edge angle

$$x = 1 \qquad dy/dx = -0.234$$

(4) Nose shape

$$x = 0.1 \qquad y = 0.078$$

The following equation satisfying approximately the above-mentioned conditions represents a profile having a thickness of approximately 20 percent of the chord.

$$\pm y = 0.29690\sqrt{x} - 0.12600x - 0.35160x^2 + 0.28430x^3 - 0.10150x^4$$

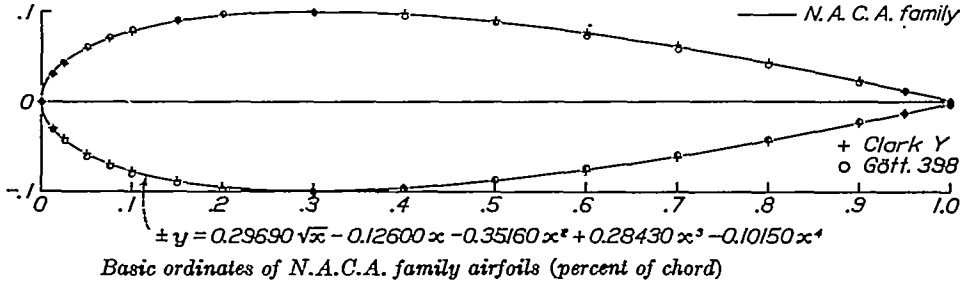

Basic ordinates of N.A.C.A. family airfoils (percent of chord)

Sta	0	1.25	2.5	5.0	7.5	10	15	20	25	30	40	50	60	70	80	90	95	100
Ord	0	3.157	4.358	5.925	7.000	7.805	8.909	9.563	9.902	10.003	9.672	8.823	7.606	6.107	4.372	2.413	1.344	0.210

L.E. radius, 4.40.

FIGURE 1.—Thickness variation.

The tests were made in the variable-density wind tunnel of the National Advisory Committee for Aeronautics during the period from April 1931 to February 1932.

DESCRIPTION OF AIRFOILS

Well-known airfoils of a certain class including the Göttingen 398 and the Clark Y, which have proved to be efficient, are nearly alike when their camber is removed (mean line straightened) and they are reduced to the same maximum thickness. A thickness variation similar to that of these airfoils was therefore chosen for the development of the N.A.C.A. airfoils. An equation defining the shape was used as a method of producing fair profiles.

This equation was taken to define the basic section. The basic profile and a table of ordinates are given in figure 1. Points obtained by removing the camber from the Göttingen 398 and the Clark Y sections, and applying a factor to the ordinates of the resulting thickness curves to bring them to the same maximum thickness, are plotted on the above figure for comparison. Sections having any desired maximum thickness were obtained by multiplying the basic ordinates by the proper factor; that is

$$\pm y_t = \frac{t}{0.20}(0.29690\sqrt{x} - 0.12600x - 0.35160x^2 + 0.28430x^3 - 0.10150x^4)$$

where t is the maximum thickness. The leading-edge radius is found to be

$$r_t = \frac{1}{2}\left(\frac{t}{0.20}a_0\right)^2 = 1.10t^2$$

When the mean lines of certain airfoils in common use were reduced to the same maximum ordinate and compared it was found that their shapes were quite different. It was observed, however, that the range of shapes could be well covered by assuming some simple shape and varying the maximum ordinate and its position along the chord. The mean line was, therefore, arbitrarily defined by two parabolic equations of the form

$$y_c = b_0 + b_1 x + b_2 x^2$$

where the leading end of the mean line is at the origin and the trailing end is on the x axis at $x=1$. The values of the constants for both equations were then expressed in terms of the above variables; namely,

(1) Mean-line extremities

$x=0$ $\qquad y_c=0$

$x=1$ $\qquad y_c=0$

(2) Maximum ordinate of mean line

$x=p$ (position of maximum ordinate)

$y_c=m$(maximum ordinate)

$dy_c/dx=0$

The resulting equations defining the mean line then became

$$y_c = \frac{m}{p^2}[2px - x^2]$$

(forward of maximum ordinate)

and

$$y_c = \frac{m}{(1-p)^2}[(1-2p)+2px-x^2]$$

(aft of maximum ordinate)

The method of combining the thickness forms with the mean-line forms is best described by means of the diagram in figure 2. The line joining the extremities of the mean line is chosen as the chord. Referring to the diagram, the ordinate y_t of the thickness form is measured along the perpendicular to the mean line from a point on the mean line at the station along the chord corresponding to the value of x for which y_t was computed. The resulting upper and lower surface points are then designated:

Stations x_u and x_l
Ordinates y_u and y_l

where the subscripts u and l refer to upper and lower surfaces, respectively. In addition to these symbols, the symbol θ is employed to designate the angle between the tangent to the mean line and the x axis. This angle is given by

$$\theta = \tan^{-1}\frac{dy_c}{dx}$$

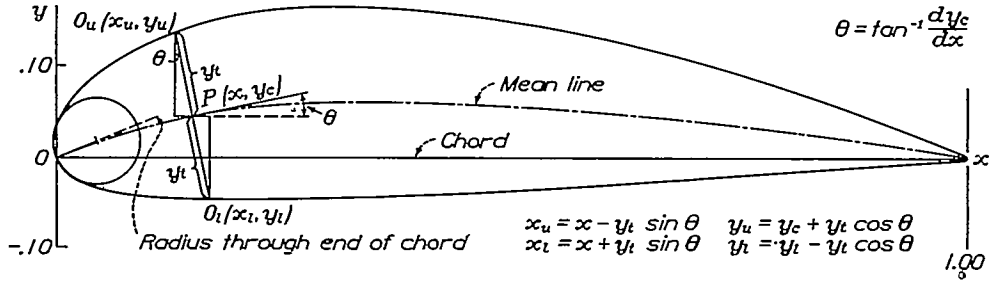

Sample calculations for derivation of N.A.C.A. 6321

x	y_t	y_c	tan θ	sin θ	cos θ	y_t sin θ	y_t cos θ	x_u	y_u	x_l	y_l
0	0	0	[1] 0.40000	0.37140	0.92840	0	0			0	0
0.01250	0.03314	0.00489	.38333	.35793	.93375	0.01186	0.03094	0.00064	0.03583	0.02436	−0.02605
.30000	.10503	.06000	0	0	1	0	.10503	.30000	.16503	.30000	−.04503
.60000	.07986	.04898	−.07347	−.07327	.99731	−.00585	.07965	.60585	.12863	.59415	−.03067
1	.00221	0	−.17143	−.16897	.98562	−.00037	.00218	1.00037	.00218	.99963	−.00218

[1] Slope of radius through end of chord.

FIGURE 2.—Method of calculating ordinates of N.A.C.A. cambered airfoils.

The following formulas for calculating the ordinates may now be derived from the diagram:

$$x_u = x - y_t \sin\theta$$
$$y_u = y_c + y_t \cos\theta$$
$$x_l = x + y_t \sin\theta$$
$$y_l = y_c - y_t \cos\theta$$

Sample calculations are given in figure 2. The center for the leading-edge radius is placed on the tangent to the mean line at the leading edge.

A family of related airfoils was derived in the manner described.* Seven values of the maximum thickness, 0.06, 0.09, 0.12, 0.15, 0.18, 0.21, and 0.25; four values of the camber, 0.00, 0.02, 0.04, and 0.06; and six values of the position of the camber, 0.2, 0.3, 0.4, 0.5, 0.6, and 0.7 were used to derive the related sections of this family. The profiles of the airfoils derived are shown collectively in figure 3.

For the purposes of this investigation the construction and tests were limited to 68 of the airfoils. Tables of ordinates at the standard stations are given in the figures presenting the aerodynamic characteristics. These ordinates were obtained graphically from the computed ordinates for all but the symmetrical sections. Two sets of trailing-edge ordinates are given. Those inclosed by parentheses, which are given to facilitate construction, represent ordinates to which the surfaces are faired. In the construction of the models the trailing edges were rounded off.

Three groups of supplementary airfoils were also constructed and tested. The derivation of these airfoils will be considered later with the discussion.

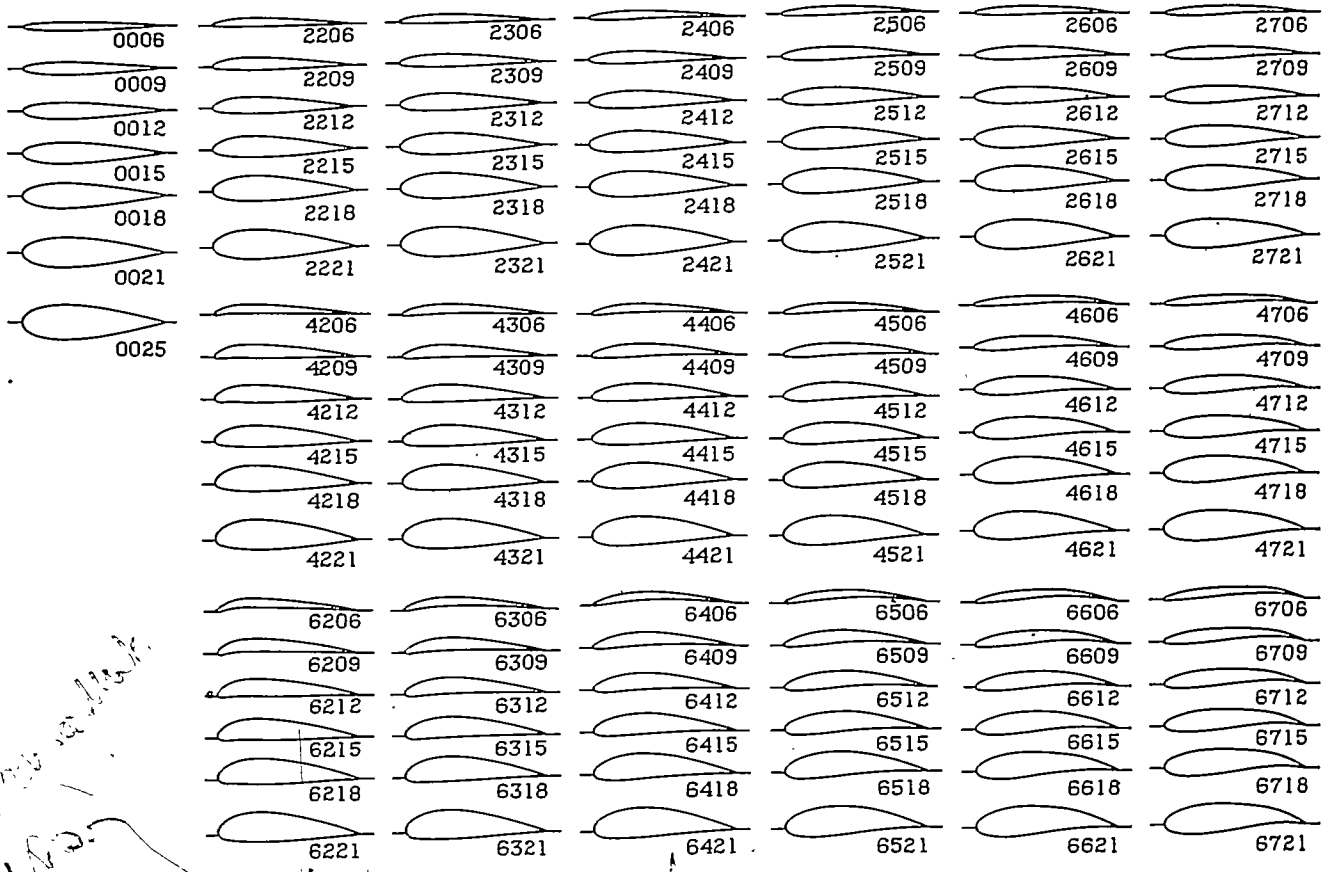

FIGURE 3.—N.A.C.A. airfoil profiles.

APPARATUS AND METHODS

A description of the variable-density wind tunnel and the method of testing is given in reference 8. The models, which are made of duralumin, have a chord of 5 inches and a span of 30 inches. They were constructed from the computed ordinates by the method described in reference 8.

Routine measurements of lift, drag, and pitching moment about a point on the chord one quarter of the chord behind its forward end were made at a Reynolds Number of approximately 3,000,000 (tank pressure, approximately 20 atmospheres). Groups of airfoils were first tested to study the variations with thickness, each group containing airfoils of different thicknesses but having the same mean line. Finally, all airfoils having a thickness of 12 percent of the chord were tested to study the variations with changes in the mean line.

RESULTS

The results are presented in the standard graphic form (figs. 4 to 80) as coefficients corrected after the method of reference 8 to give airfoil characteristics for infinite aspect ratio and aspect ratio 6. Where more than one test has been used for the analysis, the infinite aspect ratio characteristics from the earlier test have been indicated by additional points on the figure. Table I gives the important characteristics of all the airfoils.

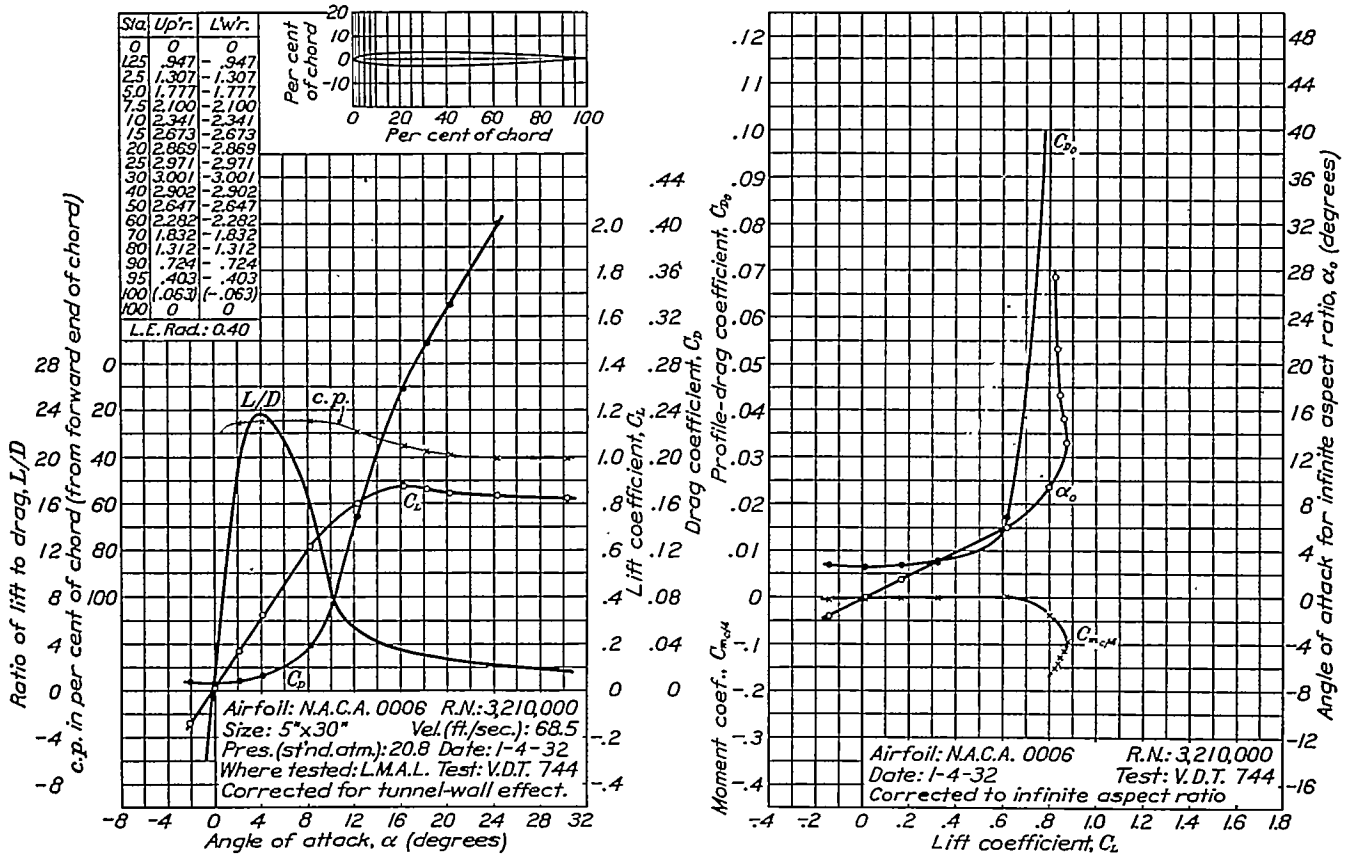

FIGURE 4.—N.A.C.A. 0006 airfoil.

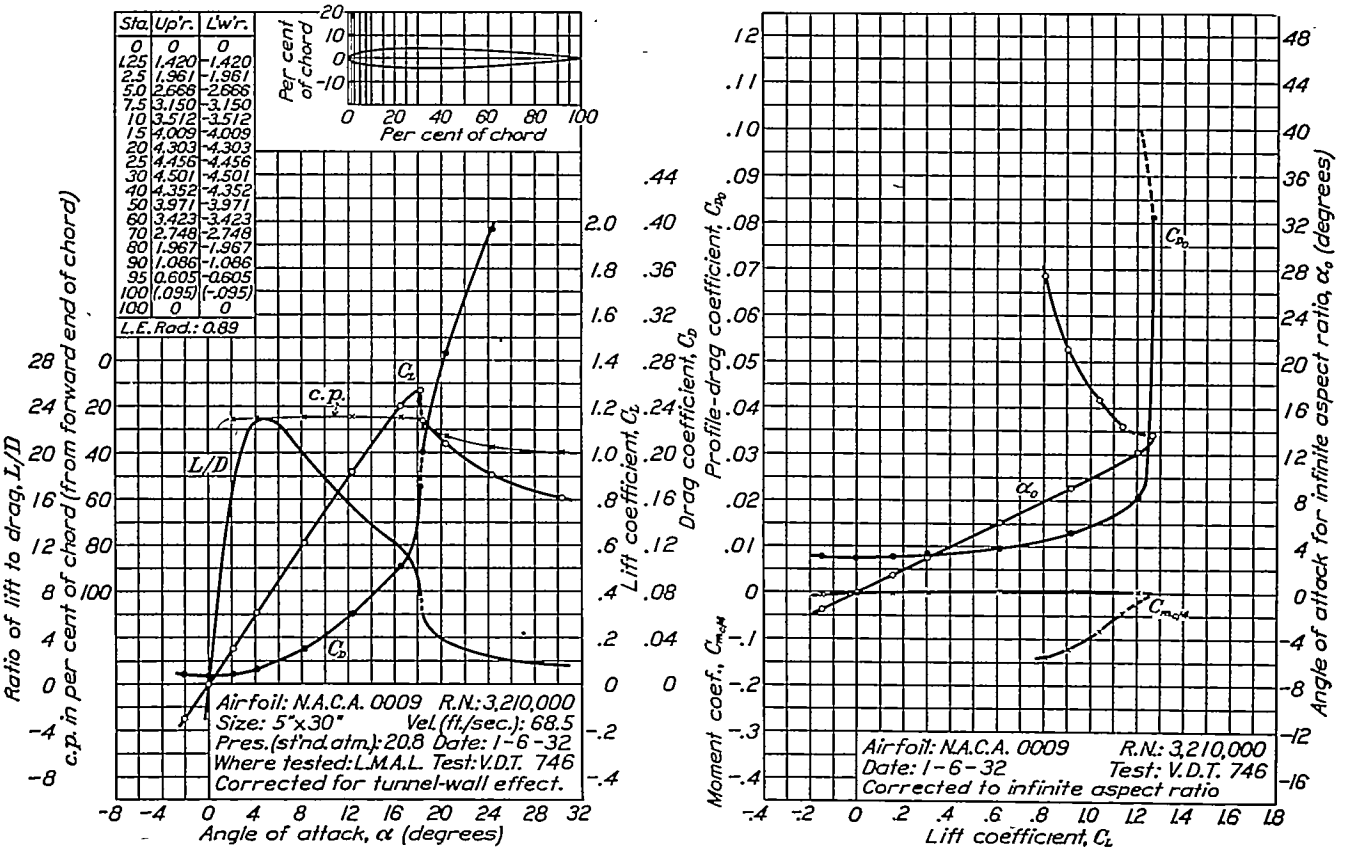

FIGURE 5.—N.A.C.A. 0009 airfoil.

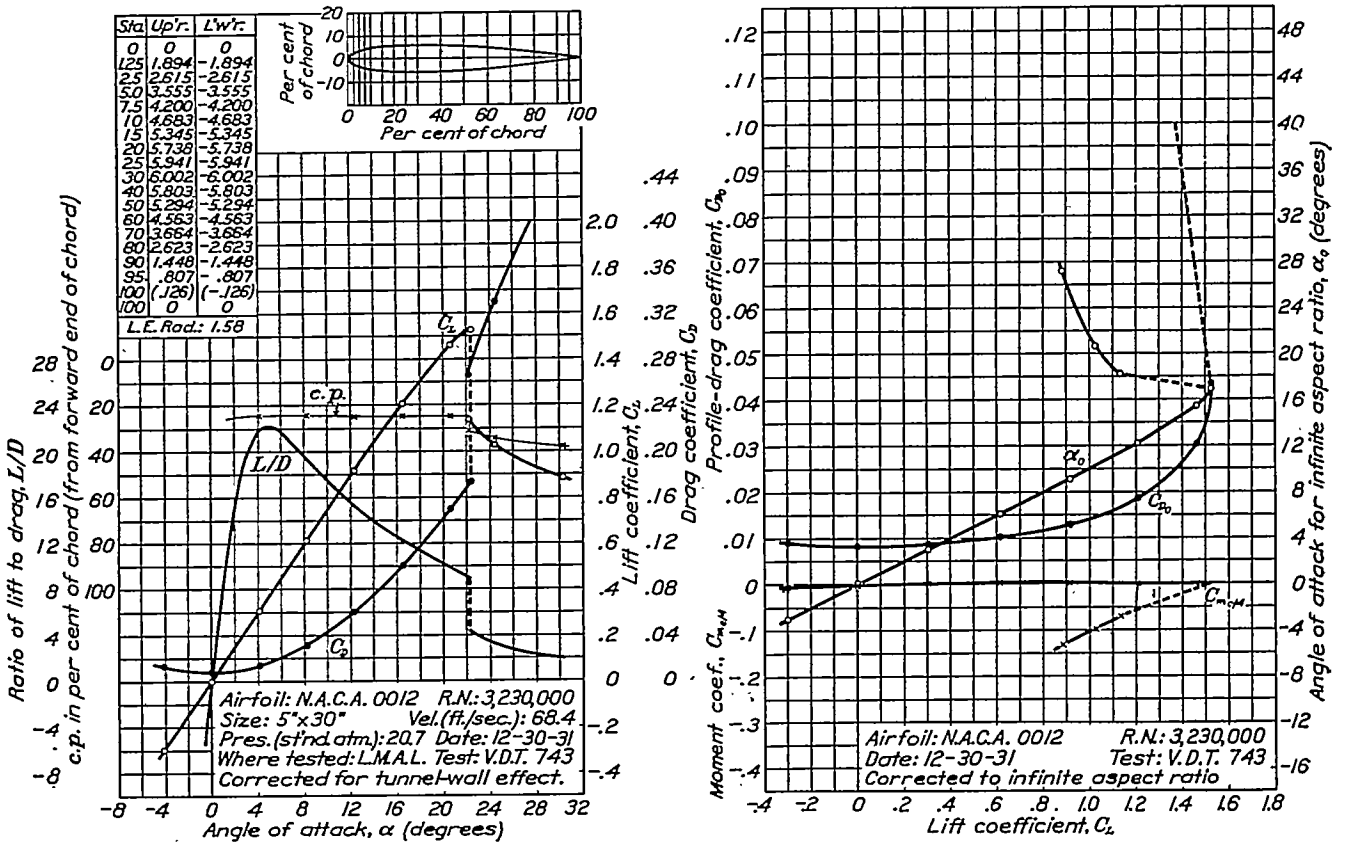

FIGURE 6.—N.A.C.A. 0012 airfoil.

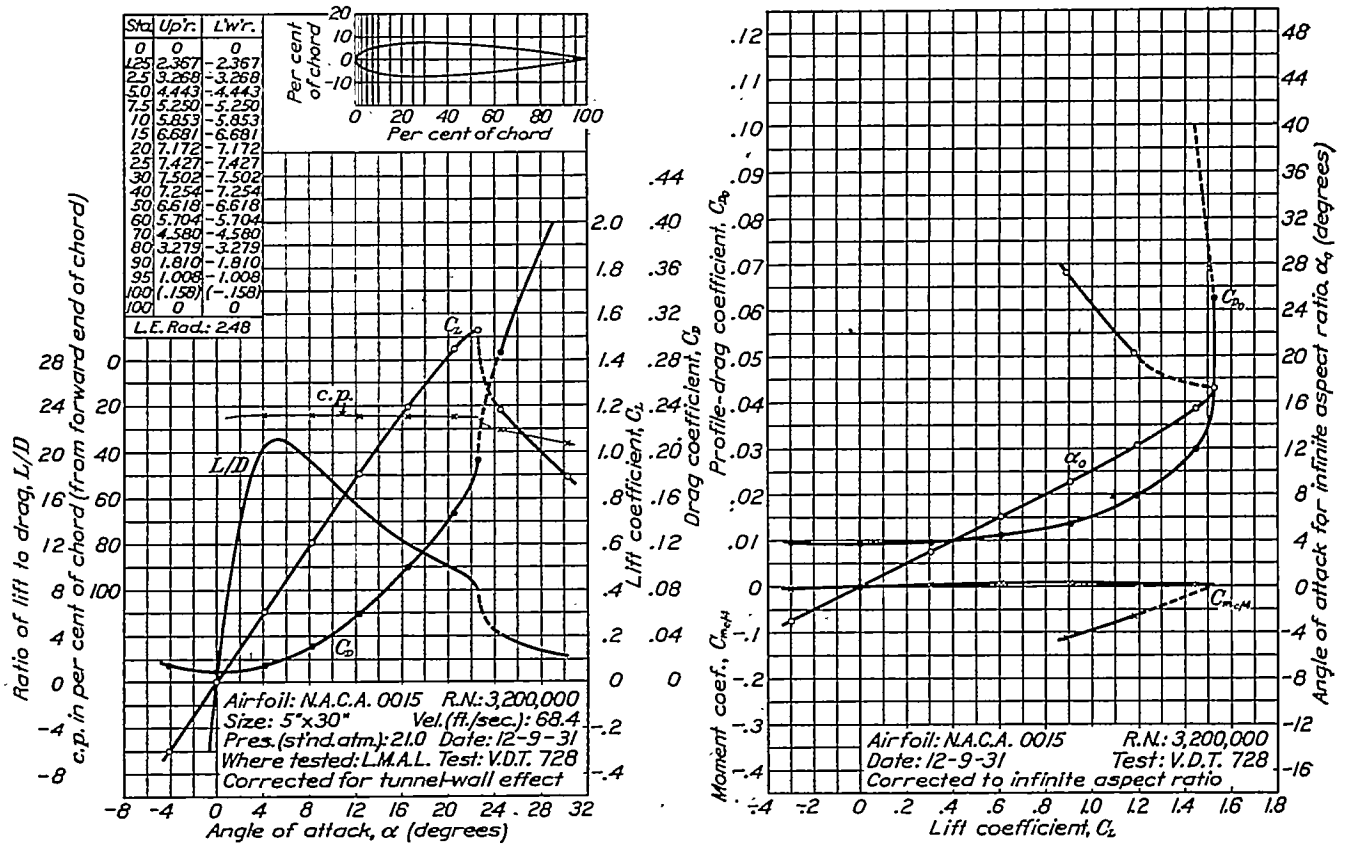

FIGURE 7.—N.A.C.A. 0015 airfoil.

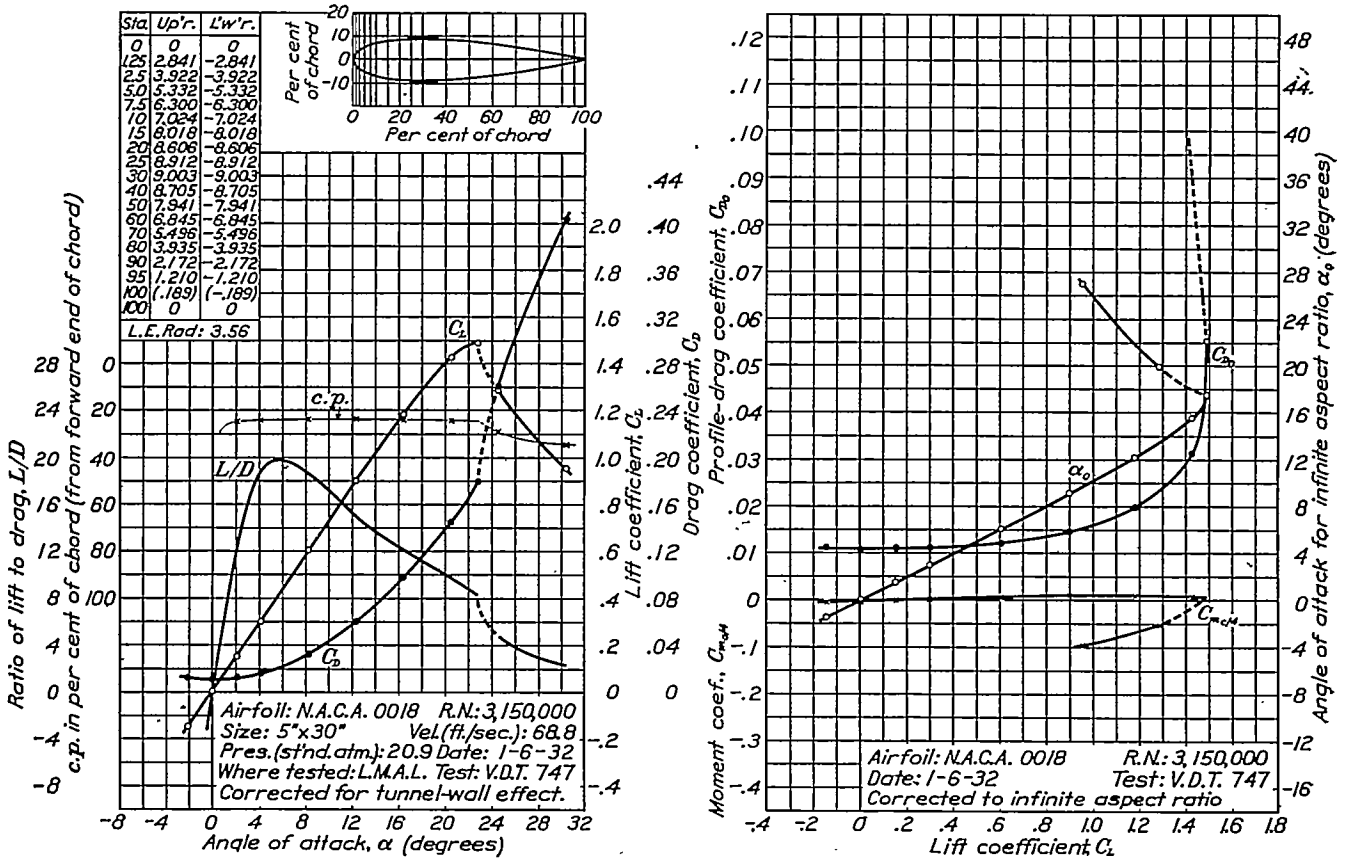

FIGURE 8.—N.A.C.A. 0018 airfoil.

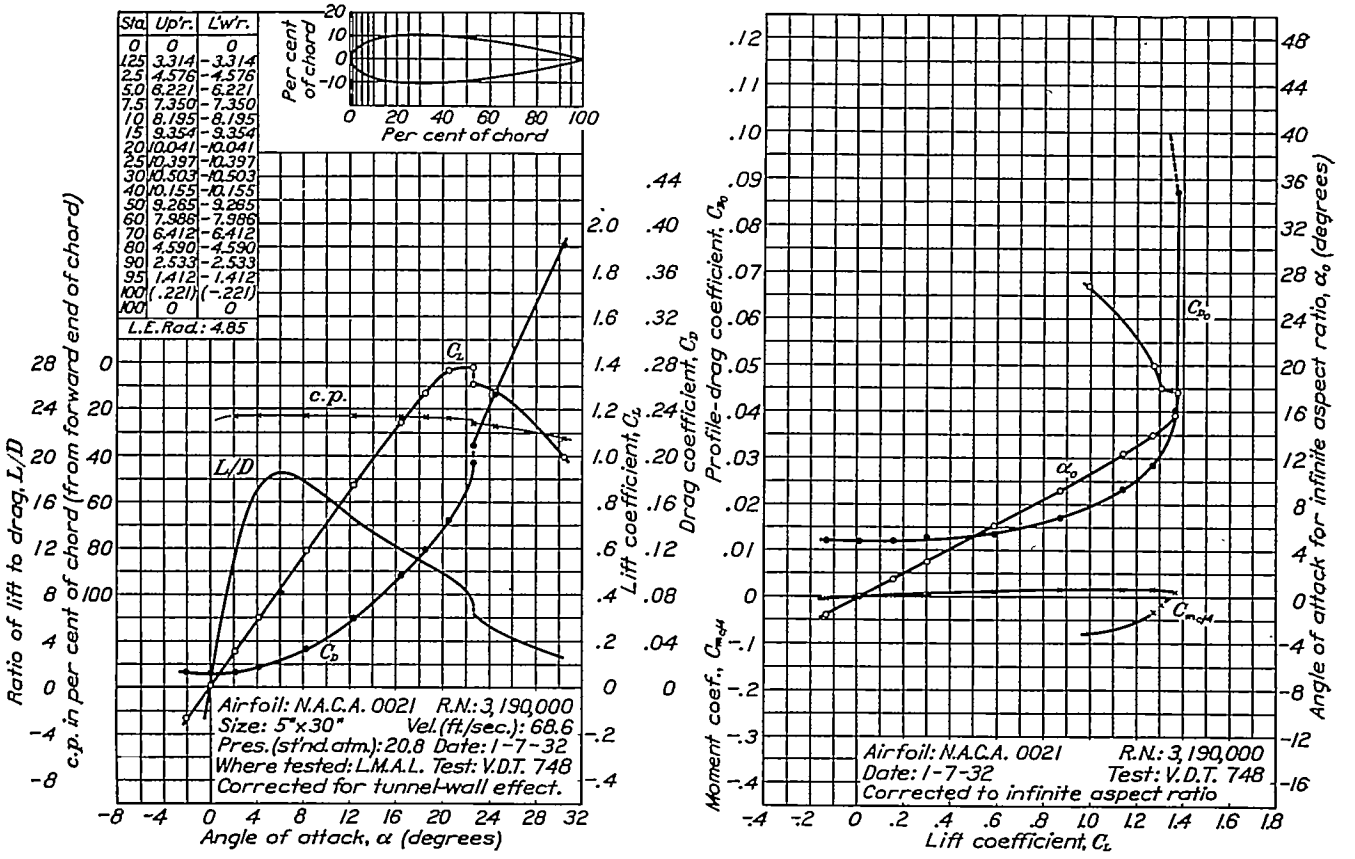

FIGURE 9.—N.A.C.A. 0021 airfoil.

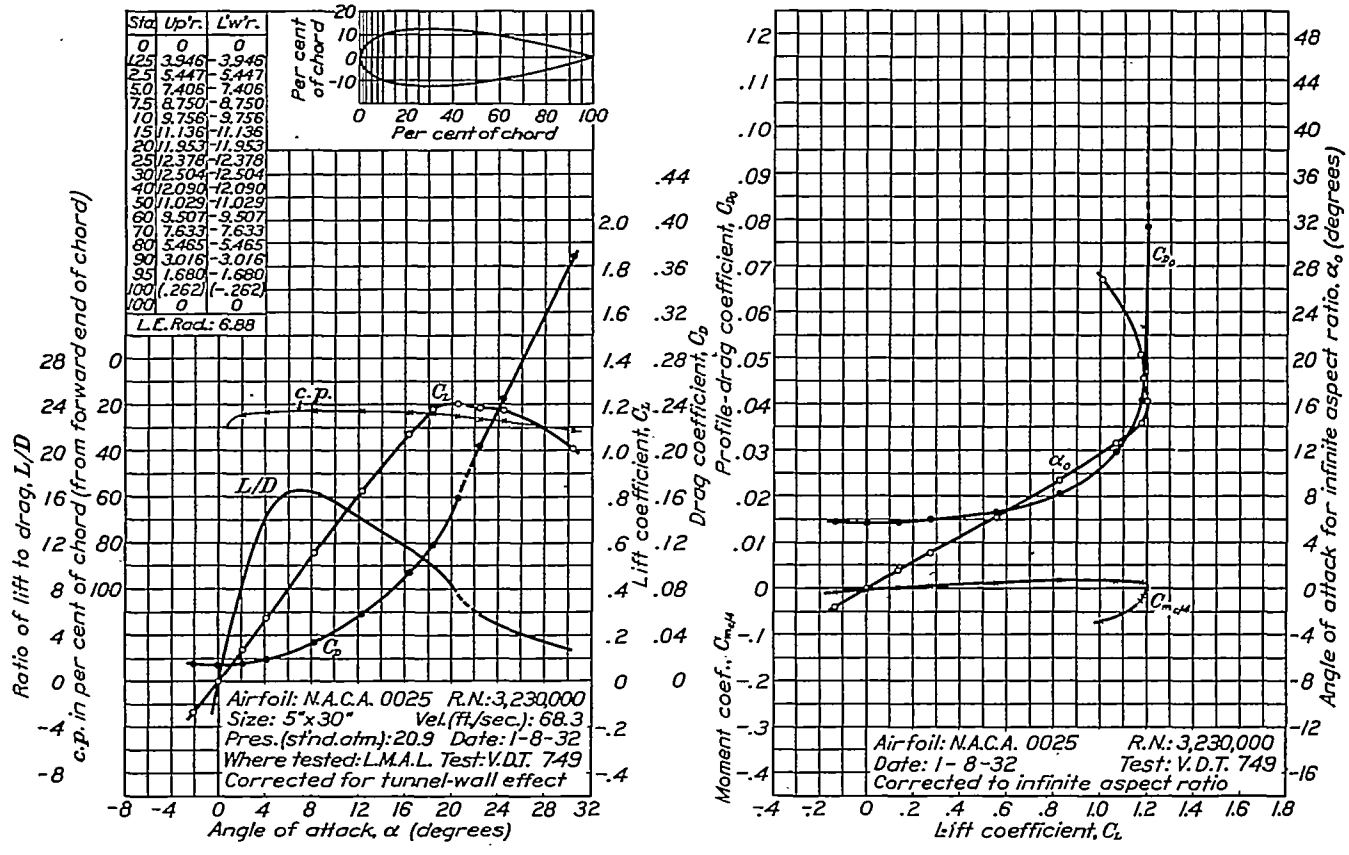

FIGURE 10.—N.A.C.A. 0025 airfoil.

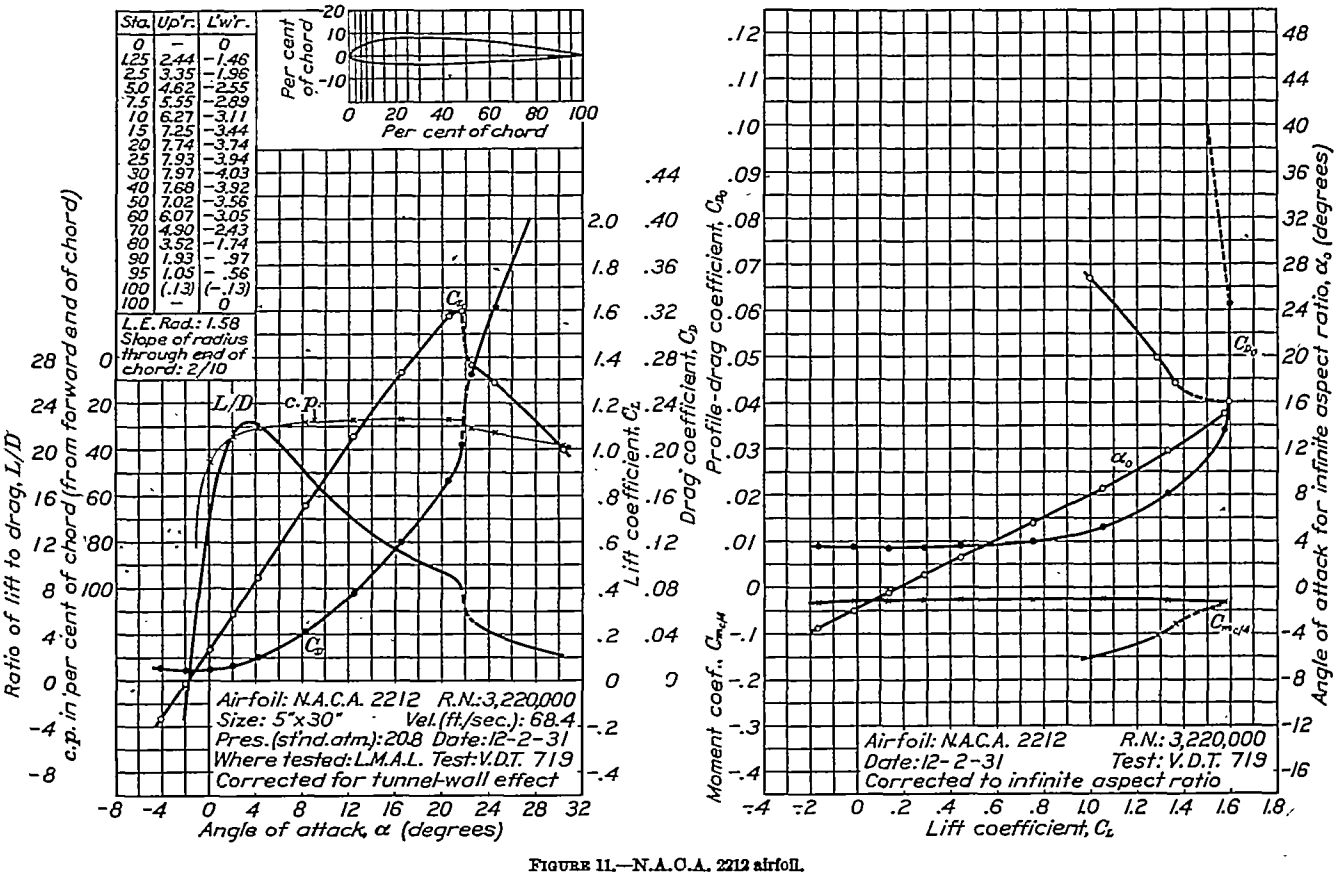

FIGURE 11.—N.A.C.A. 2212 airfoil.

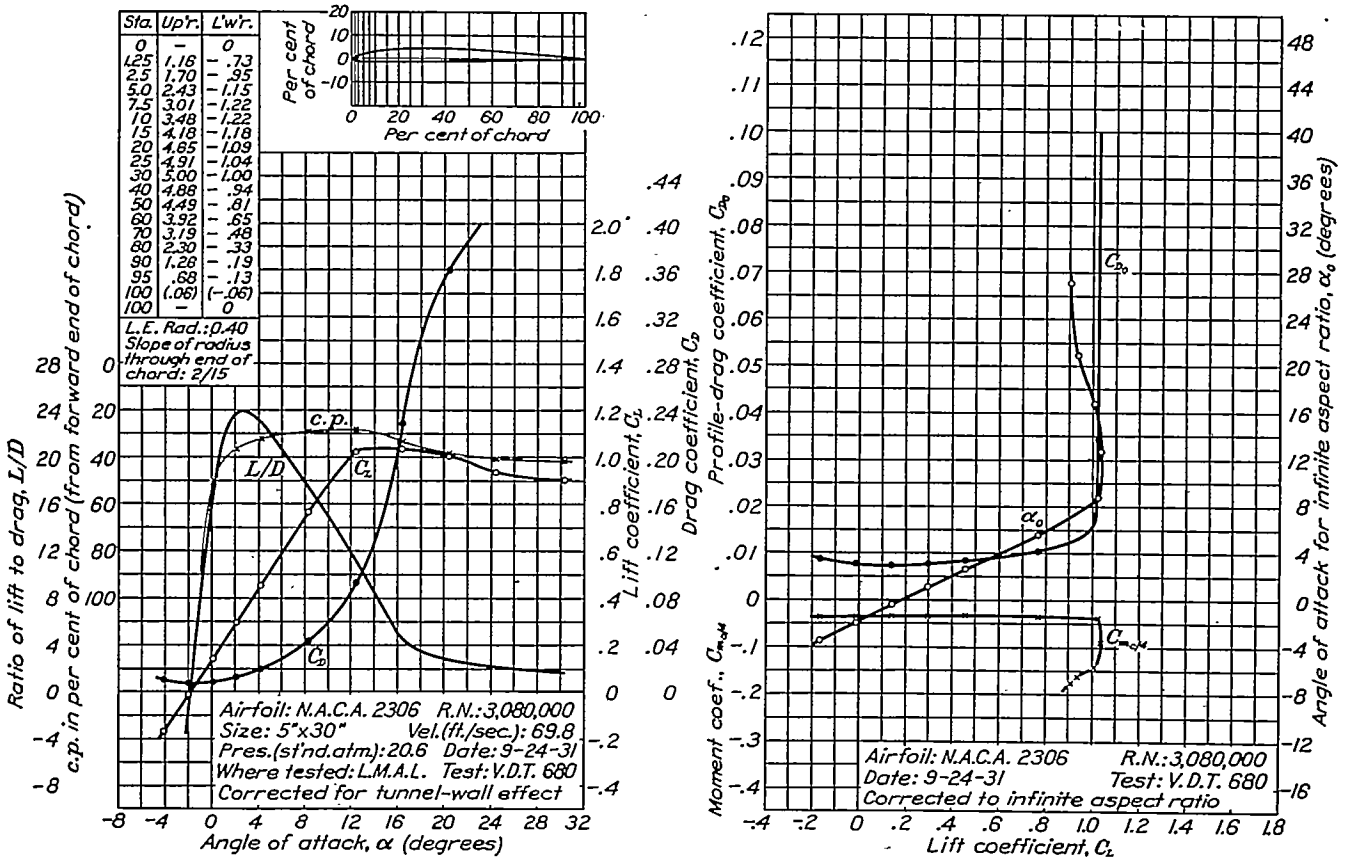

FIGURE 12.—N.A.C.A. 2306 airfoil.

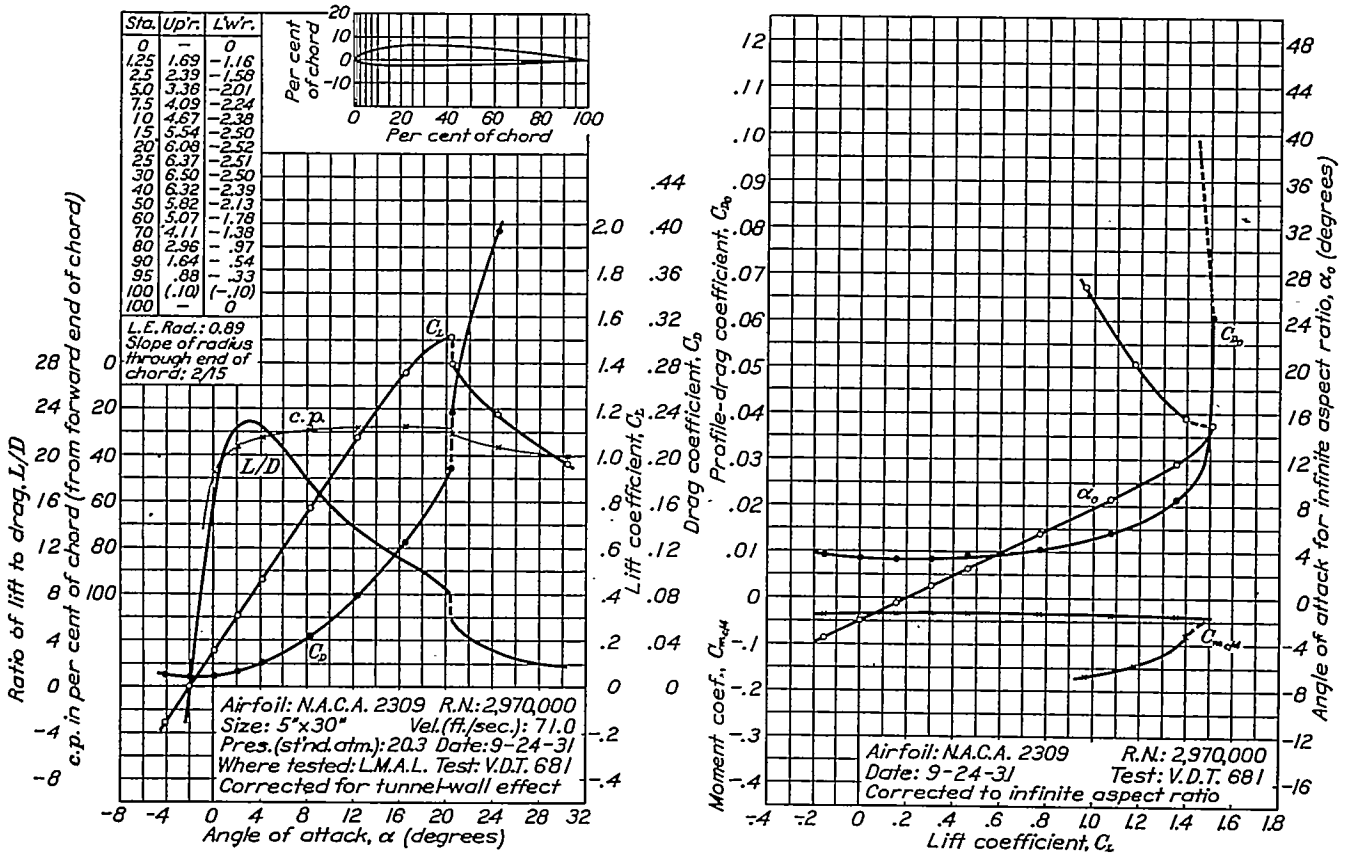

FIGURE 13.—N.A.C.A. 2309 airfoil.

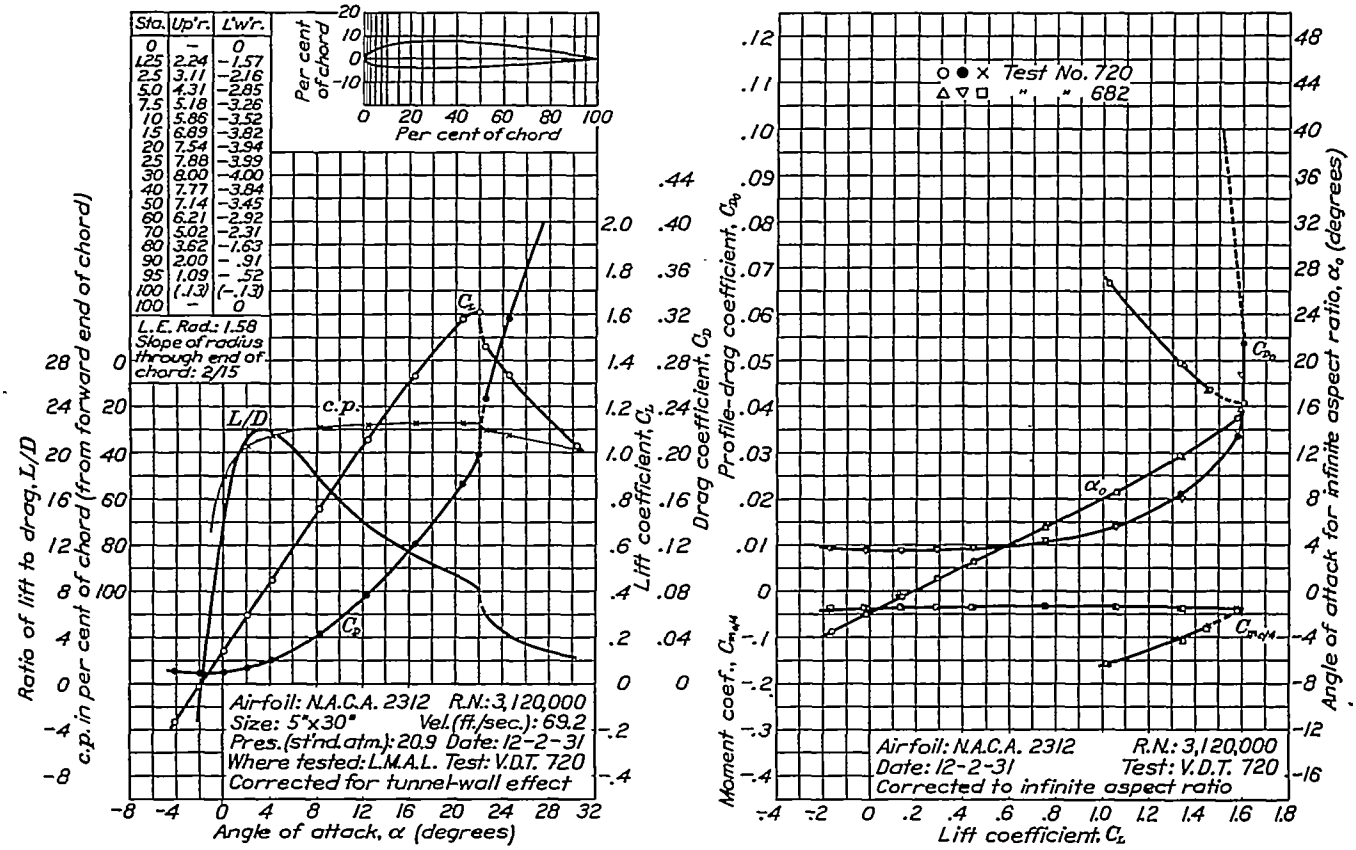

FIGURE 14.—N.A.C.A. 2312 airfoil.

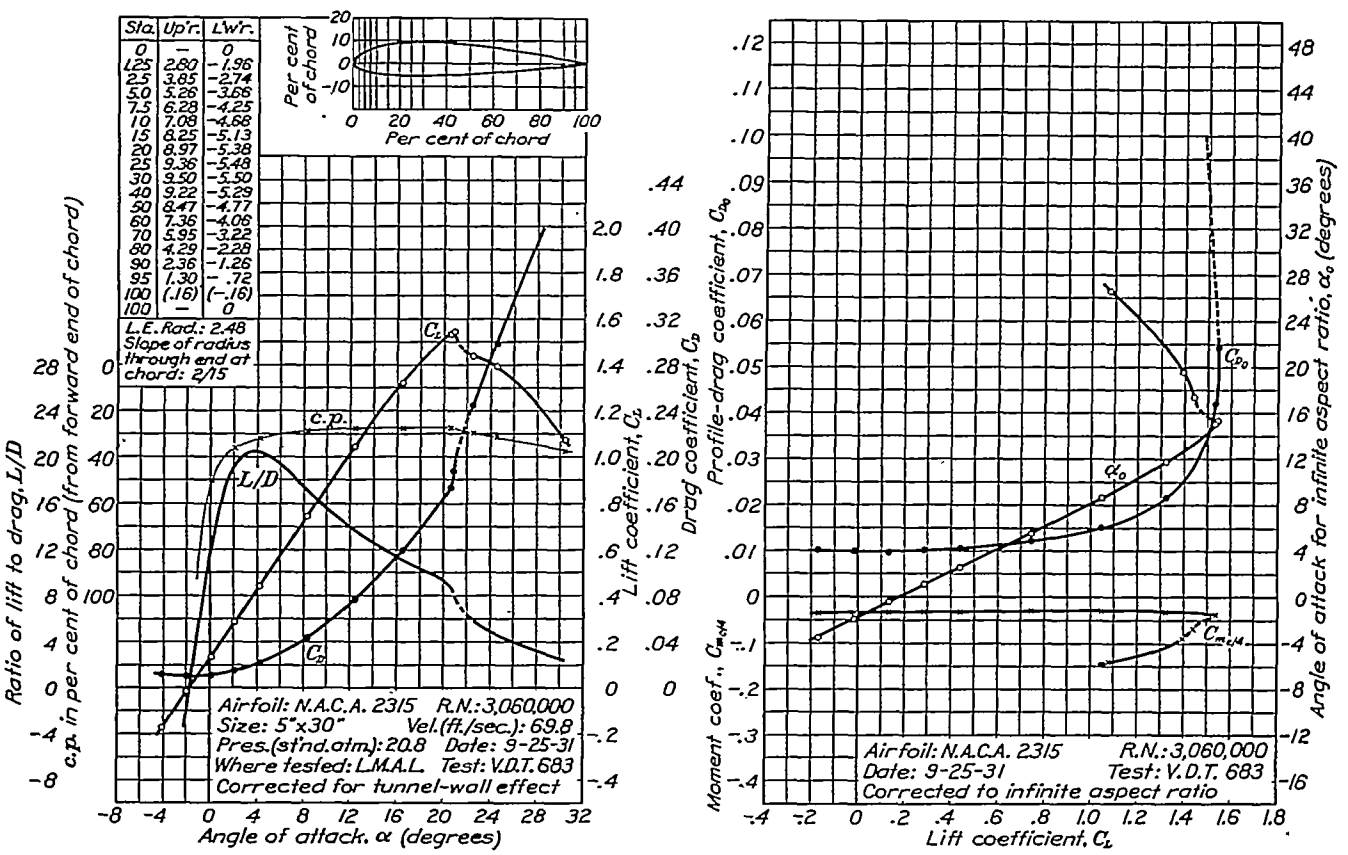

FIGURE 15.—N.A.C.A. 2315 airfoil.

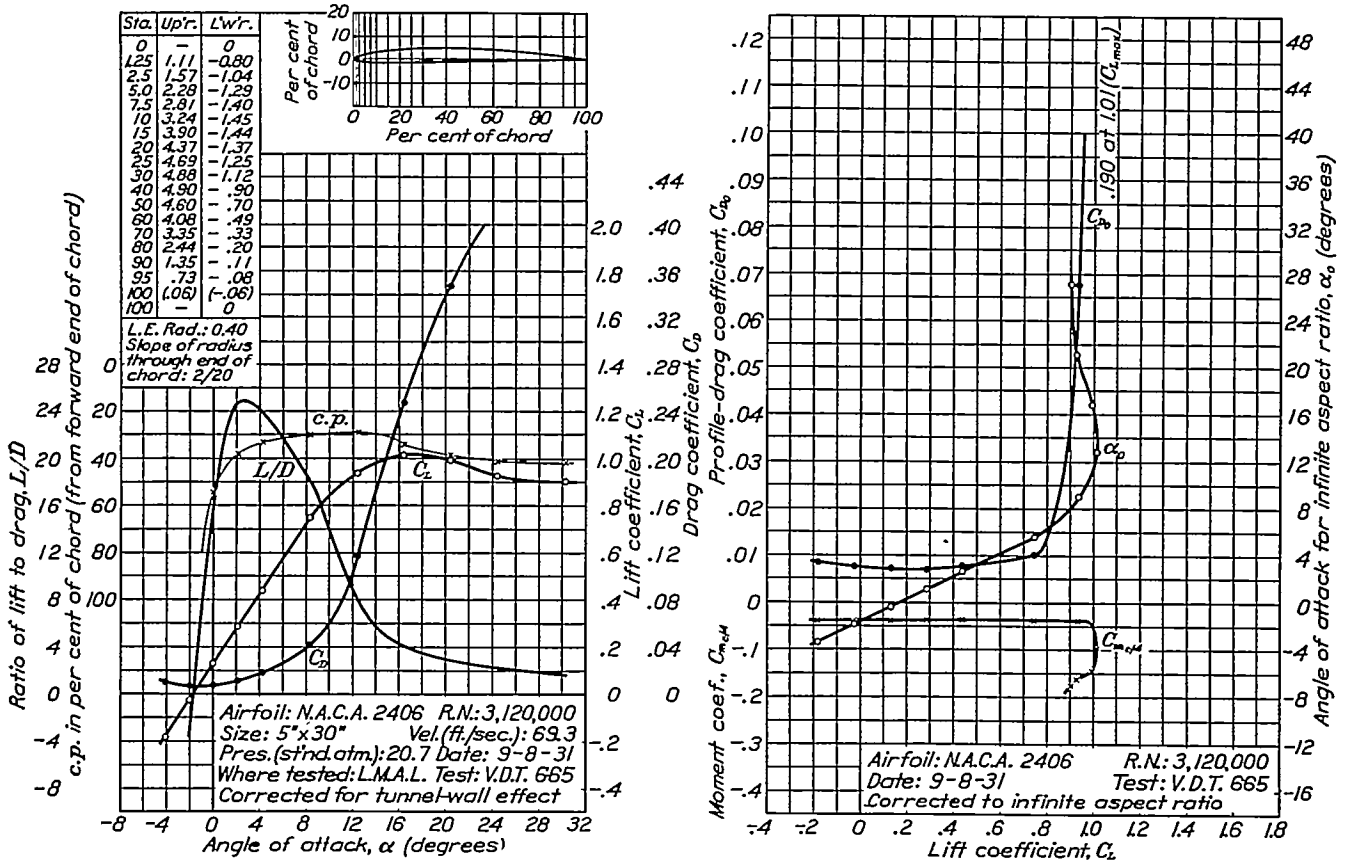

FIGURE 16.—N.A.C.A. 2406 airfoil.

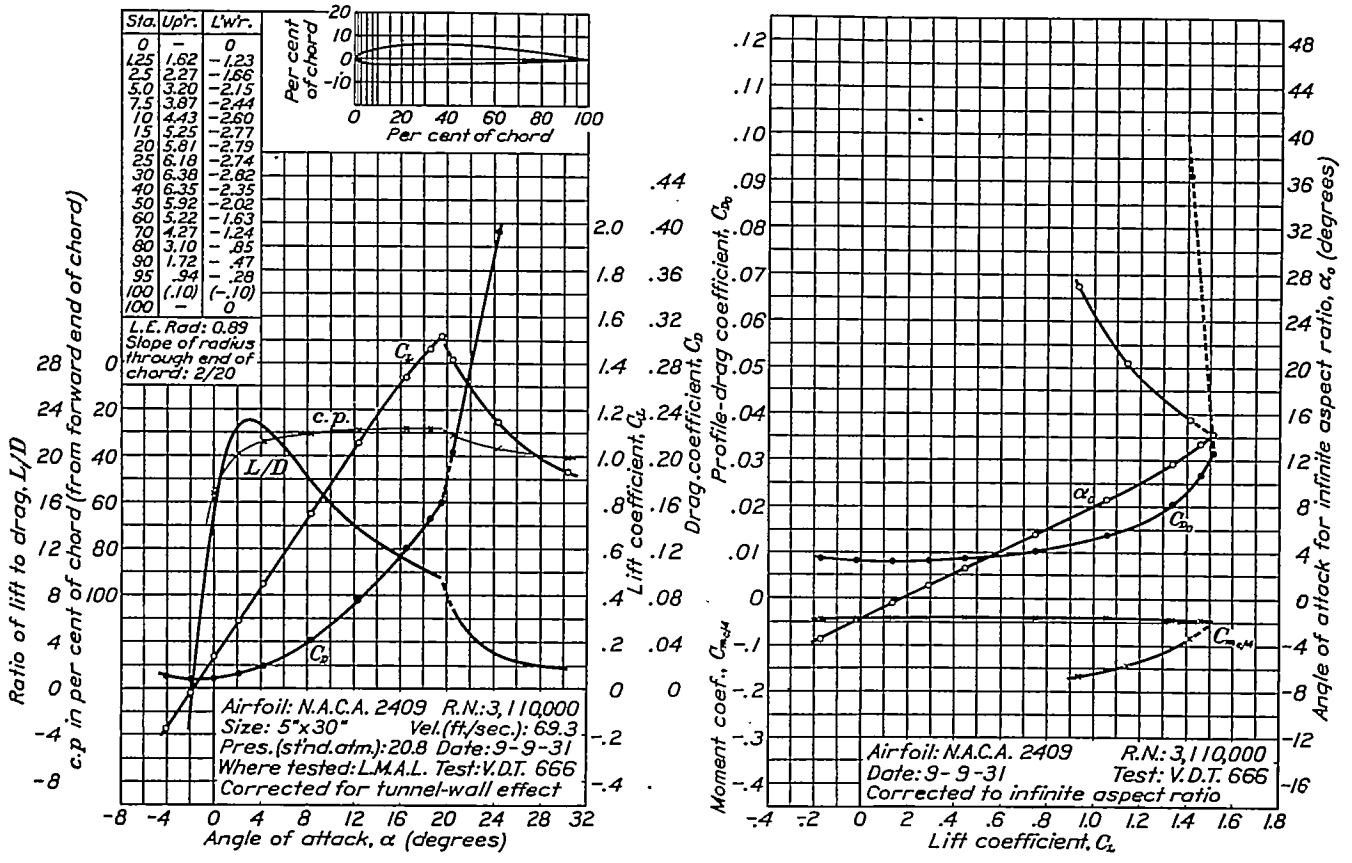

FIGURE 17.—N.A.C.A. 2409 airfoil.

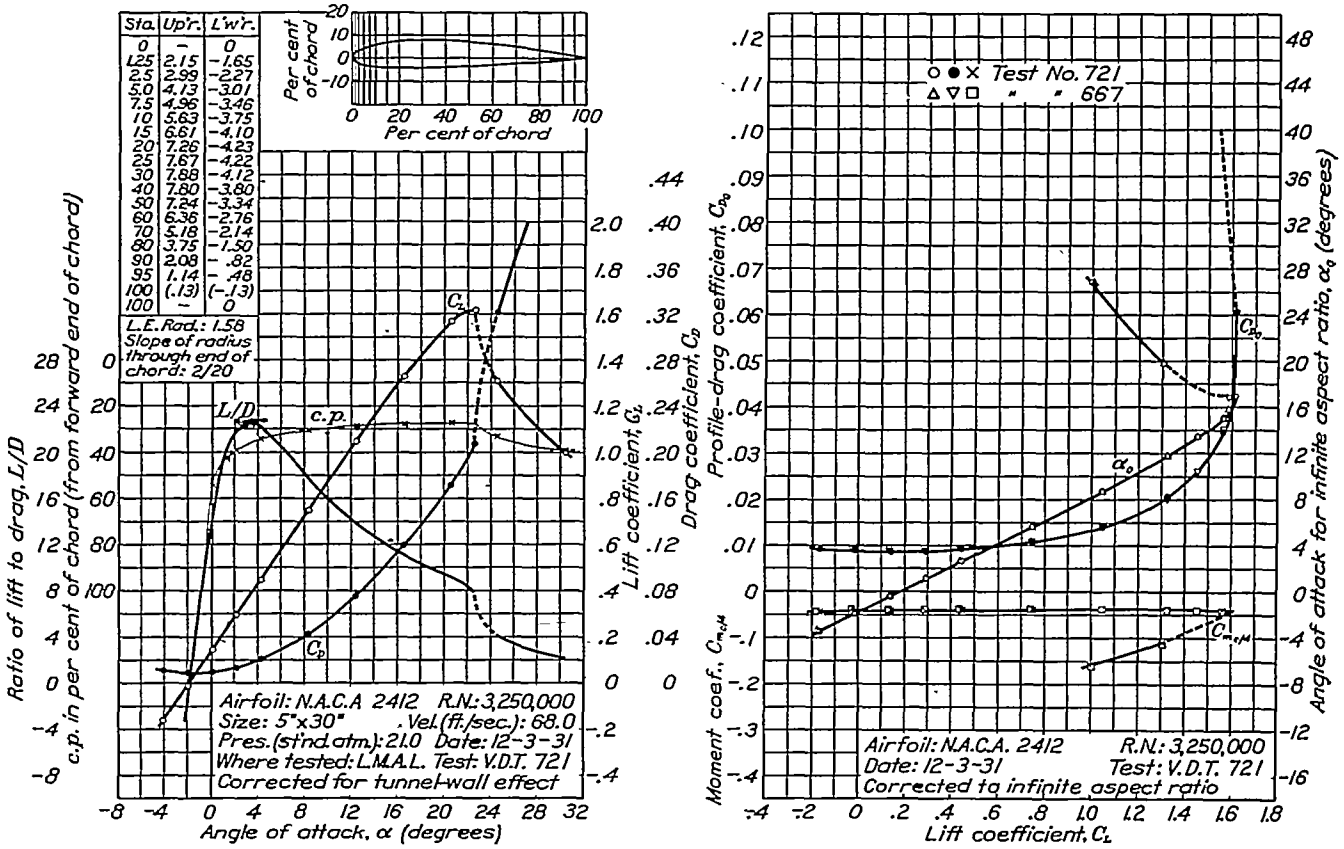

FIGURE 18.—N.A.C.A. 2412 airfoil.

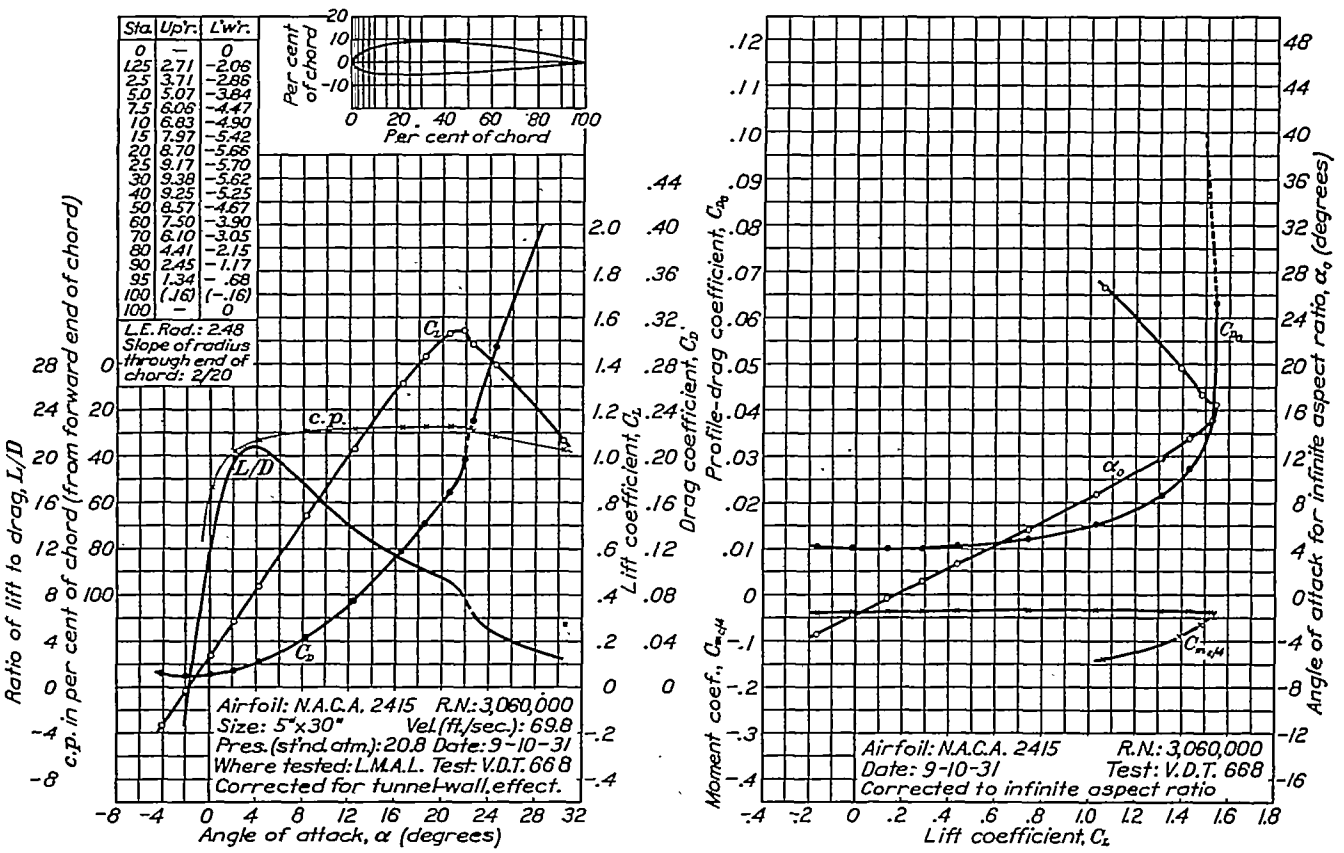

FIGURE 19.—N.A.C.A. 2415 airfoil.

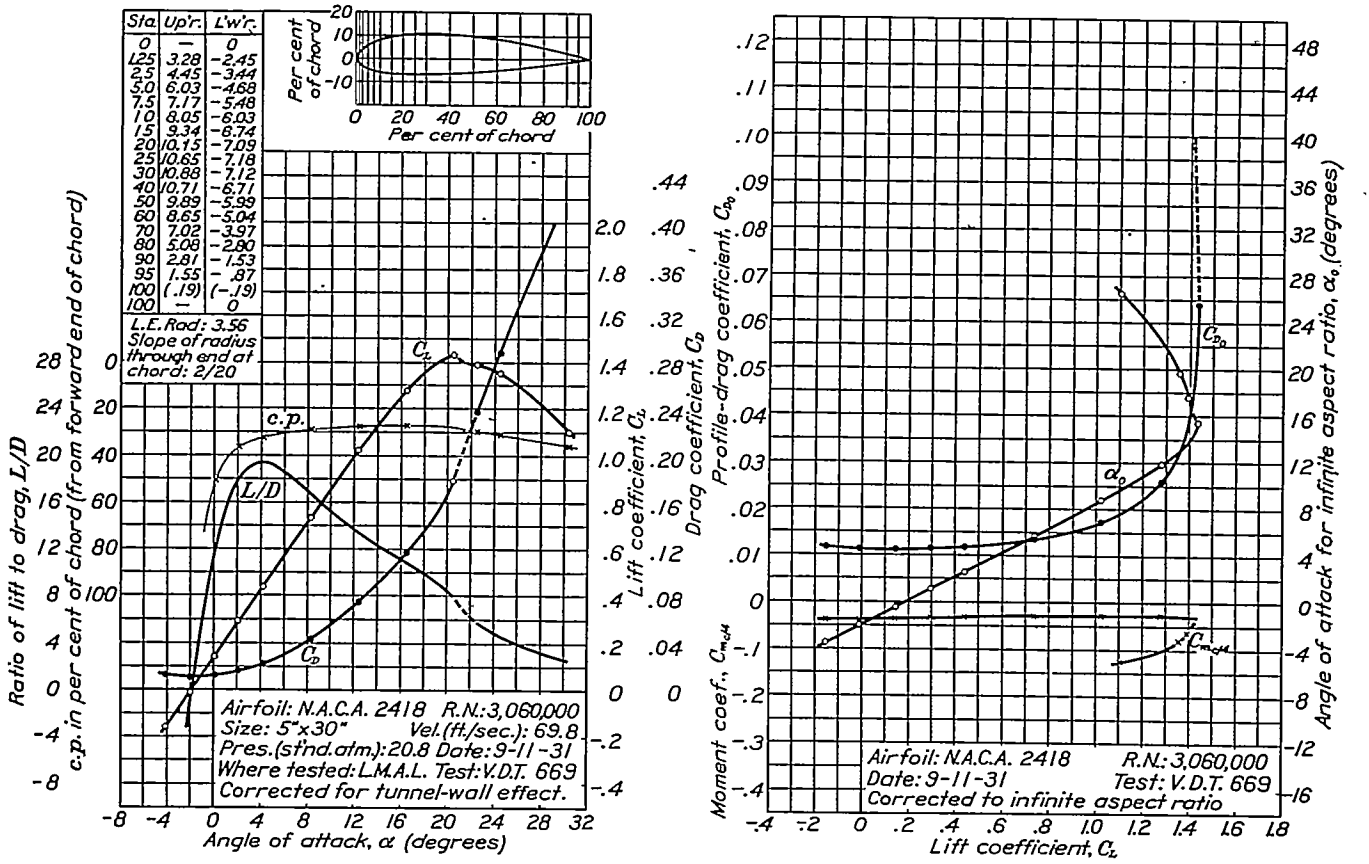

FIGURE 20.—N.A.C.A. 2418 airfoil.

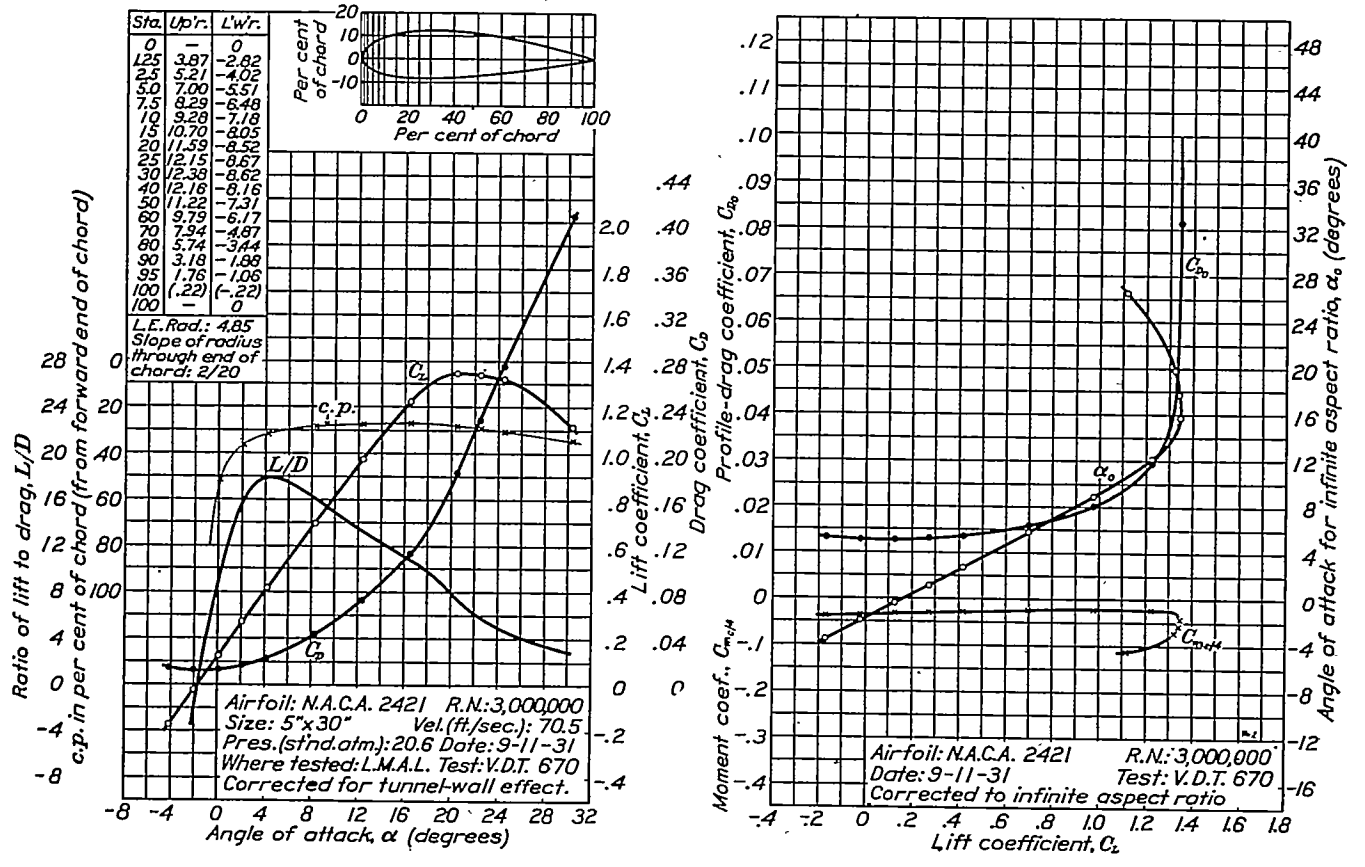

FIGURE 21.—N.A.C.A. 2421 airfoil.

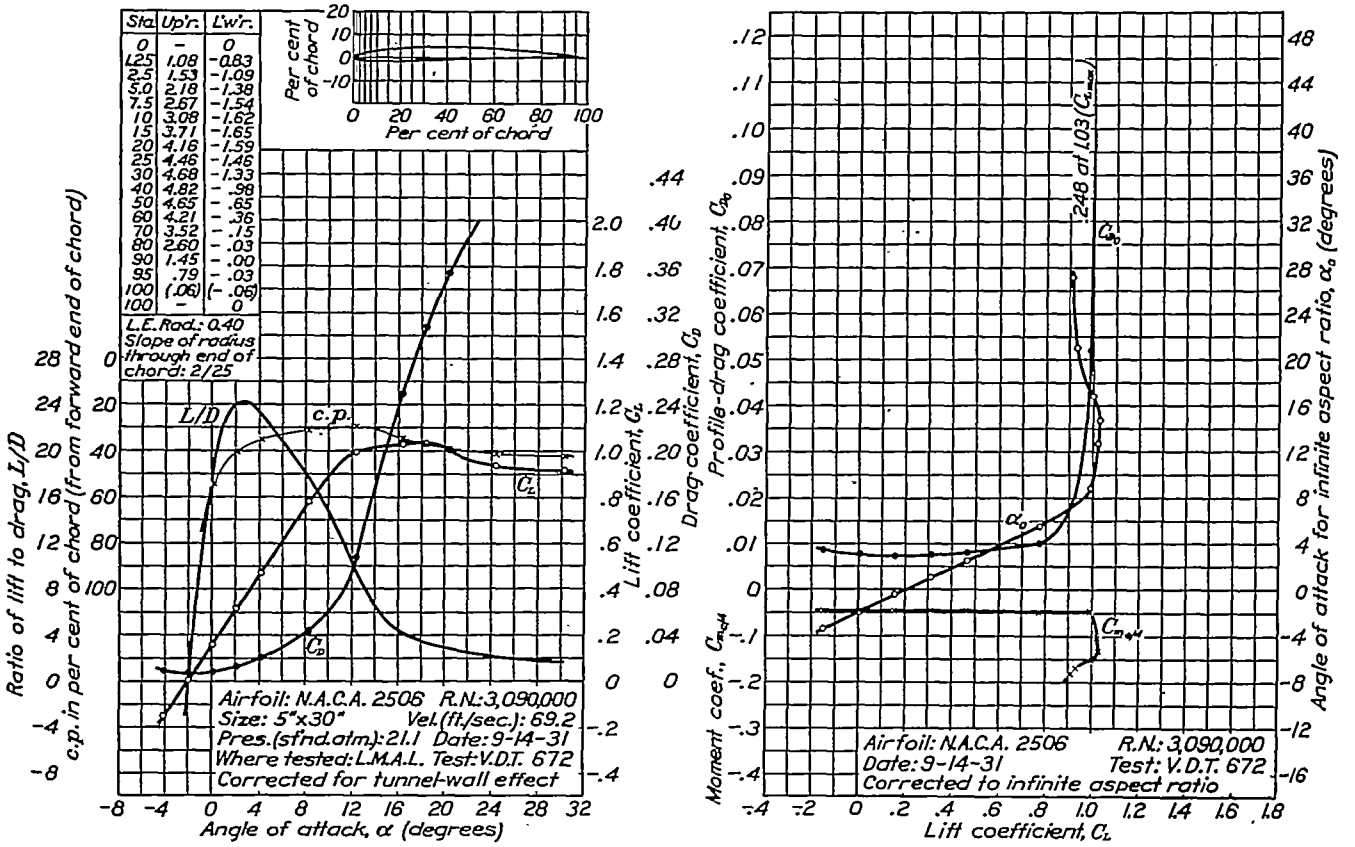

FIGURE 22.—N.A.C.A. 2506 airfoil.

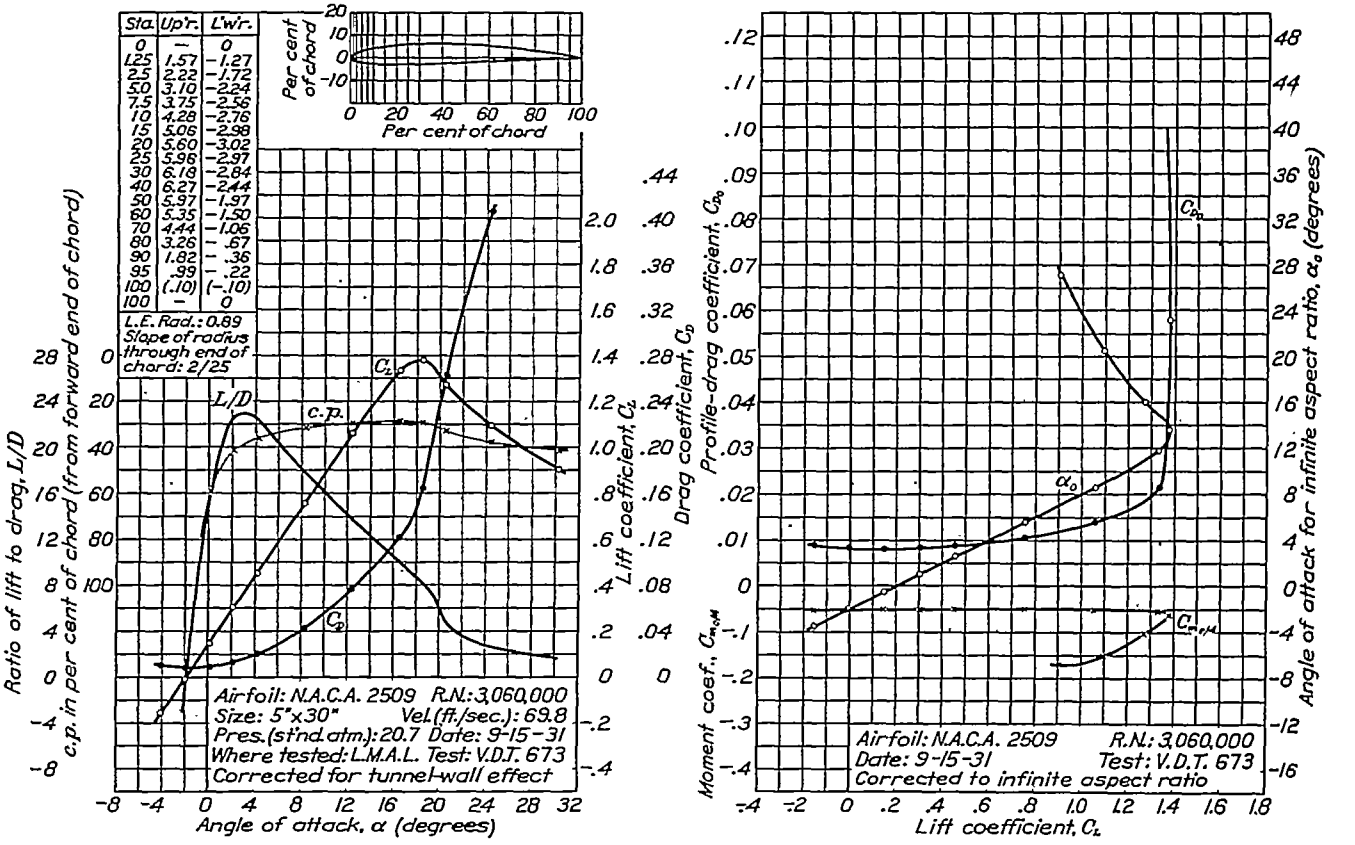

FIGURE 23.—N.A.C.A. 2509 airfoil.

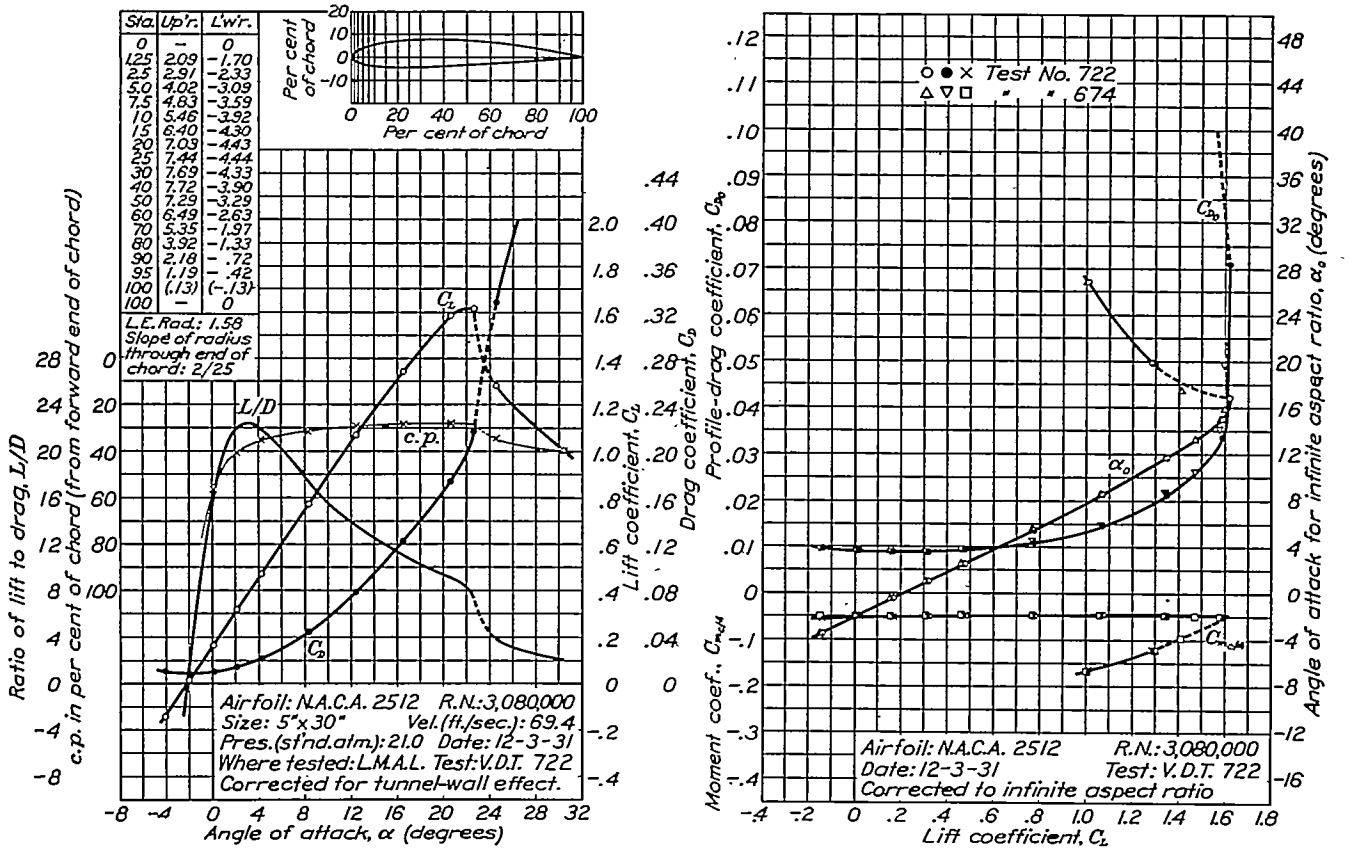

FIGURE 24.—N.A.C.A. 2512 airfoil.

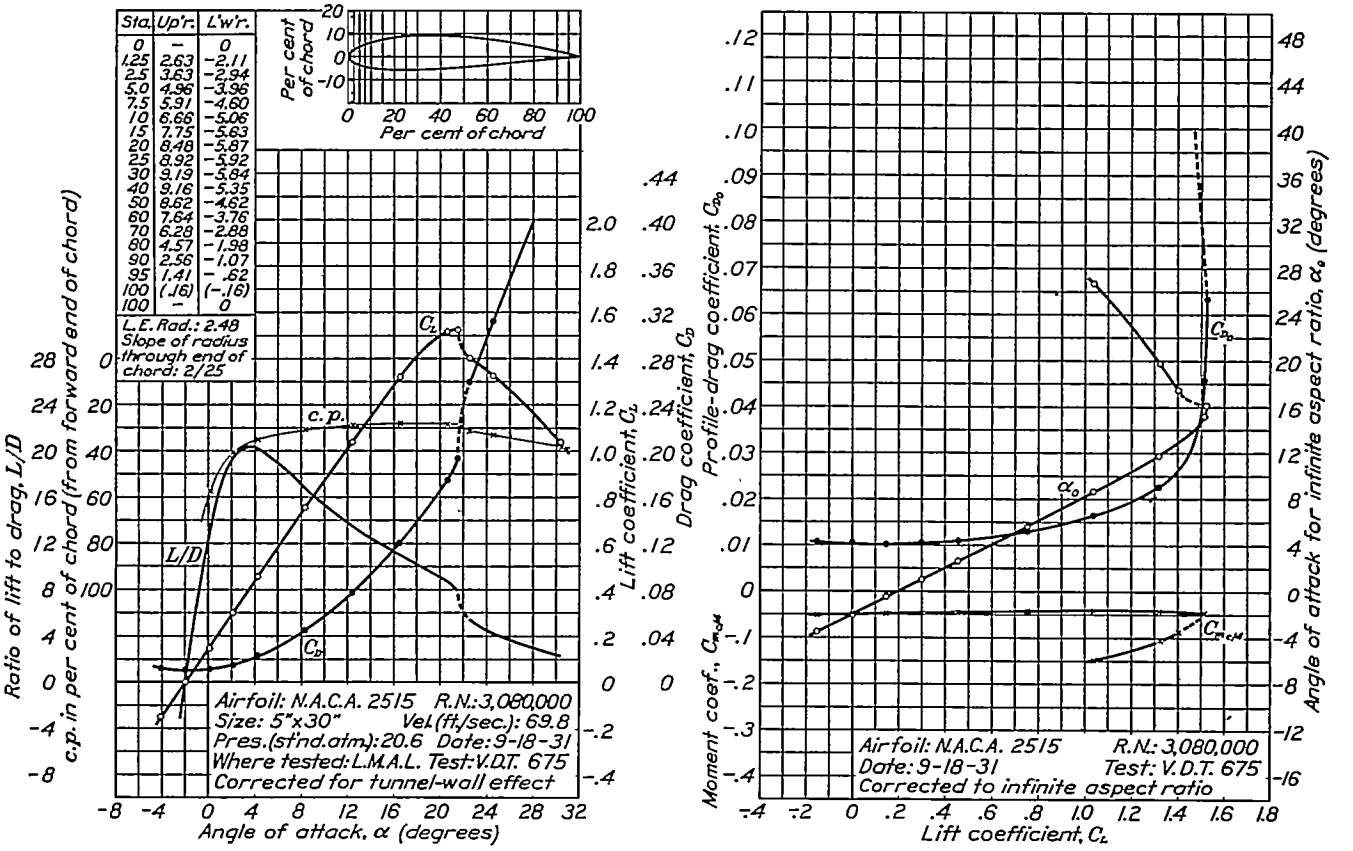

FIGURE 25.—N.A.C.A. 2515 airfoil.

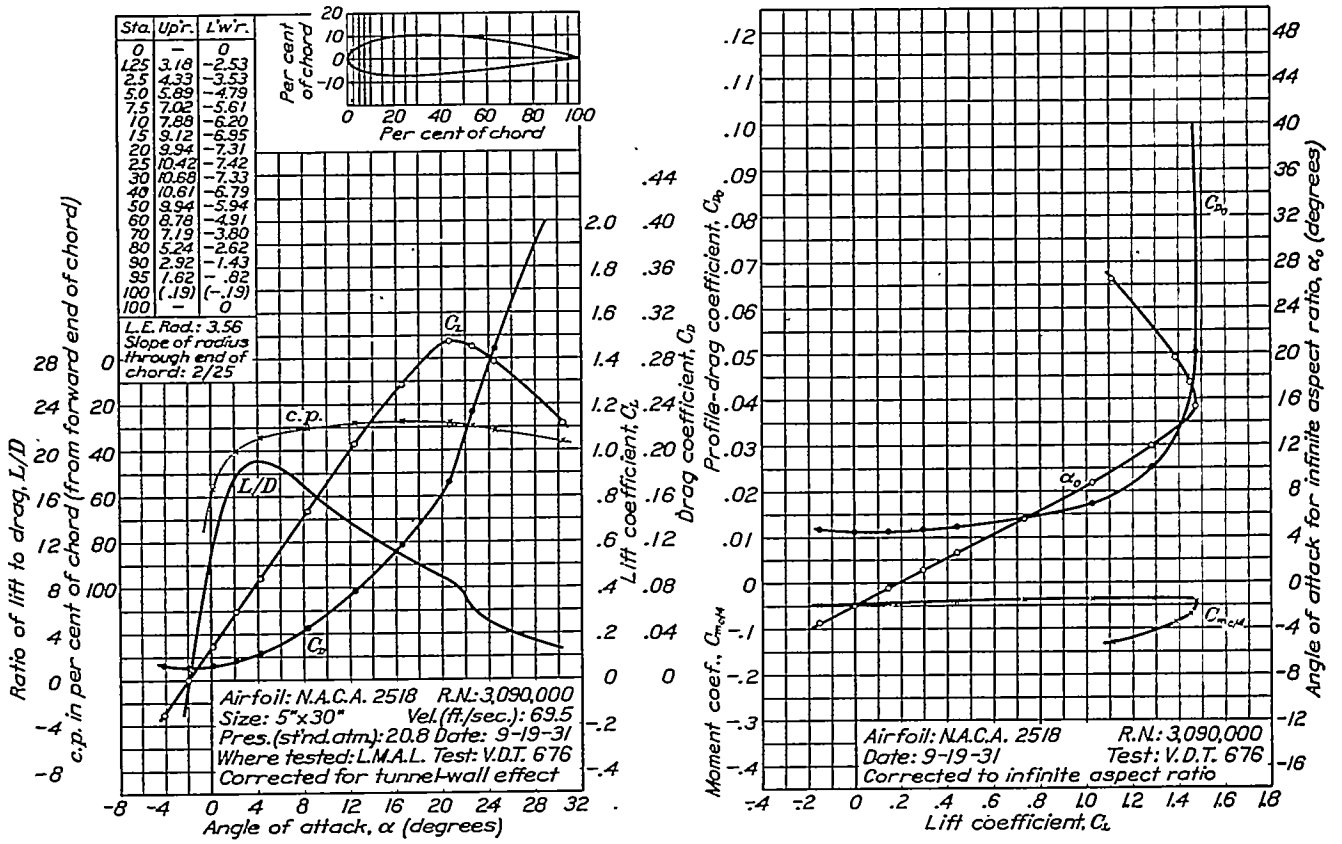

FIGURE 26.—N.A.C.A. 2518 airfoil.

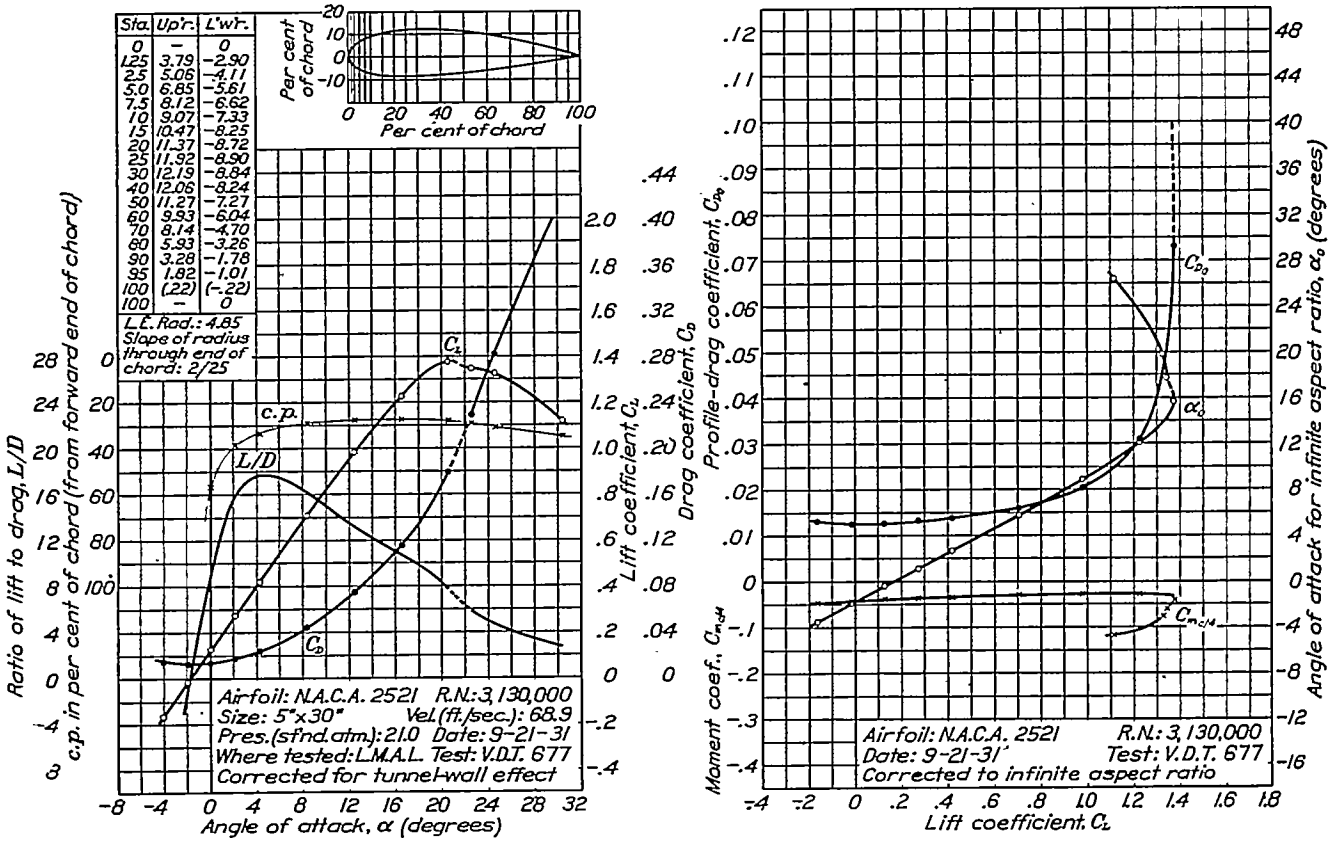

FIGURE 27.—N.A.C.A. 2521 airfoil.

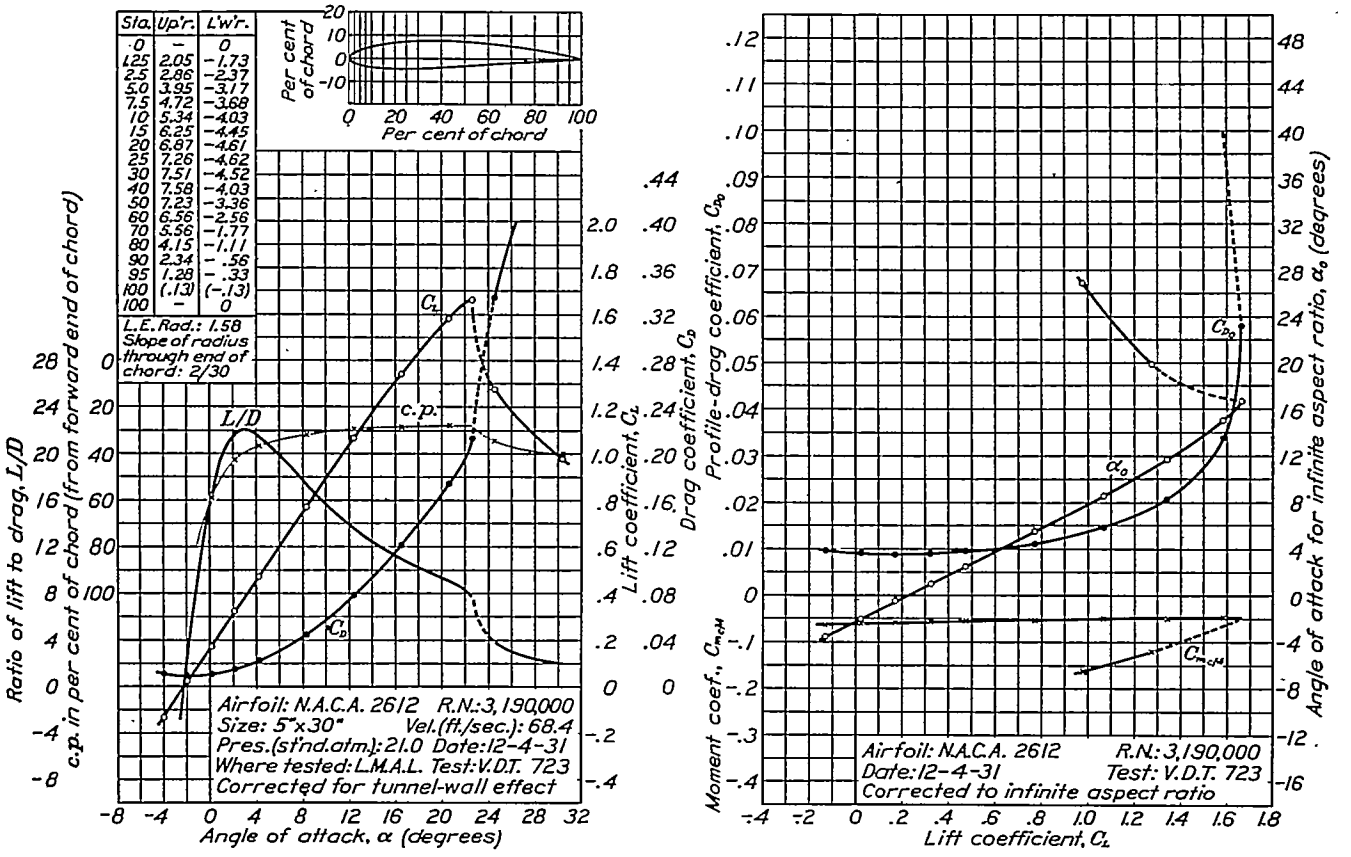

FIGURE 28.—N.A.C.A. 2612 airfoil.

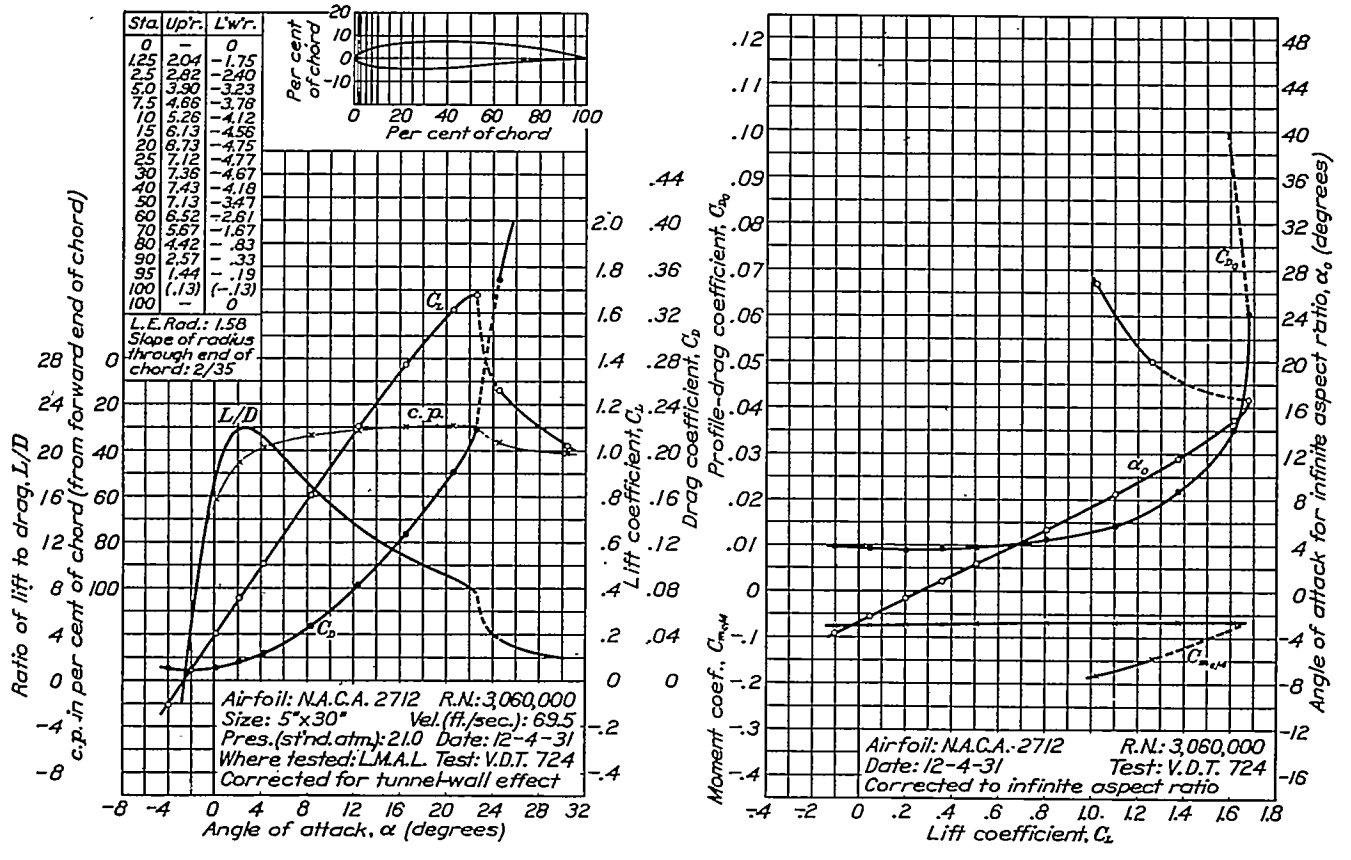

FIGURE 29.—N.A.C.A. 2712 airfoil.

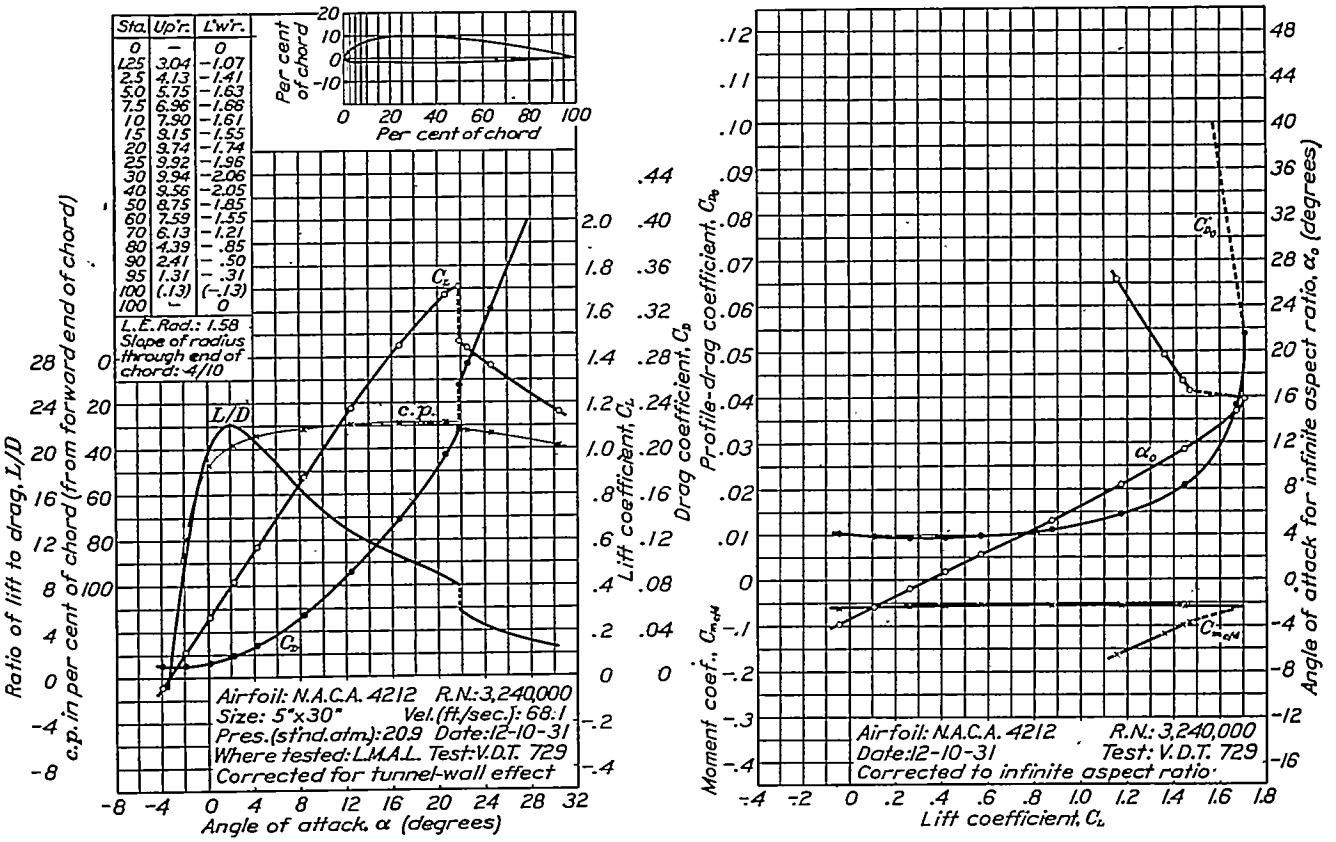

FIGURE 30.—N.A.C.A. 4212 airfoil.

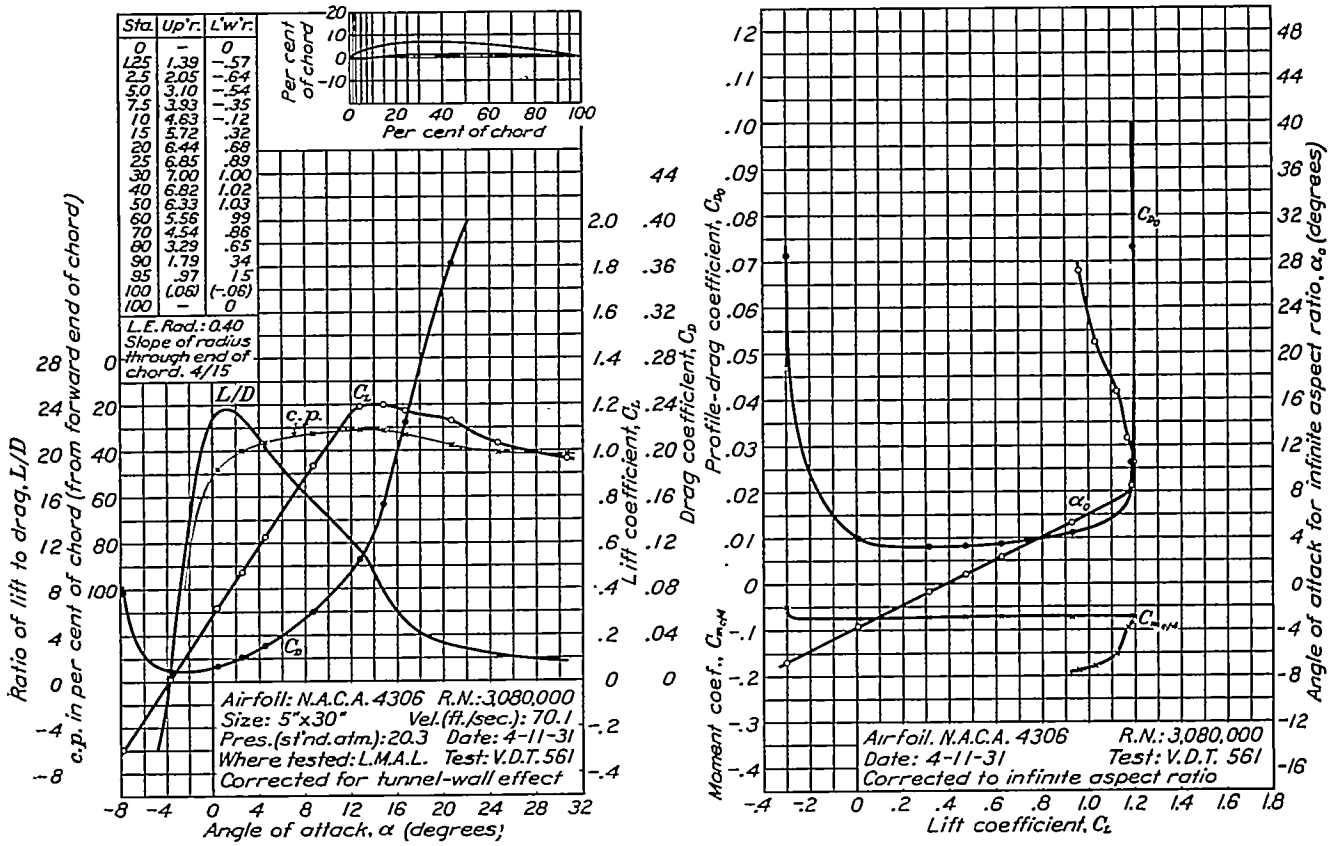

FIGURE 31.—N.A.C.A. 4306 airfoil.

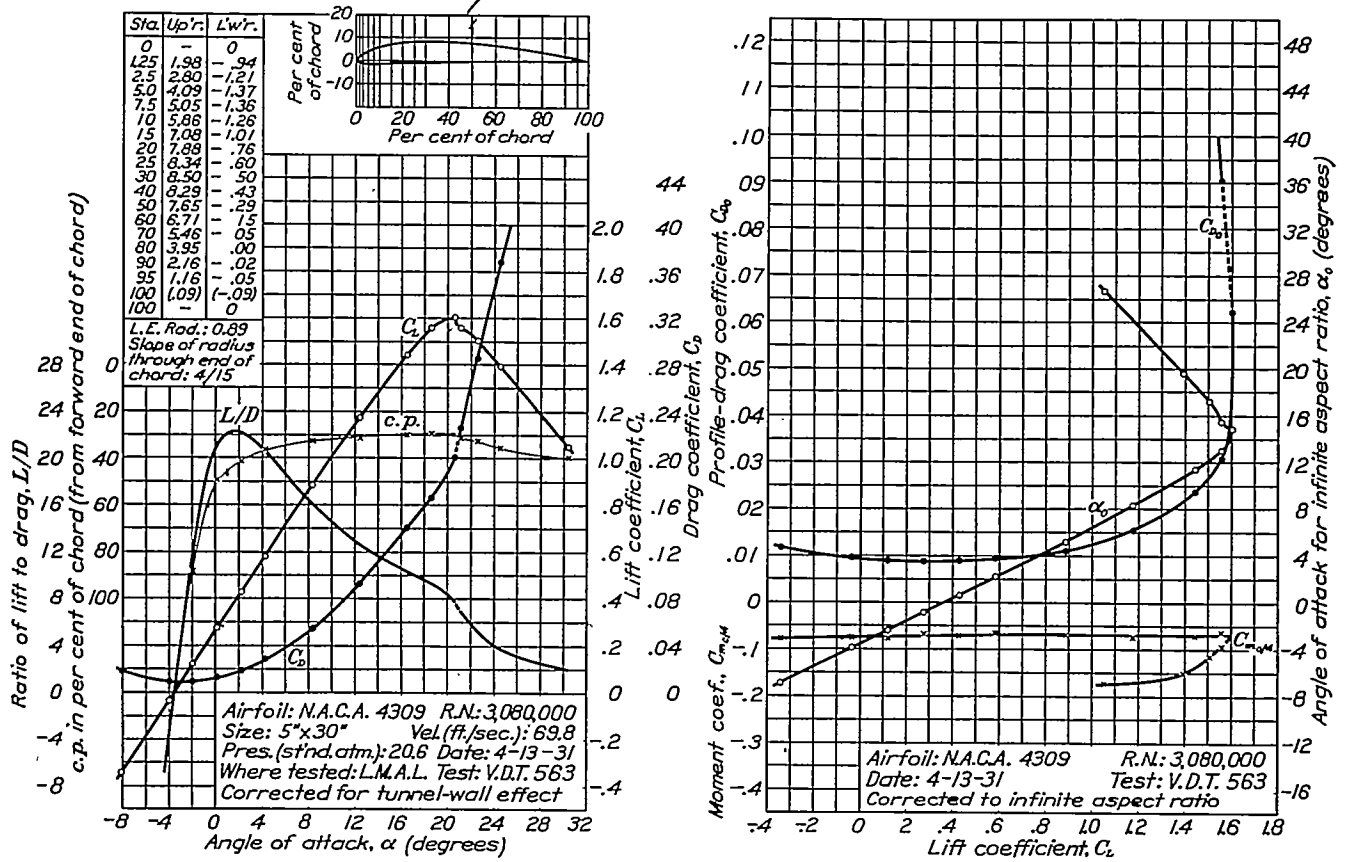

FIGURE 32.—N.A.C.A. 4309 airfoil.

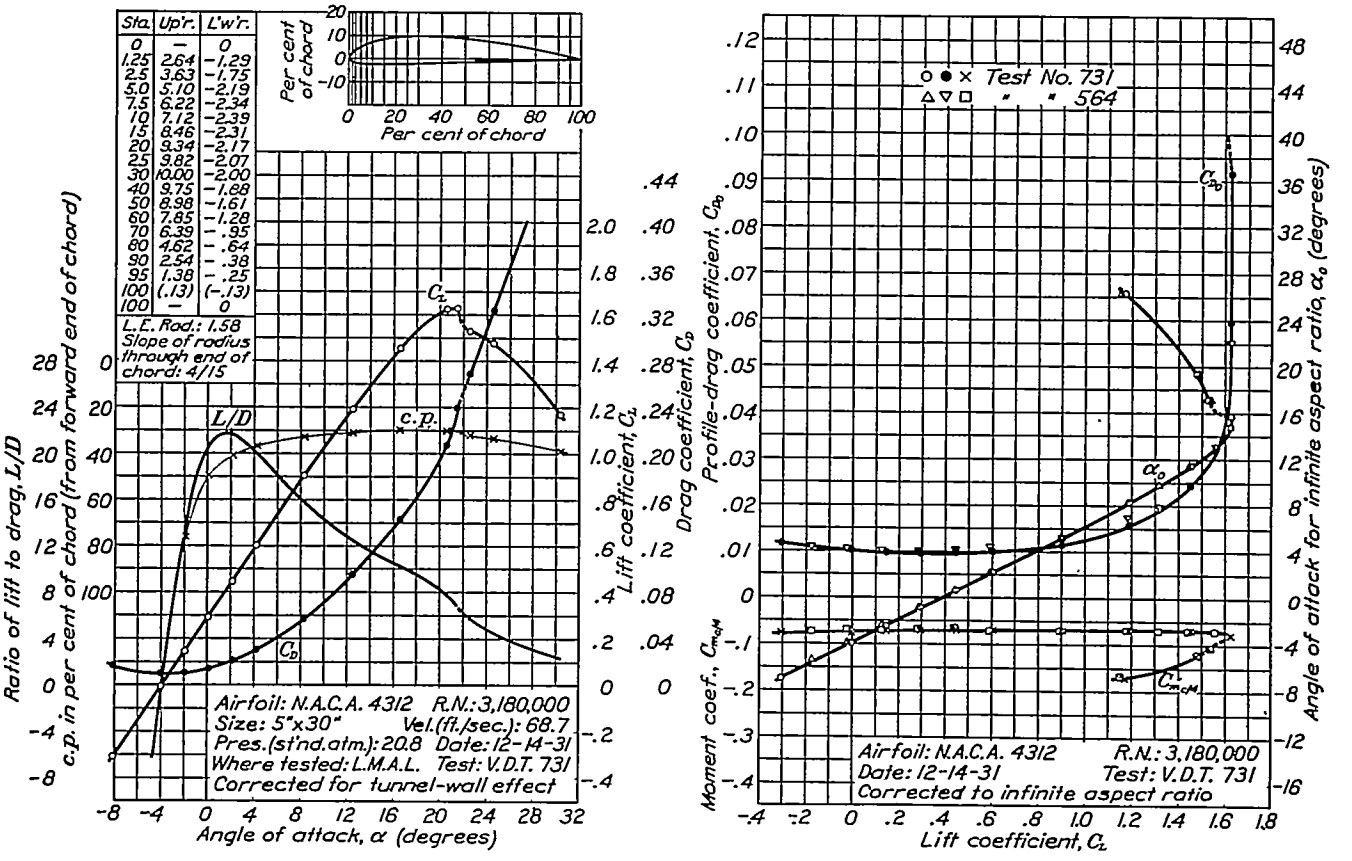

FIGURE 33.—N.A.C.A. 4312 airfoil.

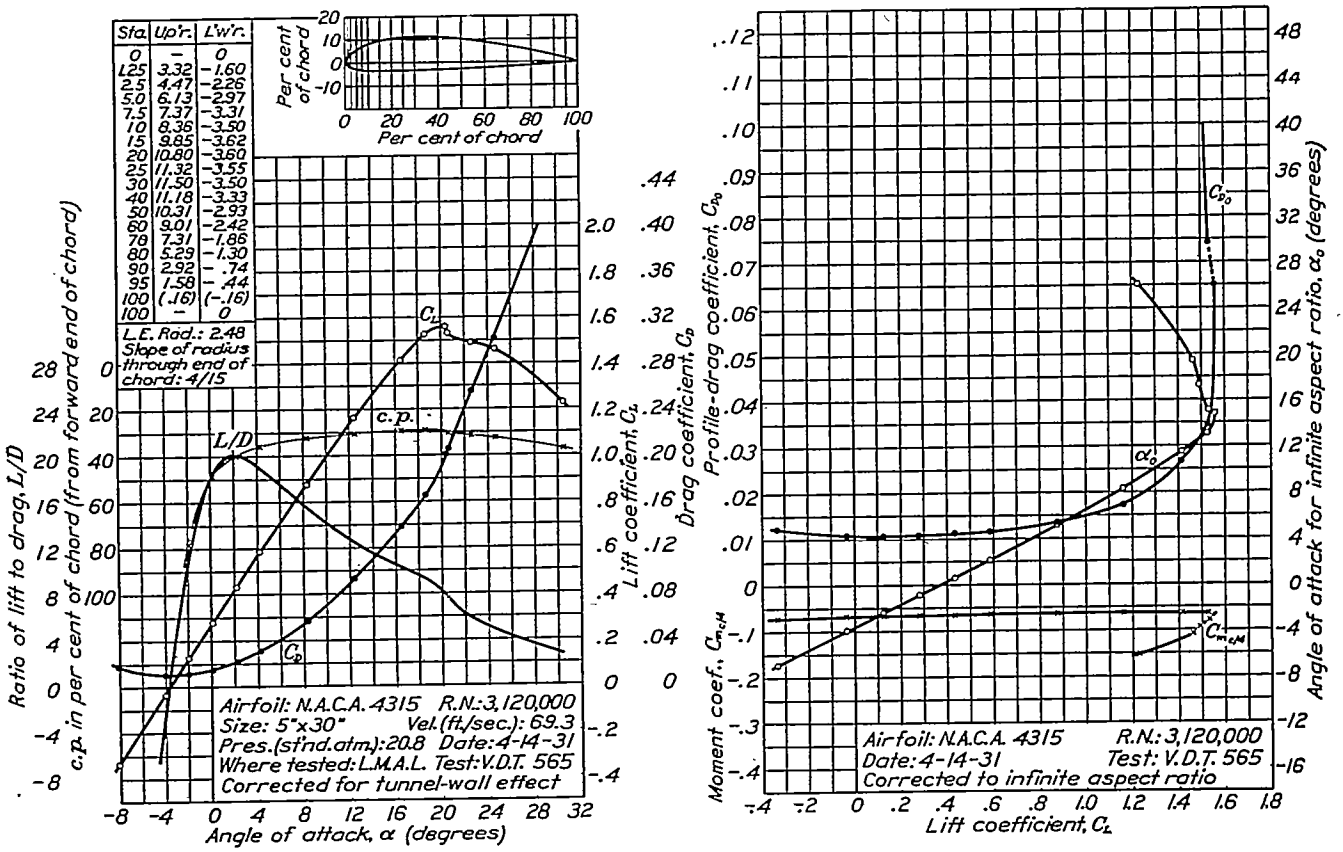

FIGURE 34.—N.A.C.A. 4315 airfoil.

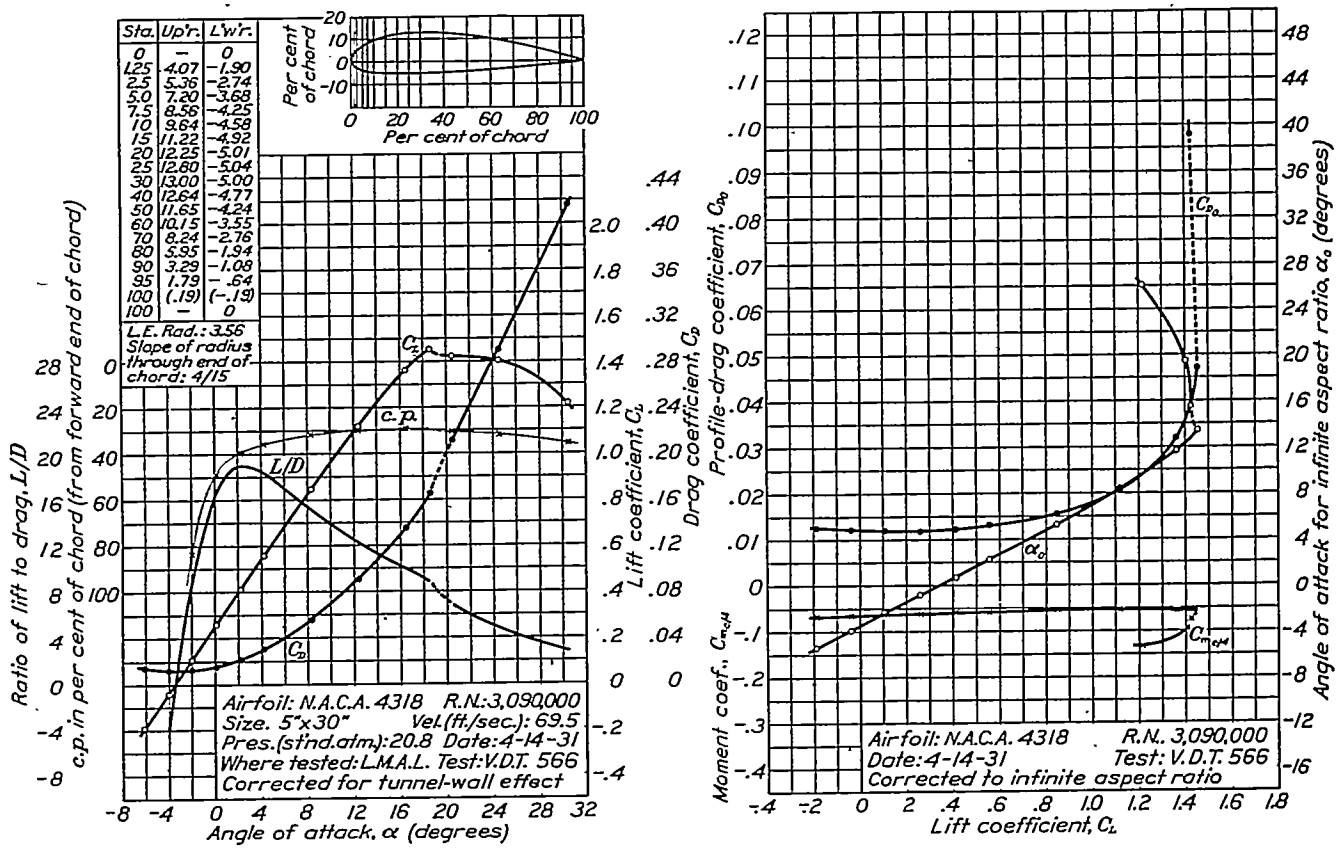

FIGURE 35.—N.A.C.A. 4318 airfoil.

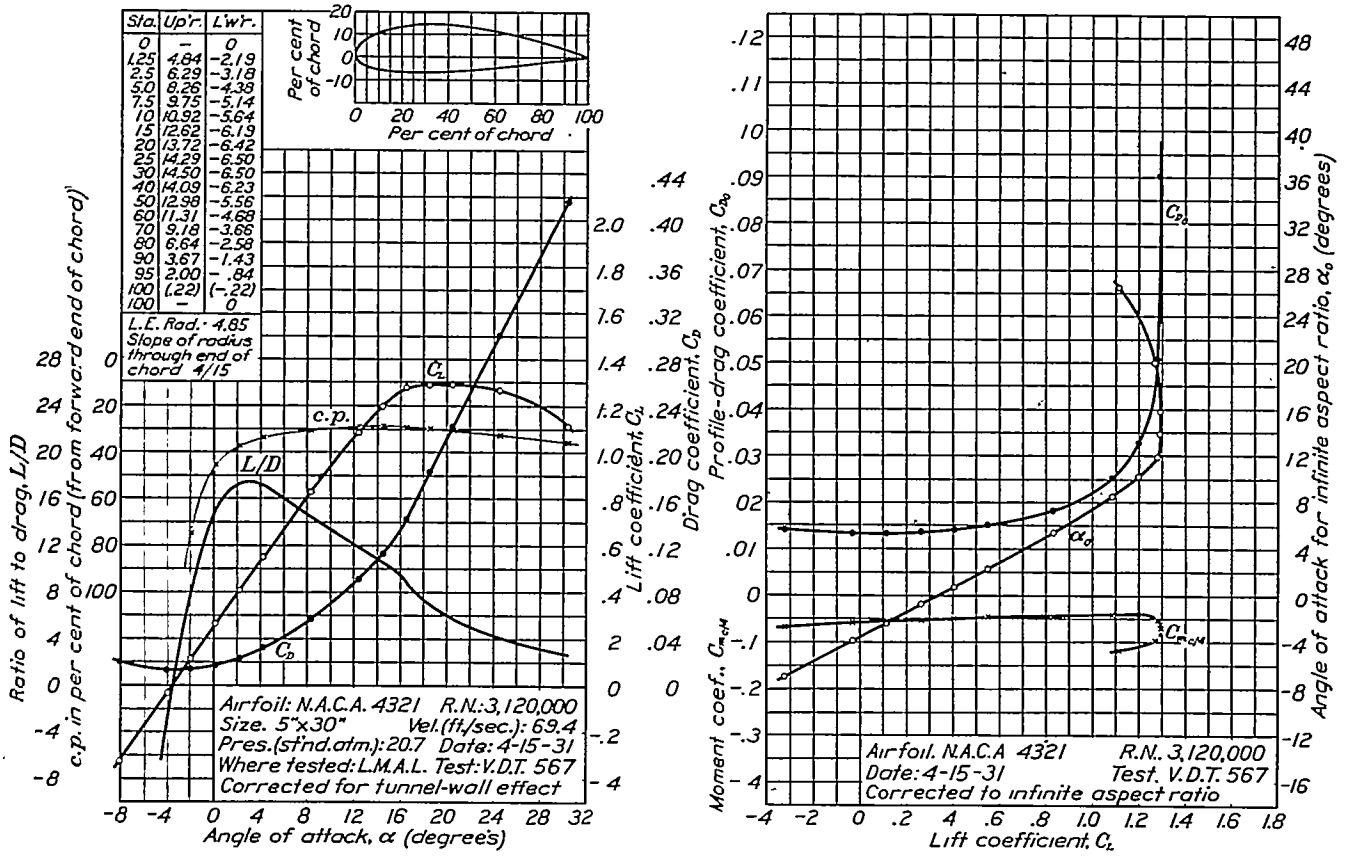

FIGURE 36.—N.A.C.A. 4321 airfoil.

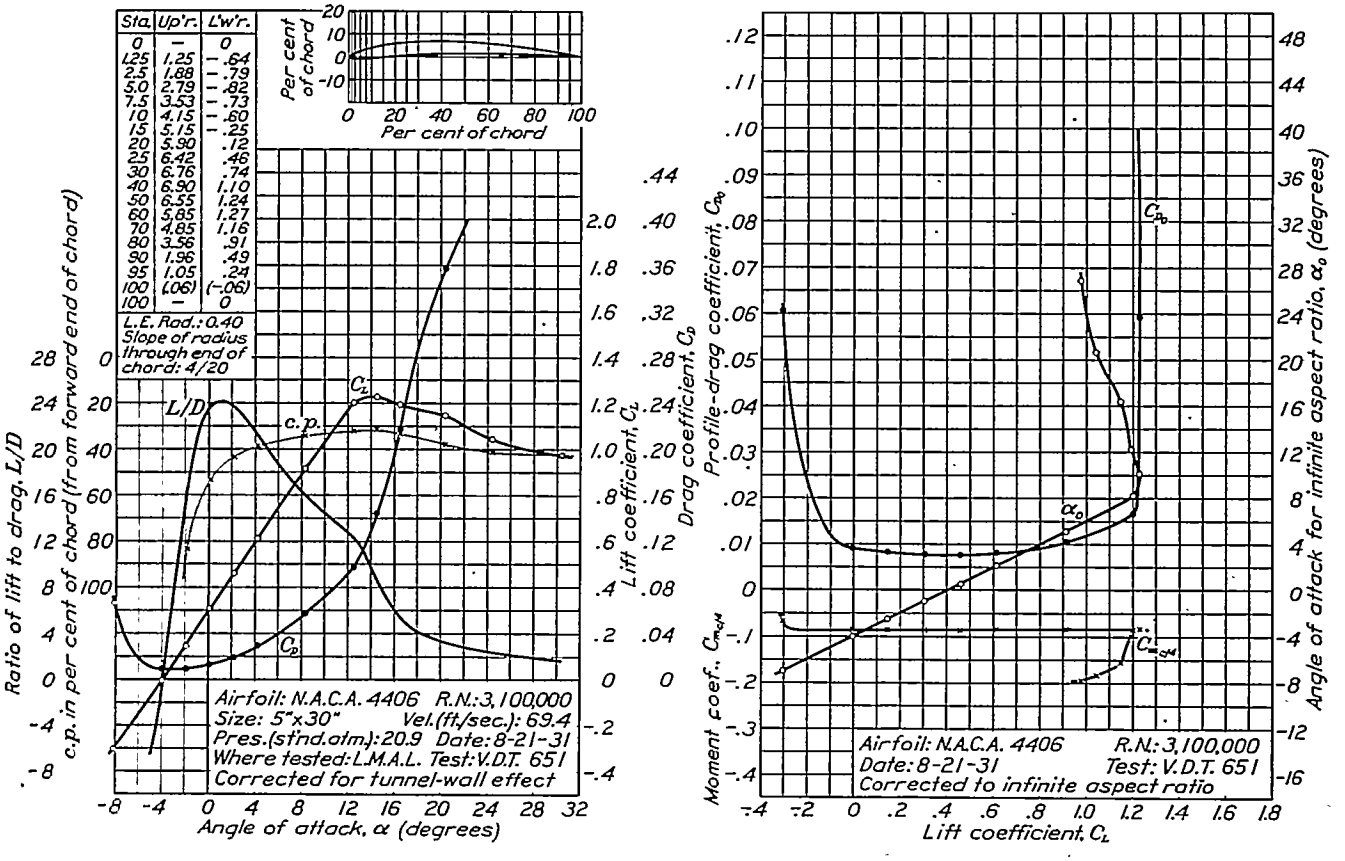

FIGURE 37.—N.A.C.A. 4406 airfoil.

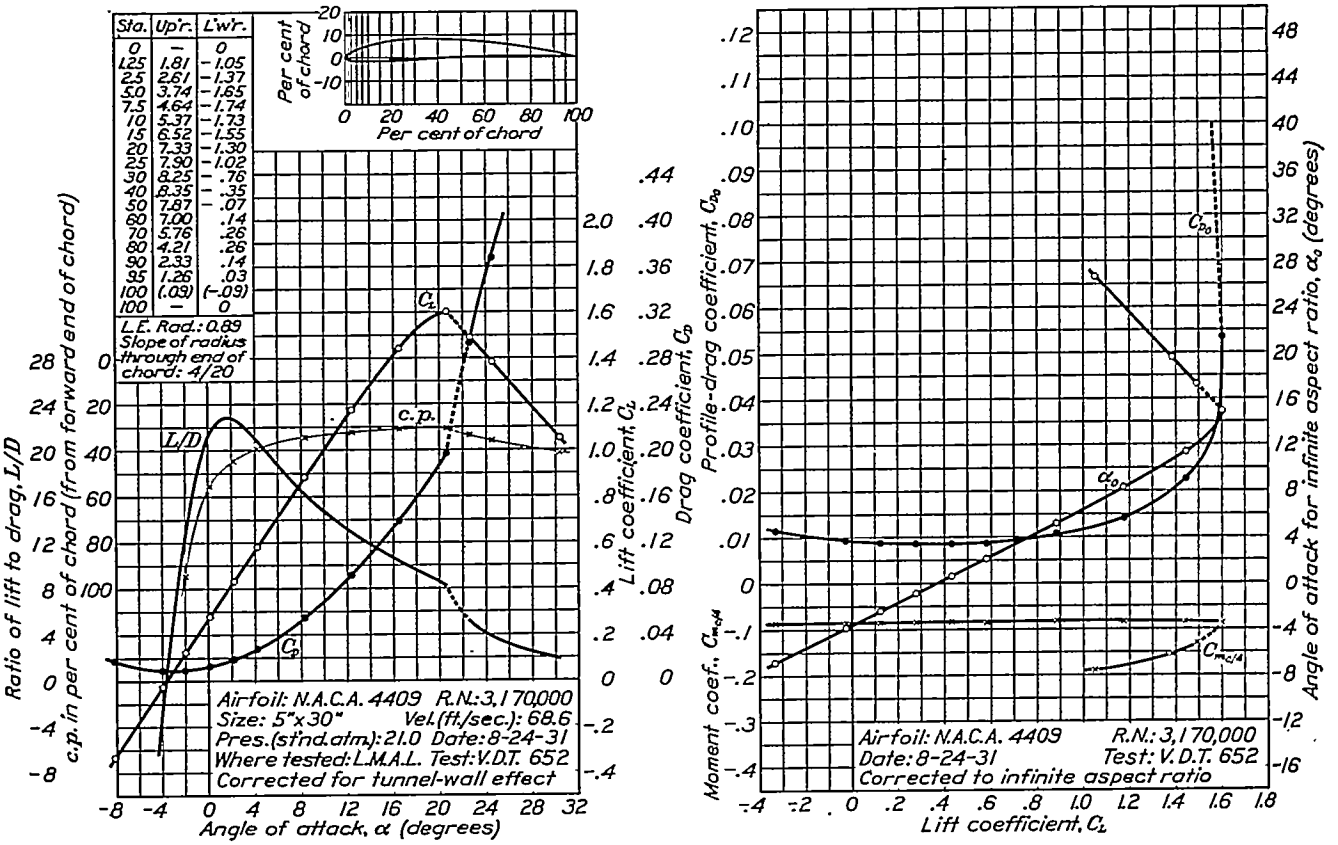

FIGURE 38.—N.A.C.A. 4409 airfoil.

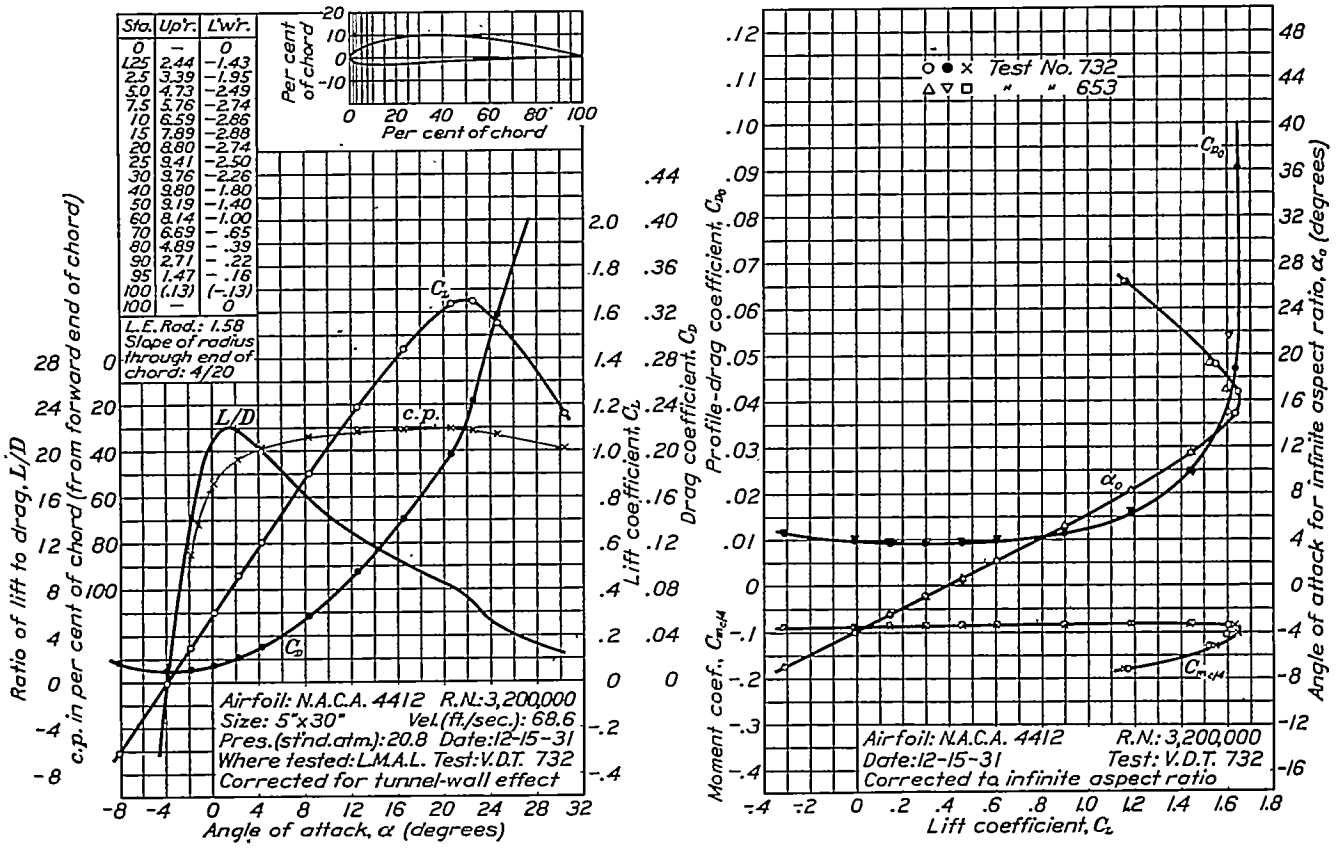

FIGURE 39.—N.A.C.A. 4412 airfoil.

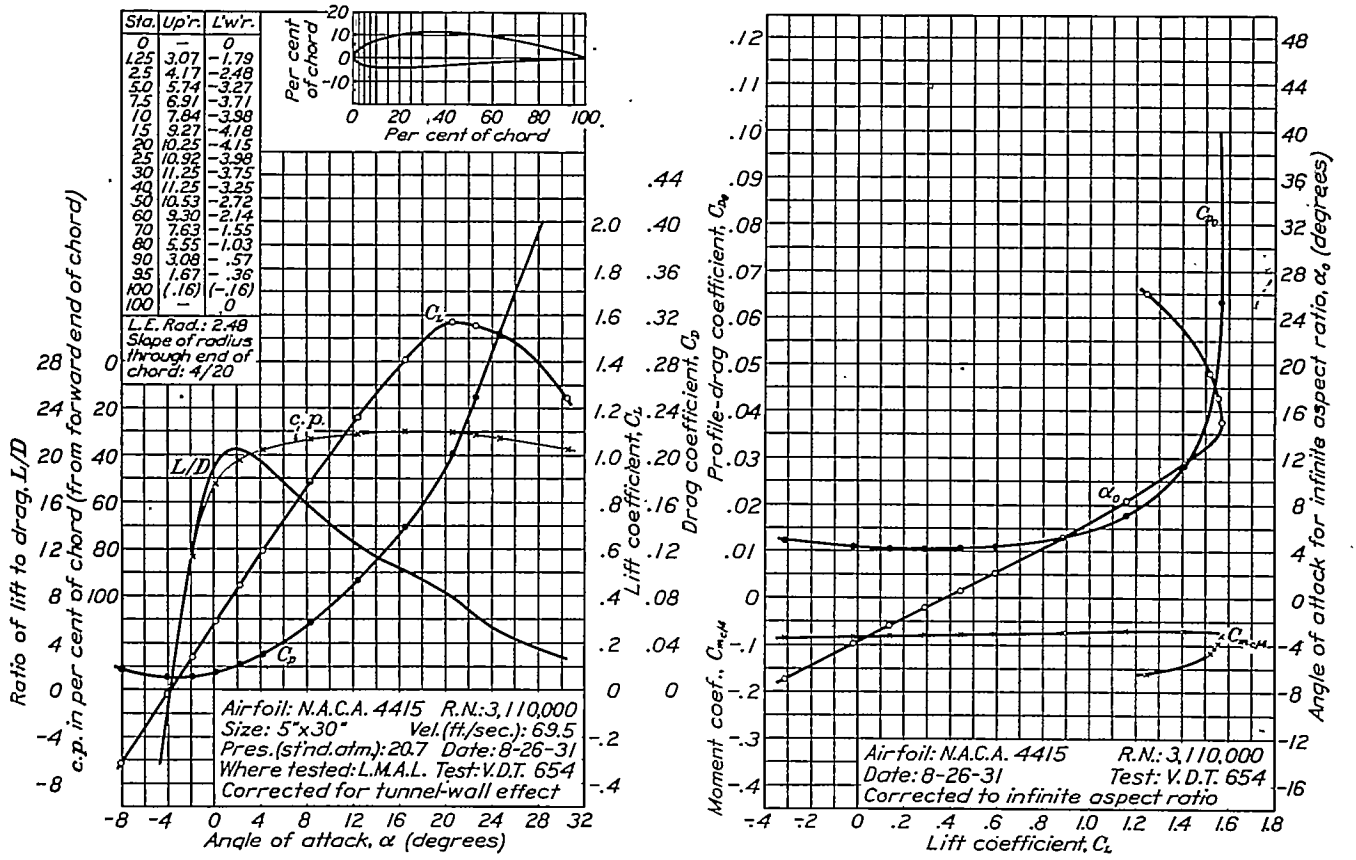

FIGURE 40.—N.A.C.A. 4415 airfoil.

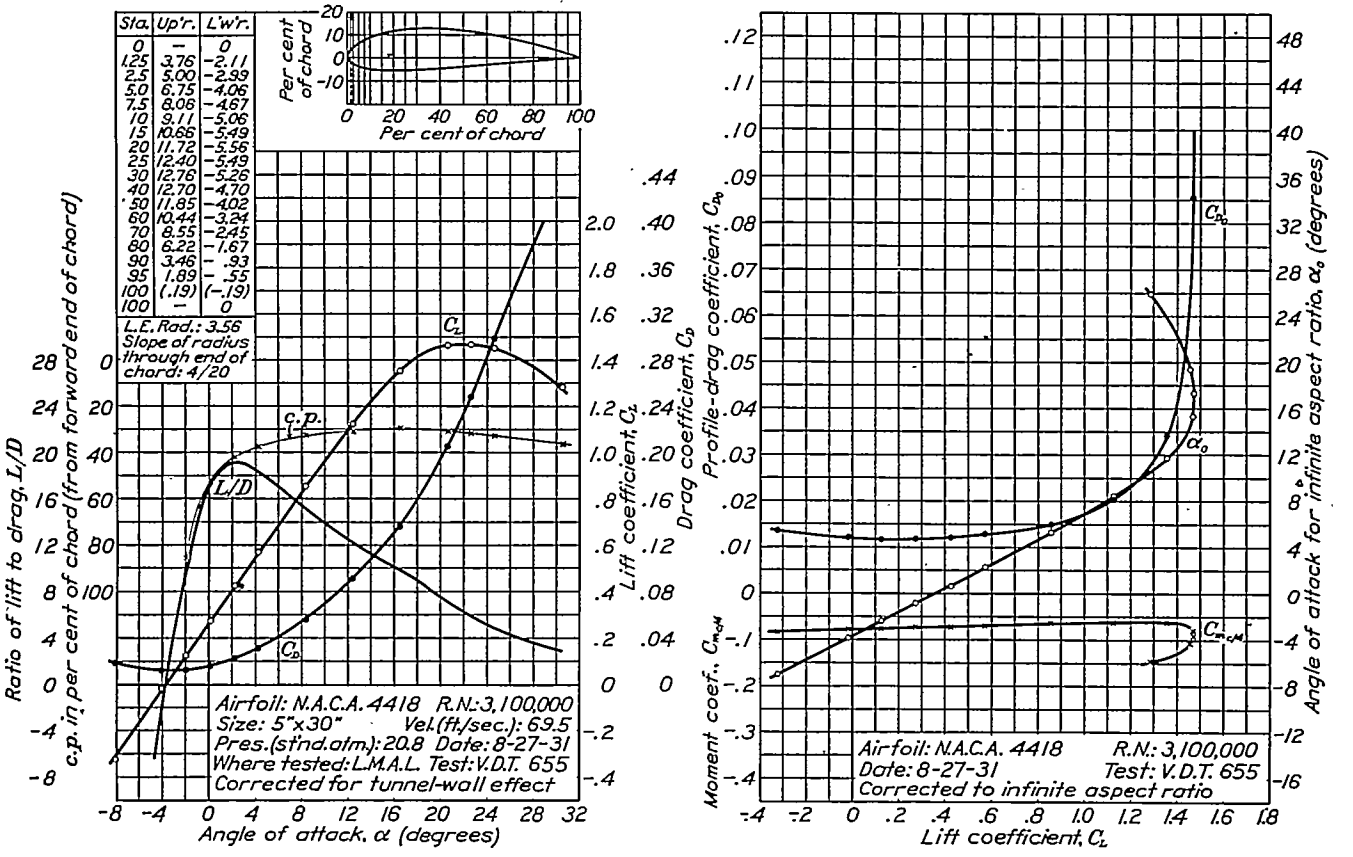

FIGURE 41.—N.A.C.A. 4418 airfoil.

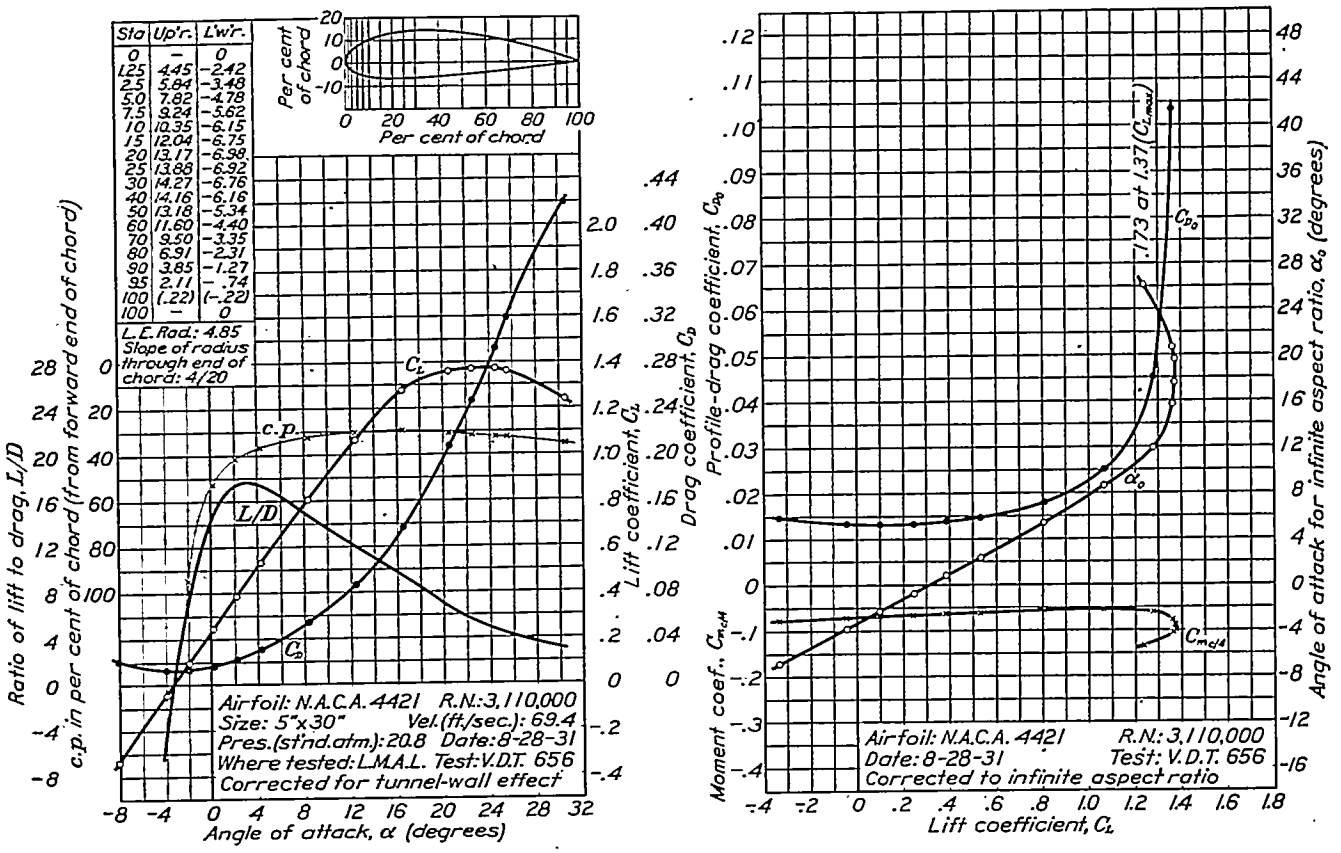

FIGURE 42.—N.A.C.A. 4421 airfoil.

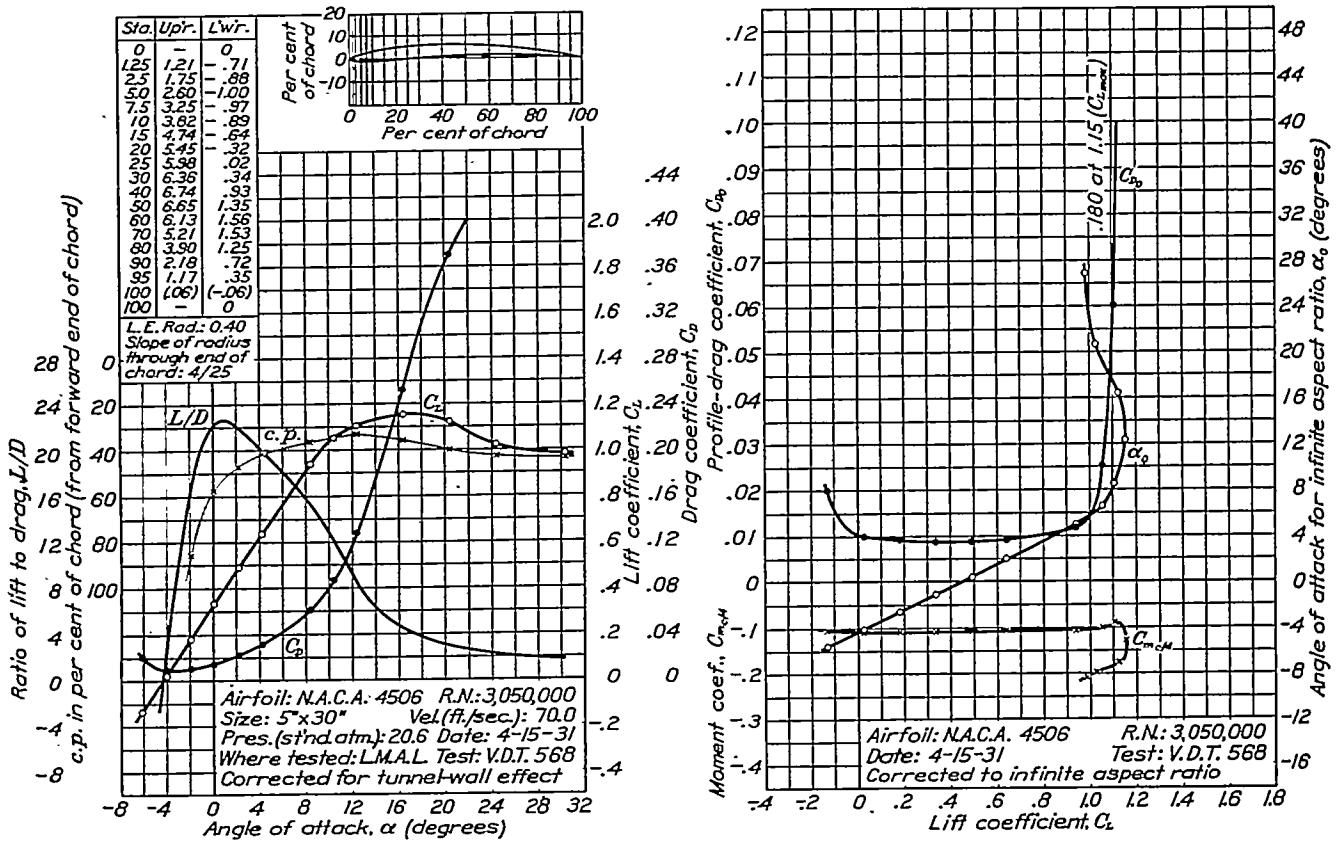

FIGURE 43.—N.A.C.A. 4506 airfoil.

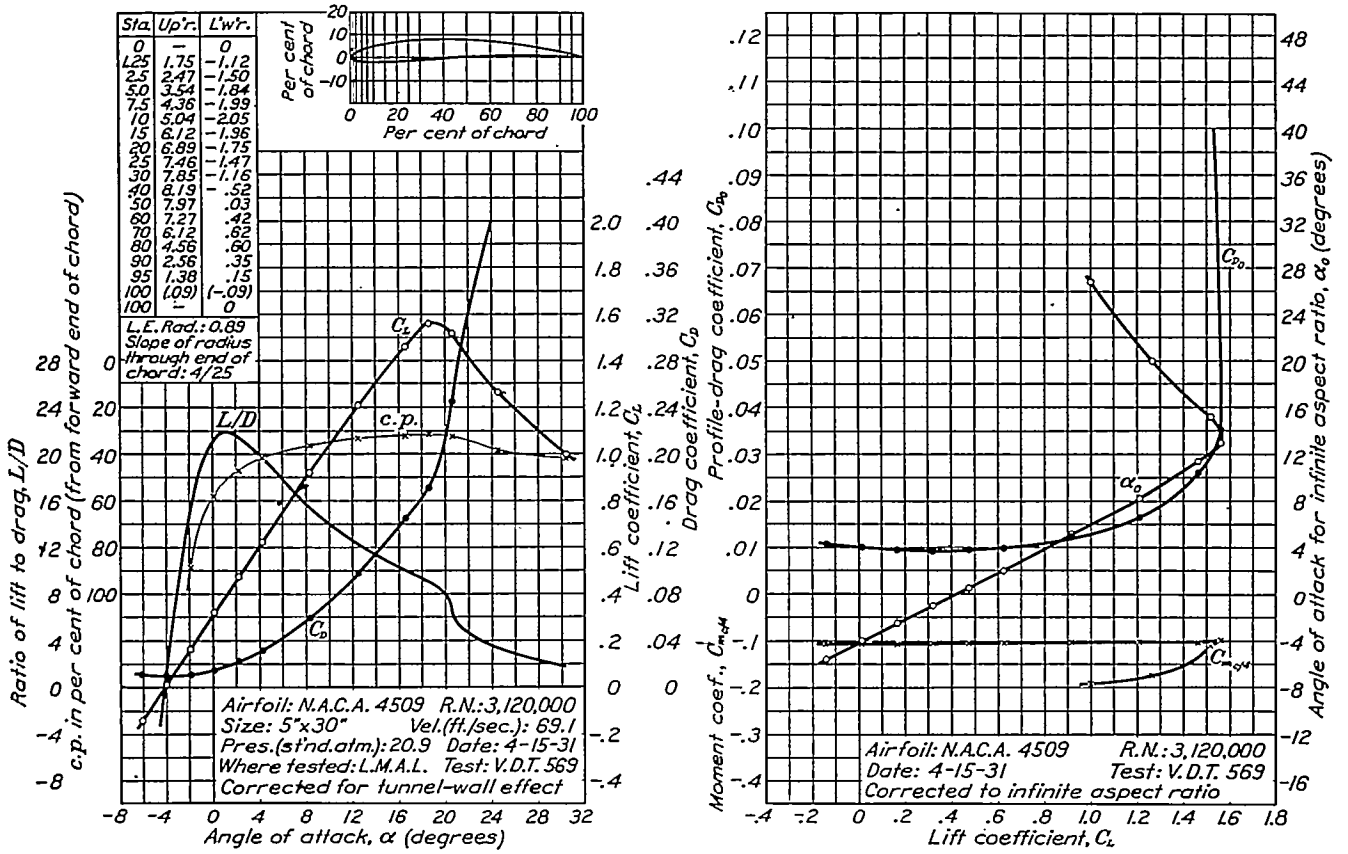

FIGURE 44.—N.A.C.A. 4509 airfoil.

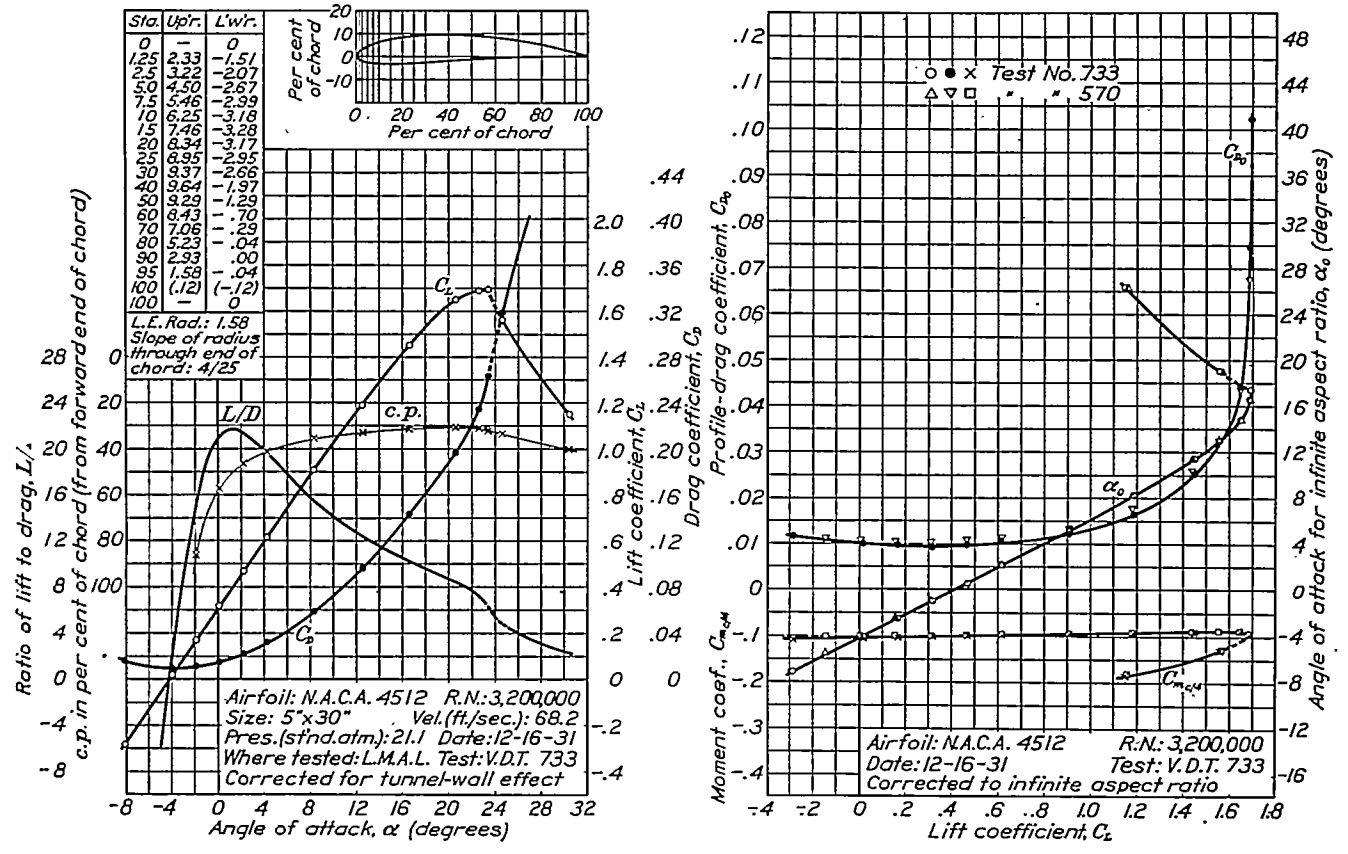

FIGURE 45.—N.A.C.A. 4512 airfoil.

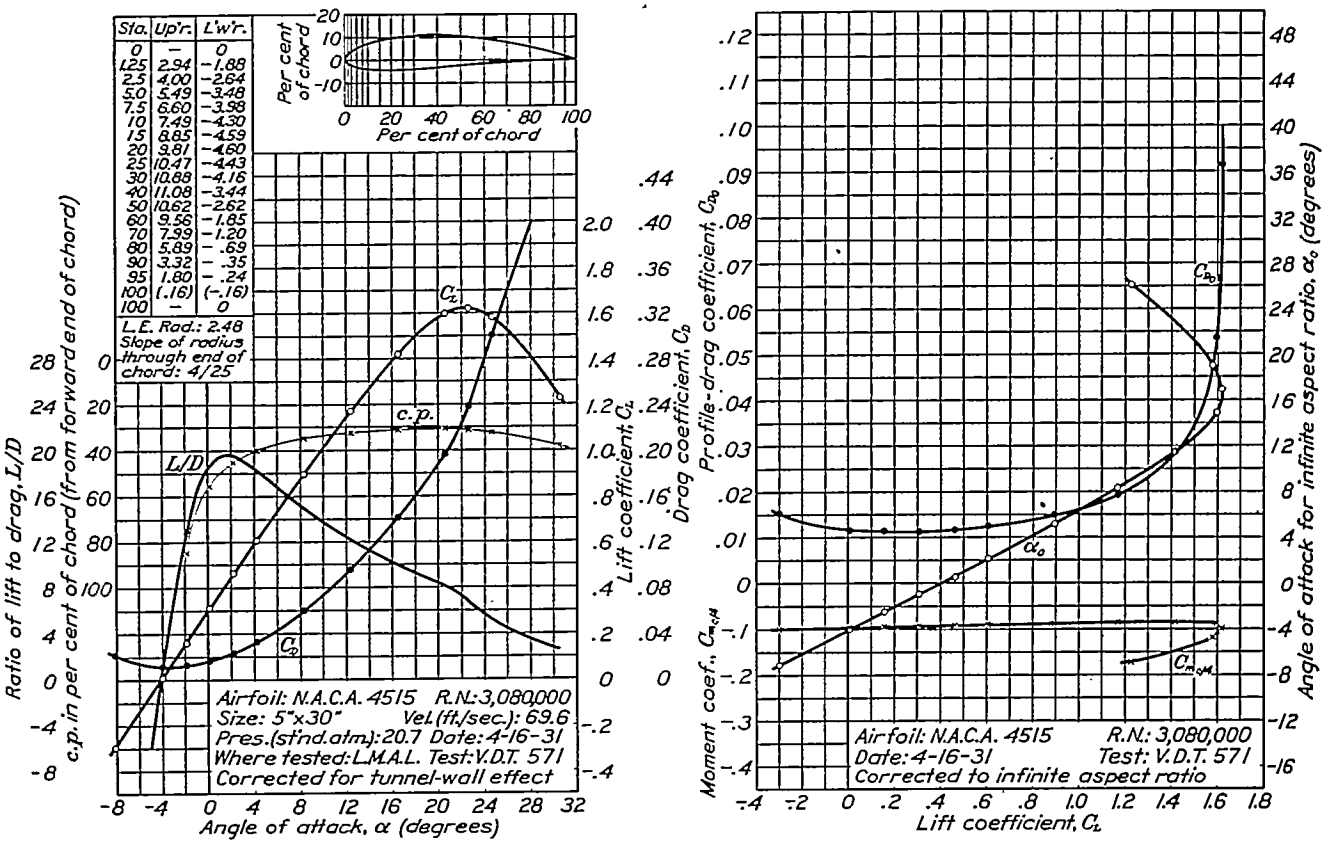

FIGURE 46.—N.A.C.A. 4515 airfoil.

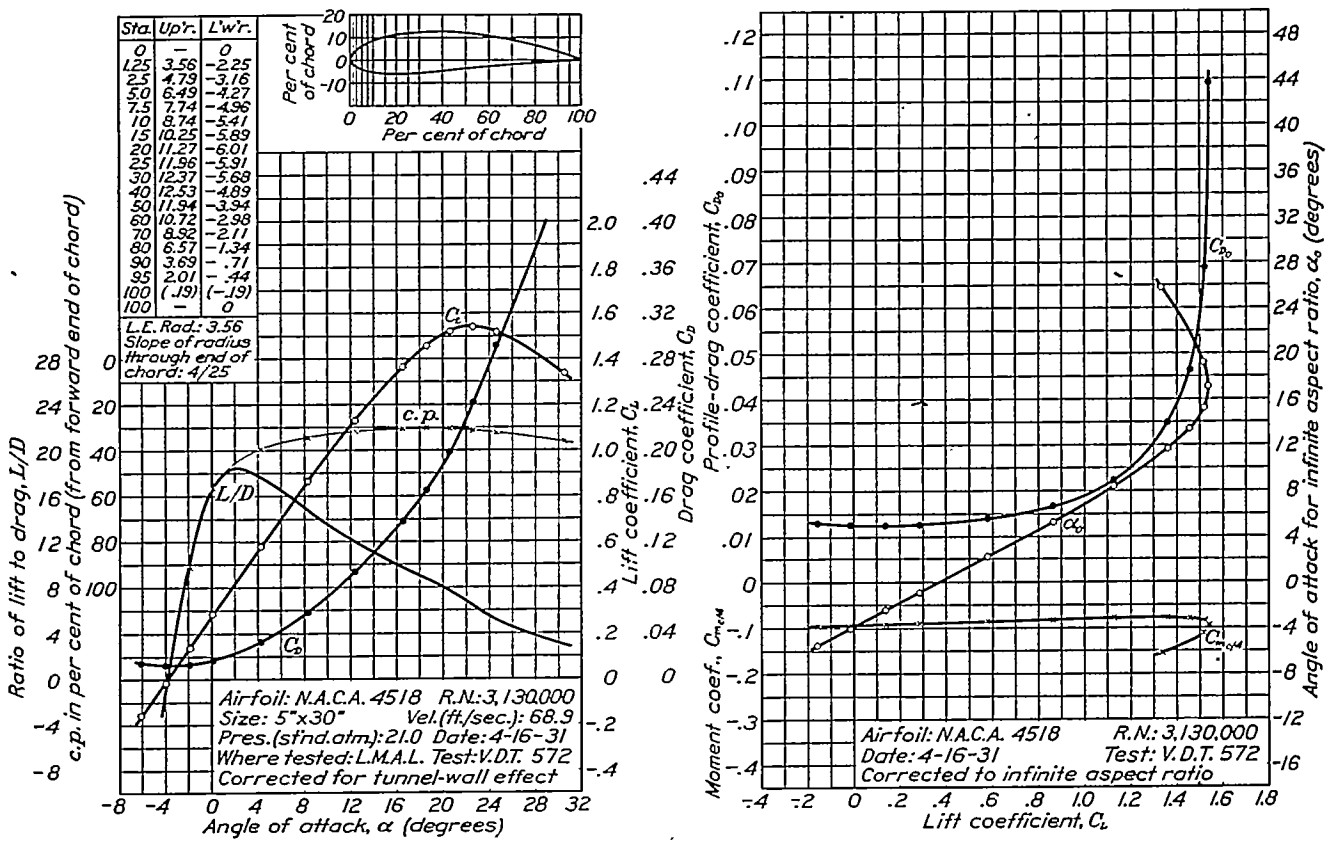

FIGURE 47.—N.A.C.A. 4518 airfoil.

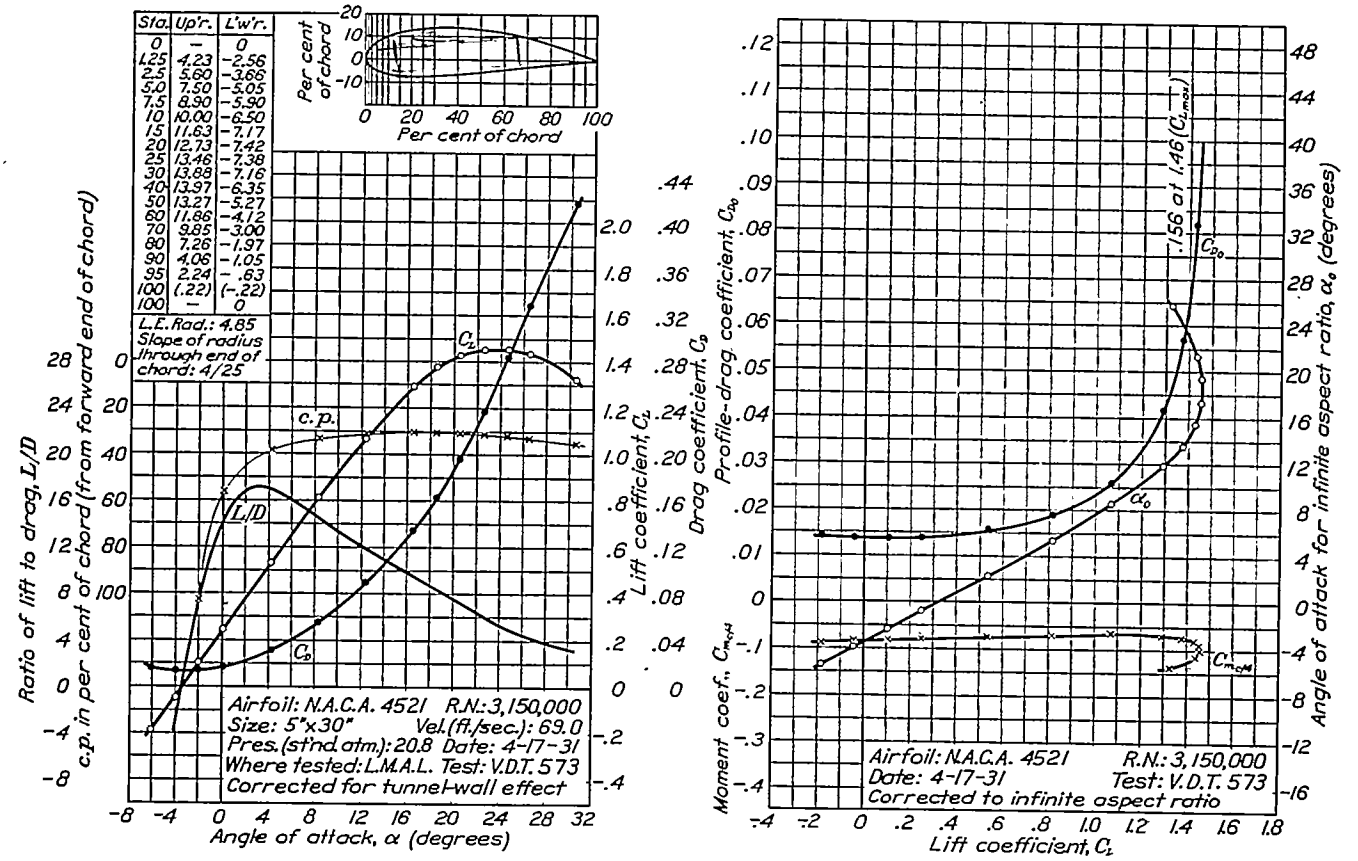

FIGURE 48.—N.A.C.A. 4521 airfoil.

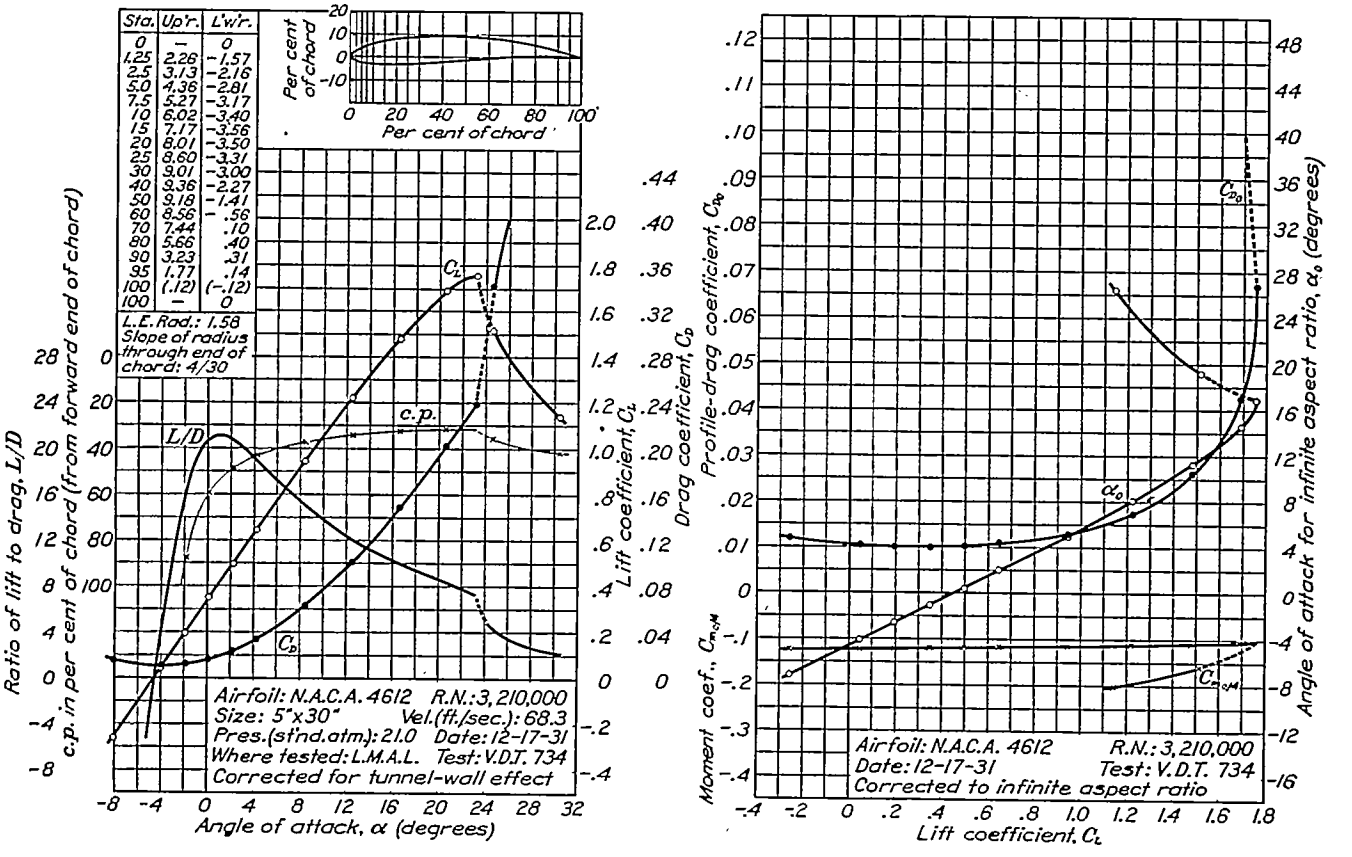

FIGURE 49.—N.A.C.A. 4612 airfoil.

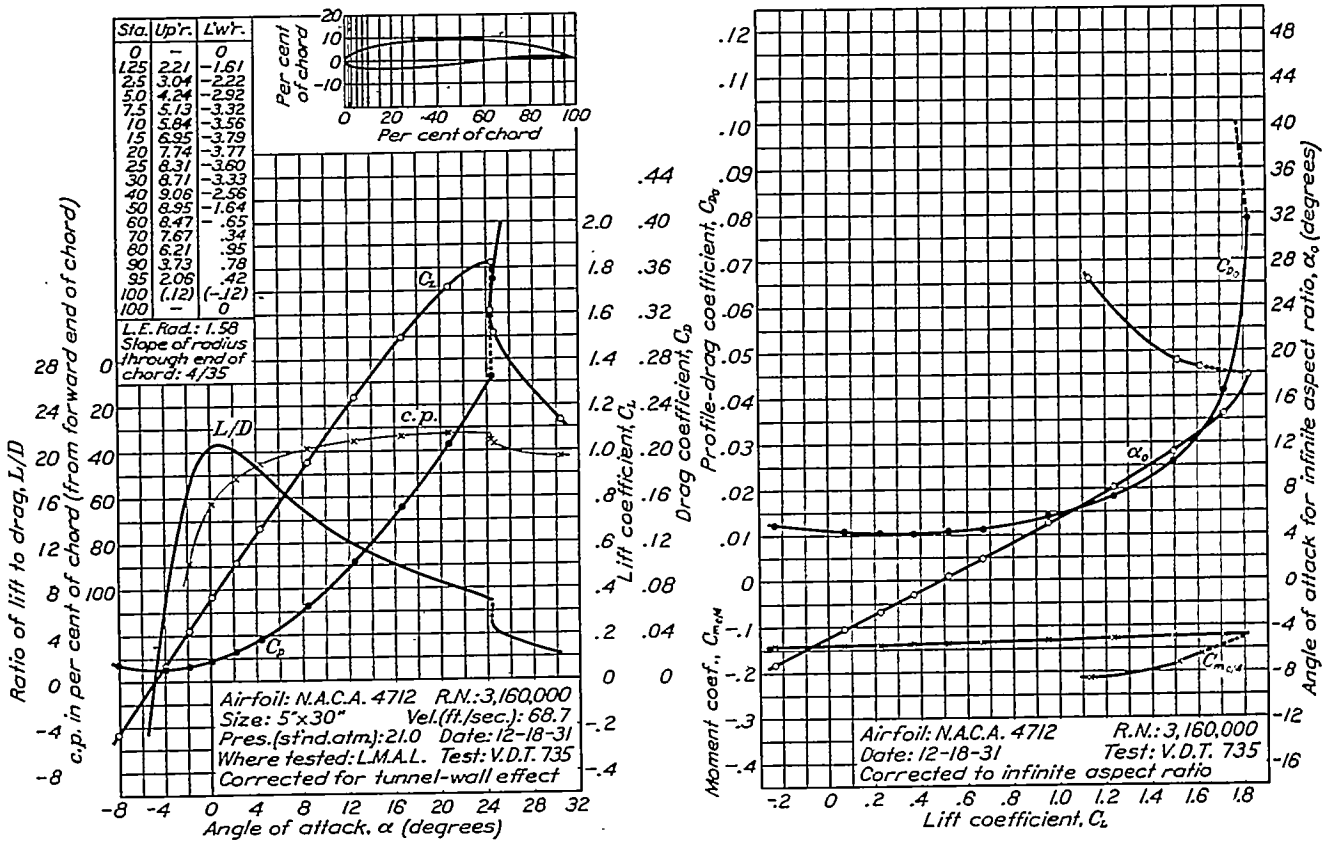

FIGURE 50.—N.A.C.A. 4712 airfoil.

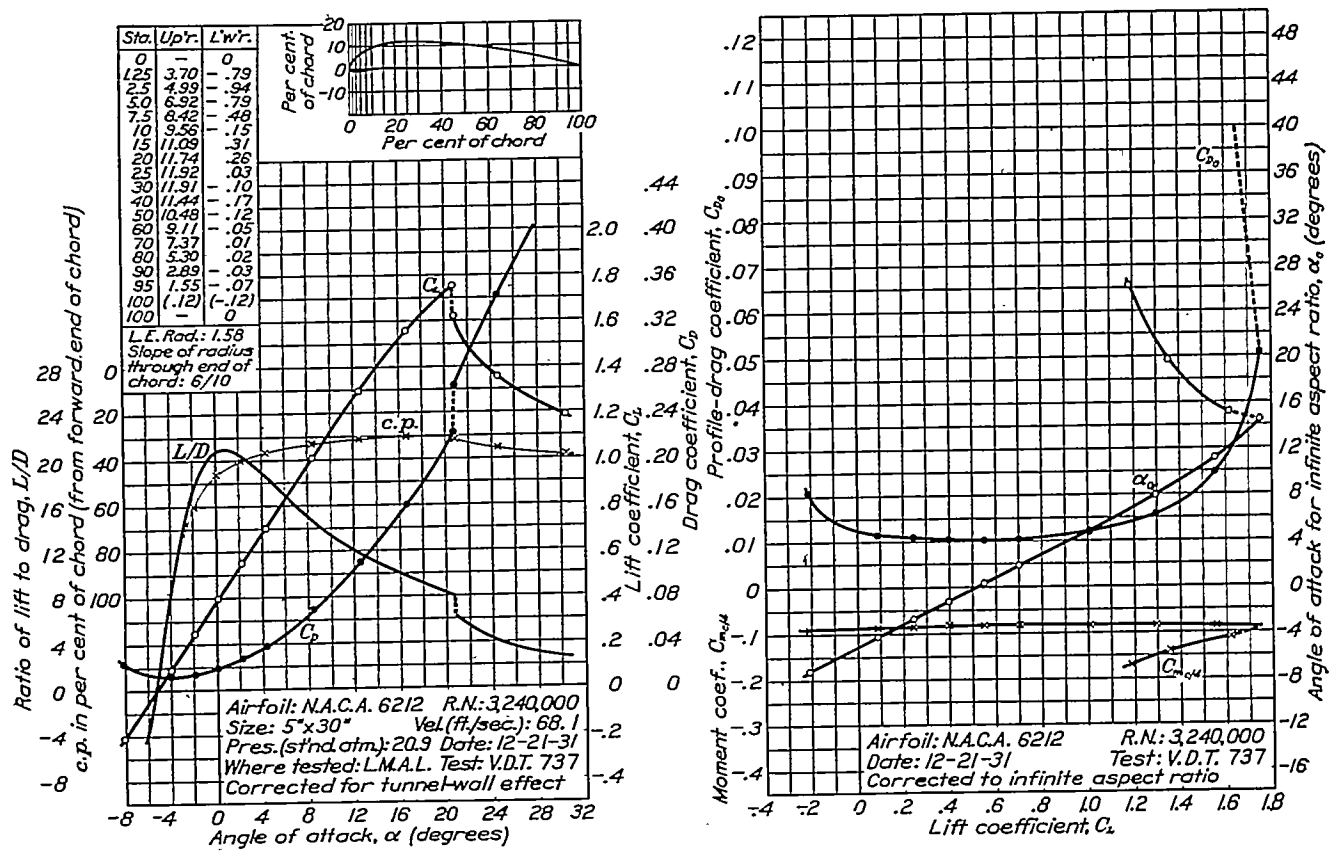

FIGURE 51.—N.A.C.A. 6212 airfoil.

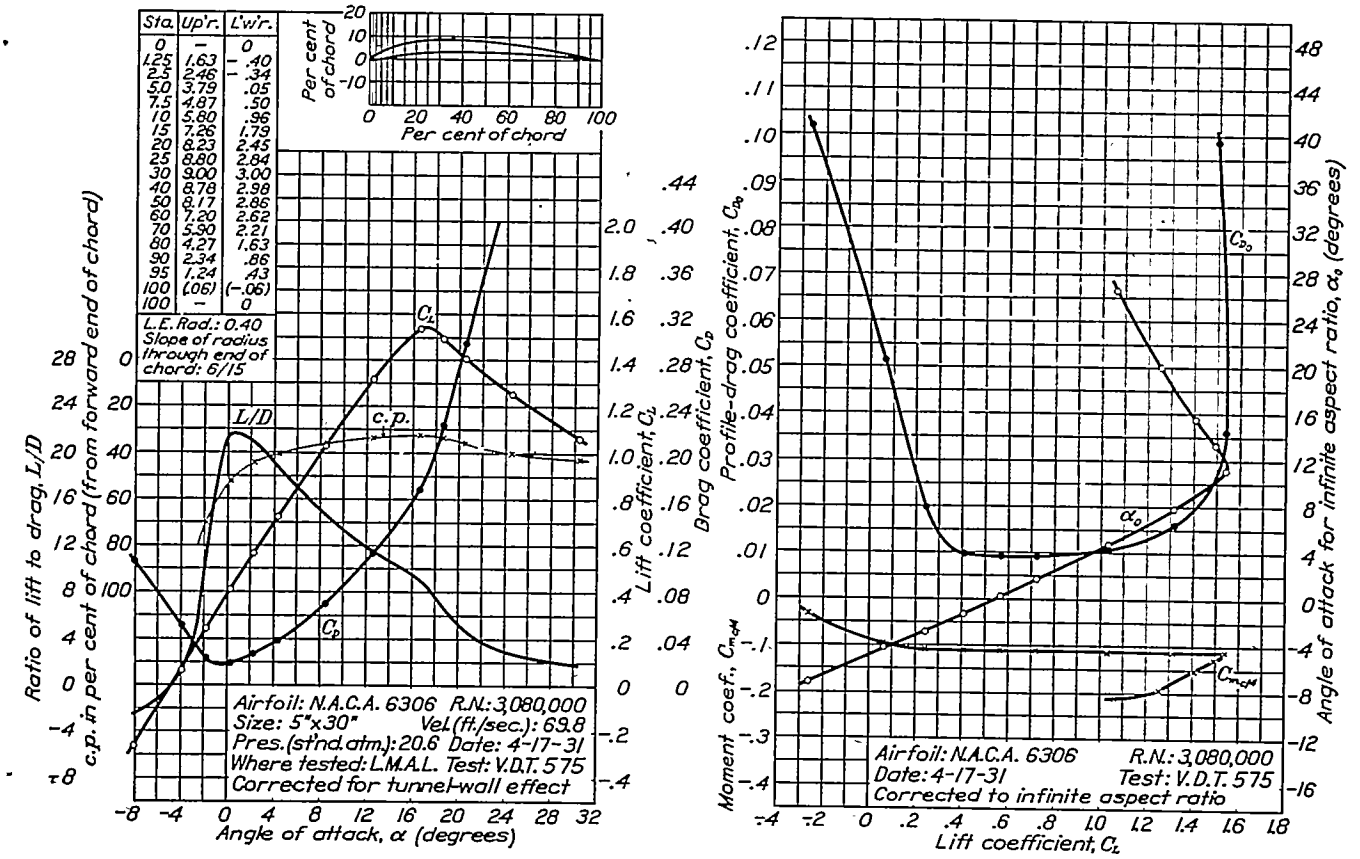

FIGURE 52.—N.A.C.A. 6306 airfoil.

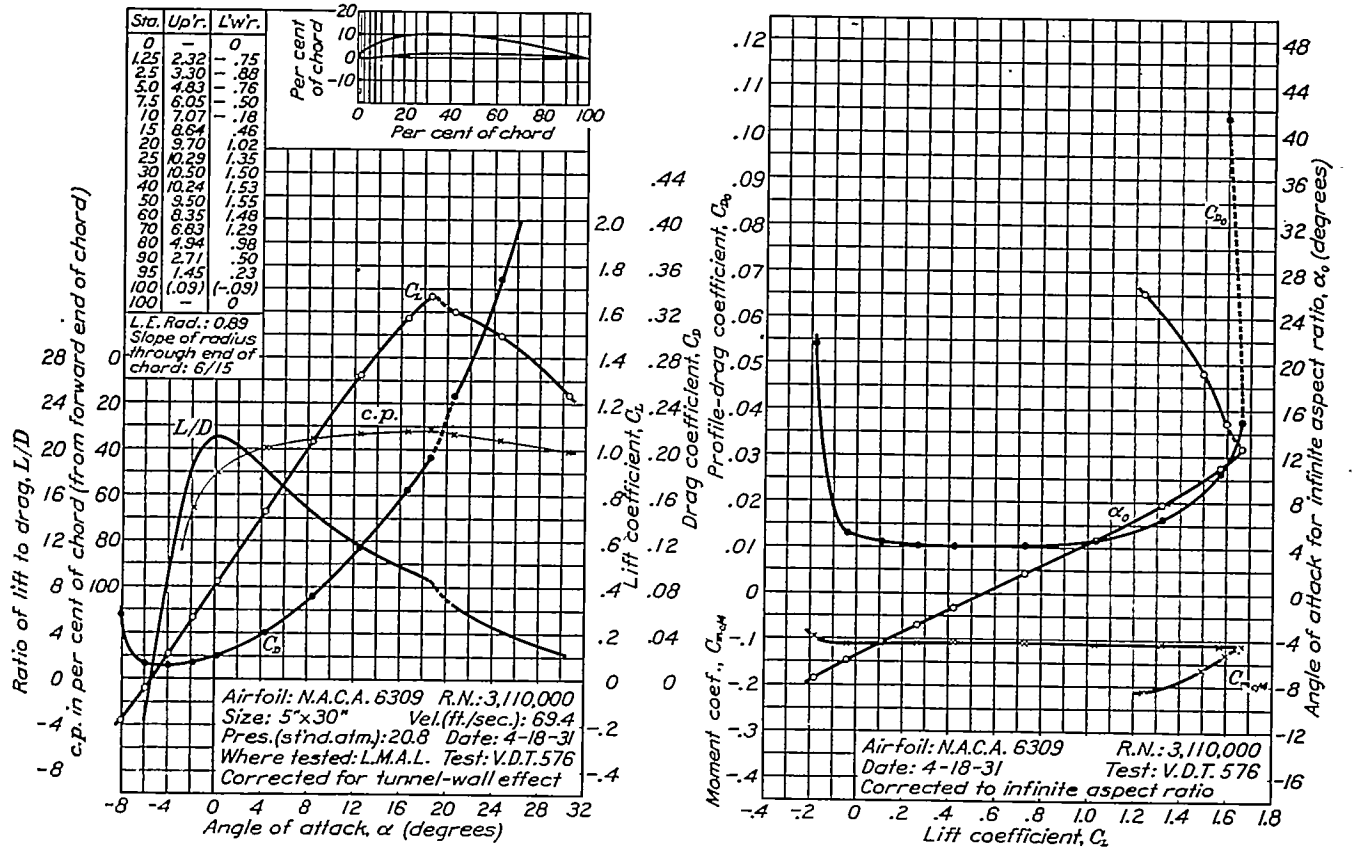

FIGURE 53.—N.A.C.A. 6309 airfoil.

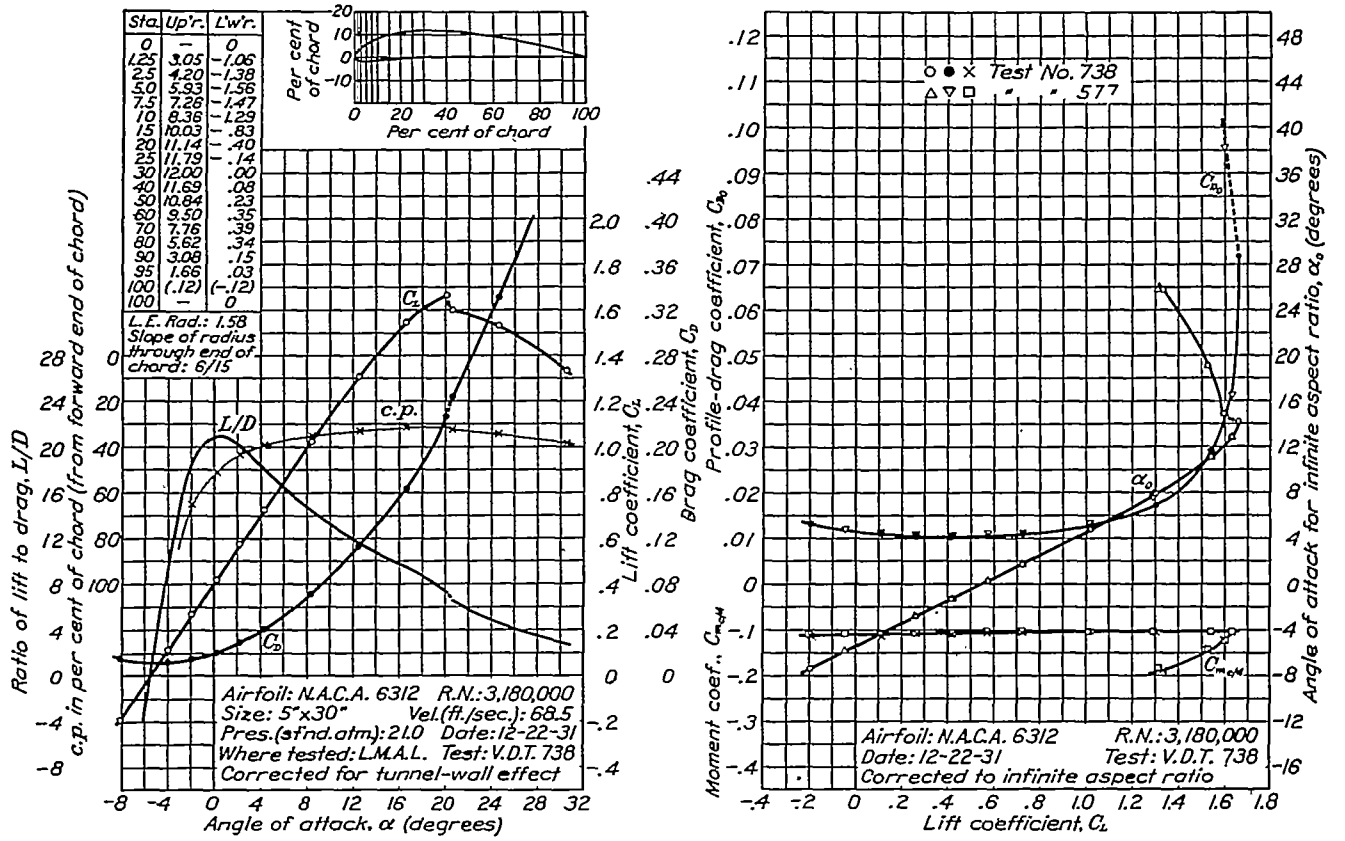

FIGURE 54.—N.A.C.A. 6312 airfoil.

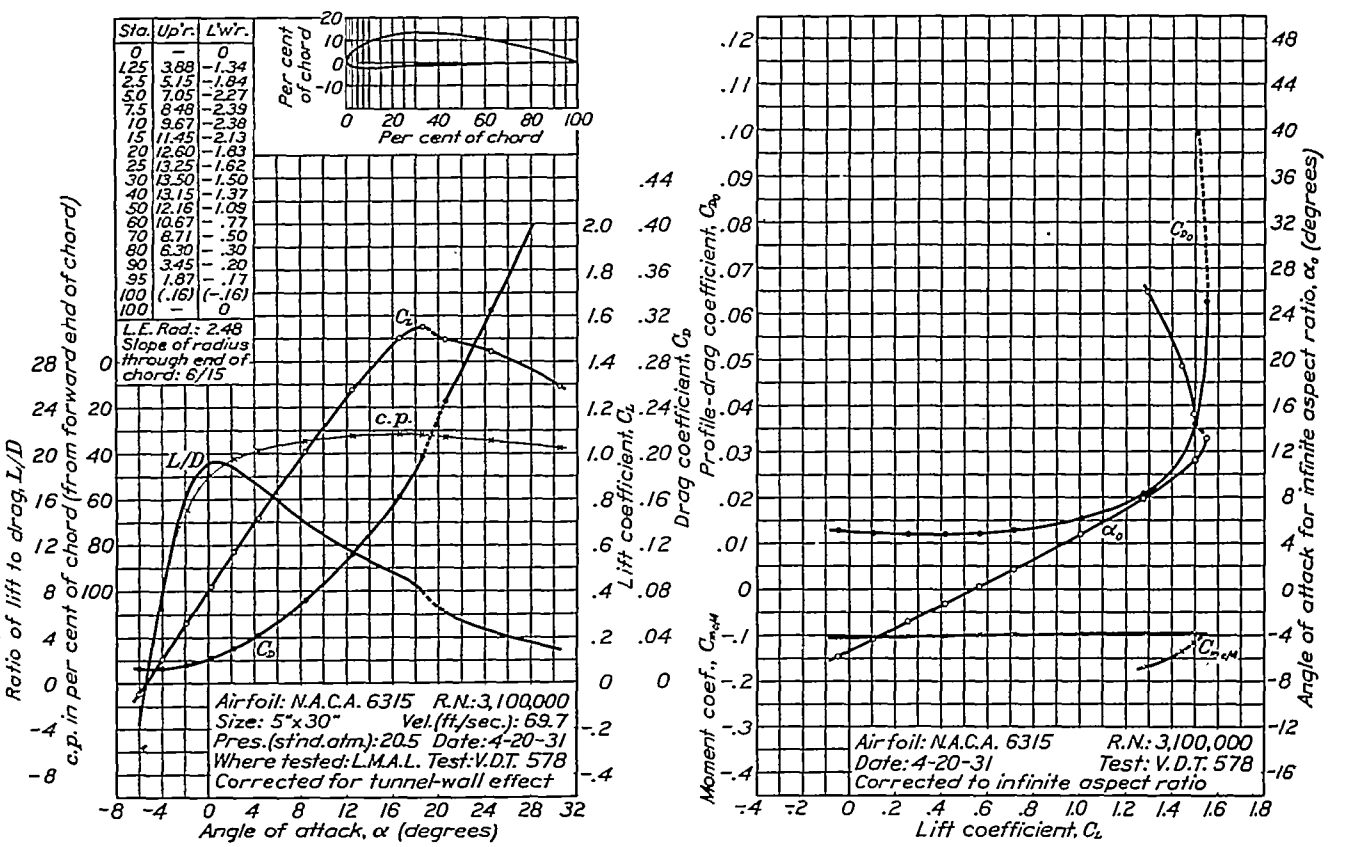

FIGURE 55.—N.A.C.A. 6315 airfoil.

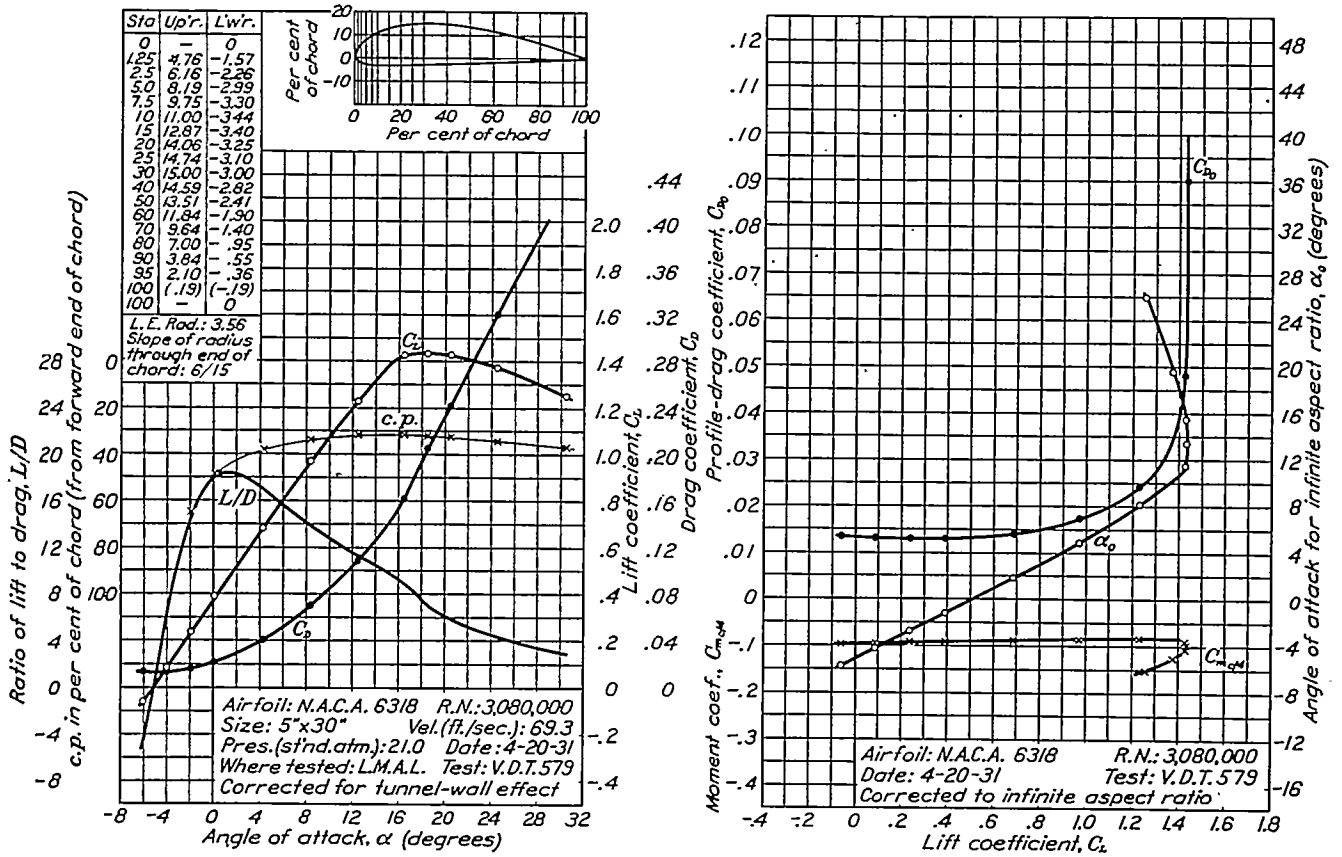

FIGURE 56.—N.A.C.A. 6318 airfoil.

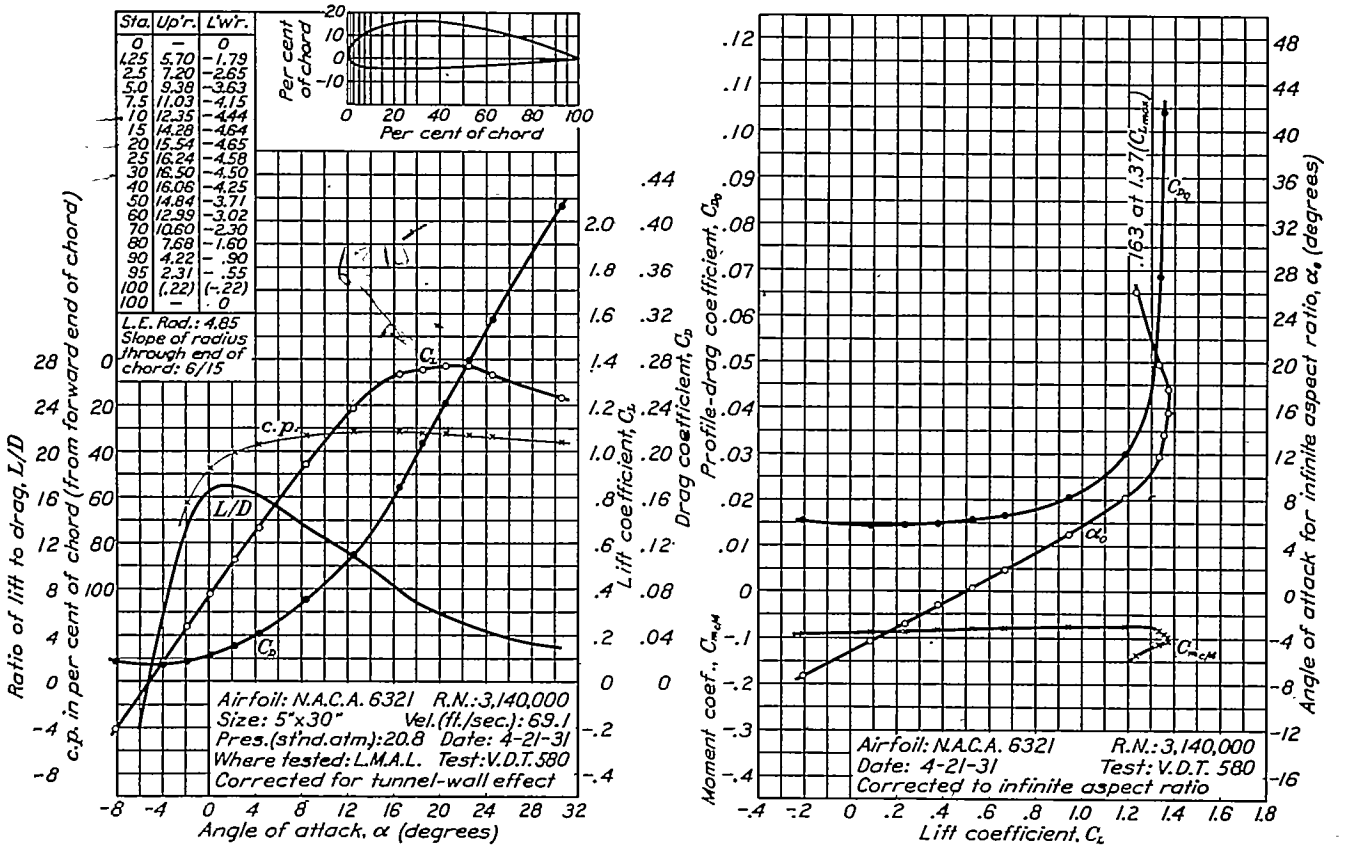

FIGURE 57.—N.A.C.A. 6321 airfoil.

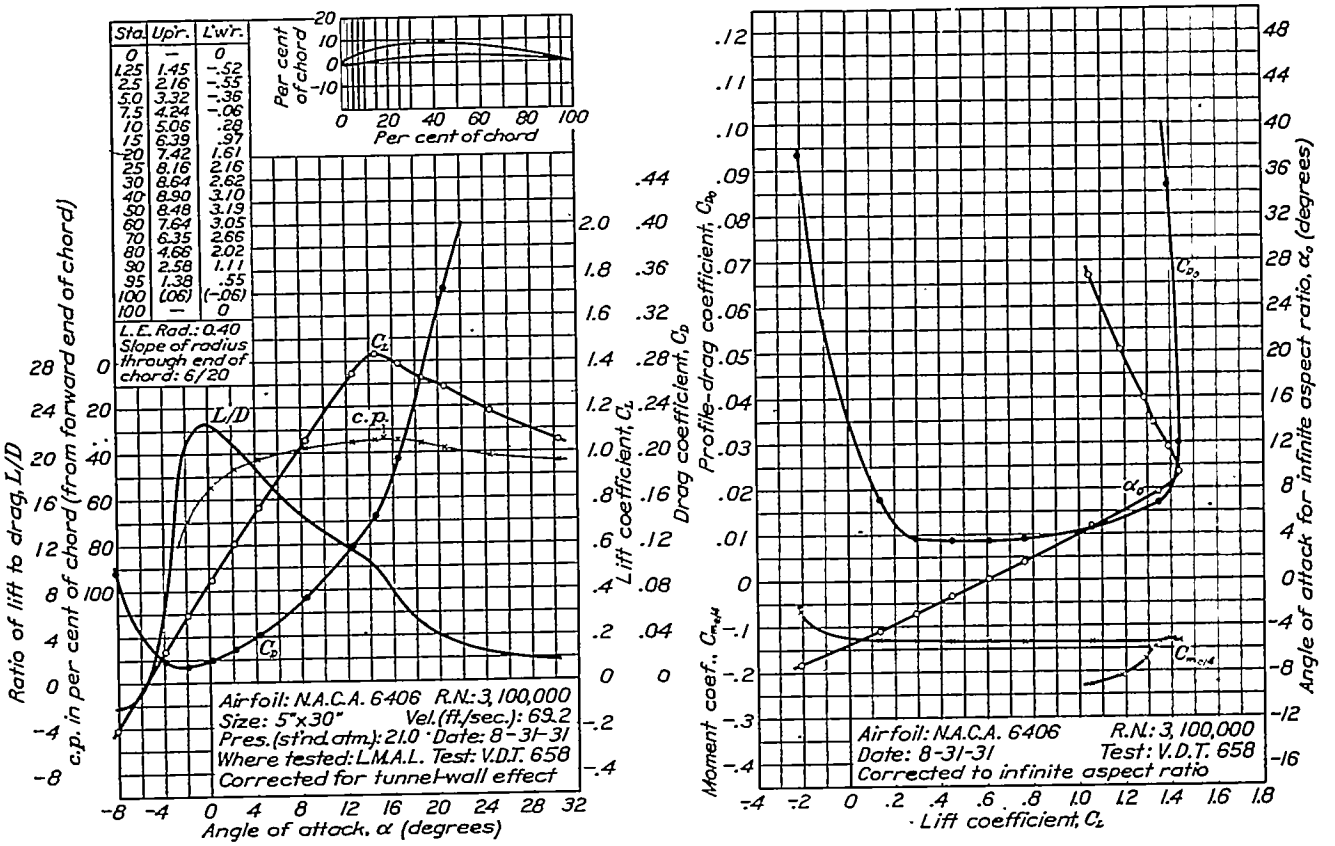

FIGURE 58.—N.A.C.A. 6406 airfoil.

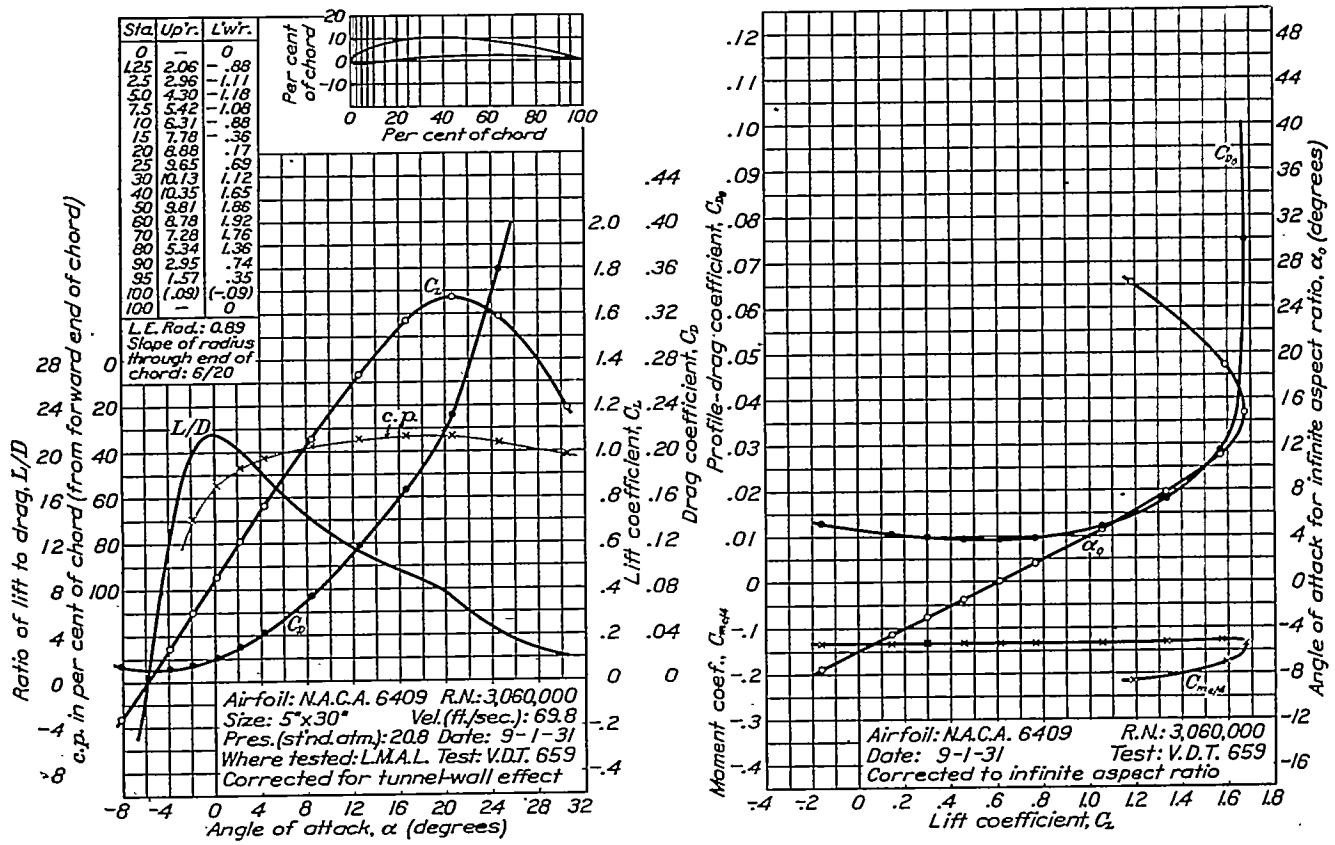

FIGURE 59.—N.A.C.A. 6409 airfoil.

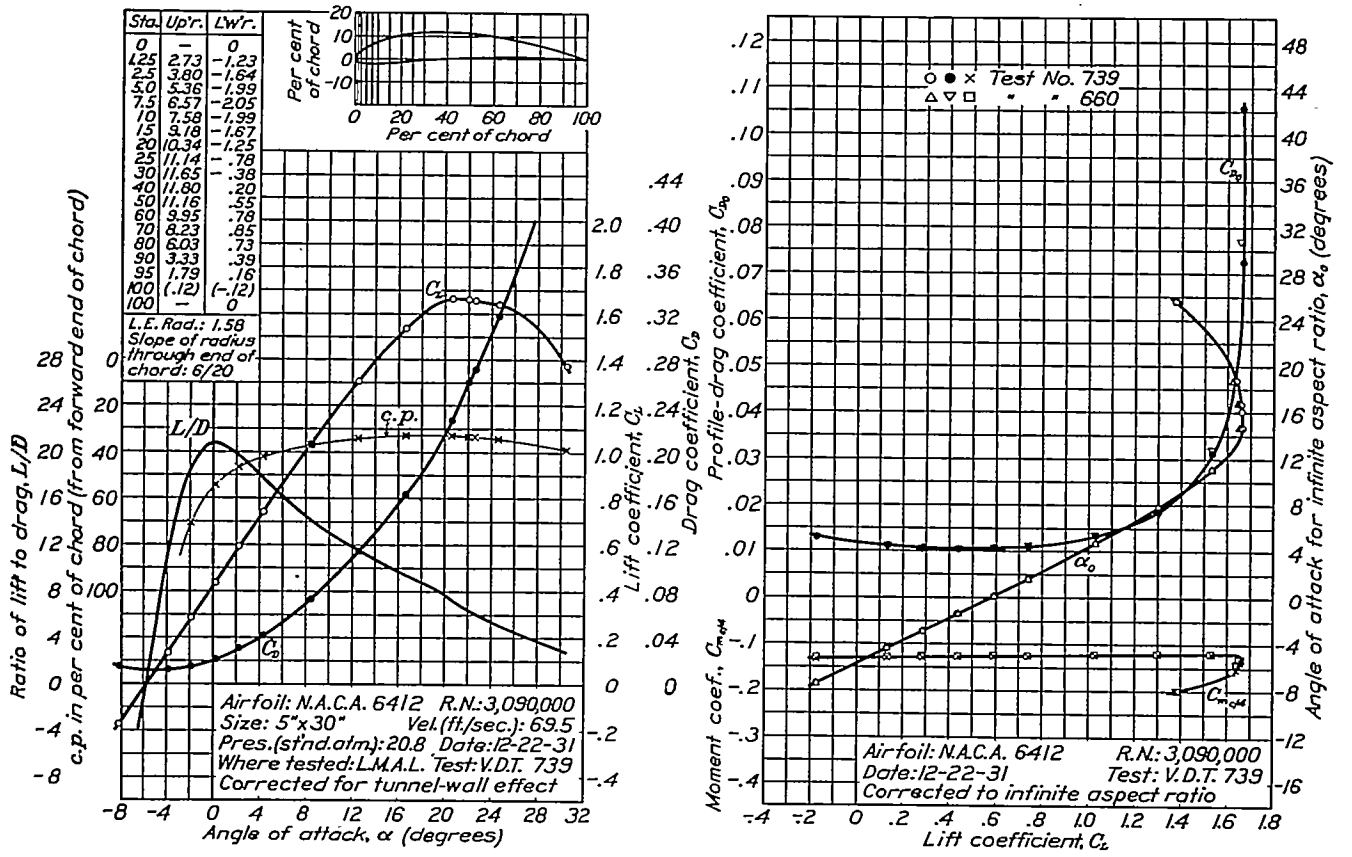

FIGURE 60.—N.A.C.A. 6412 airfoil.

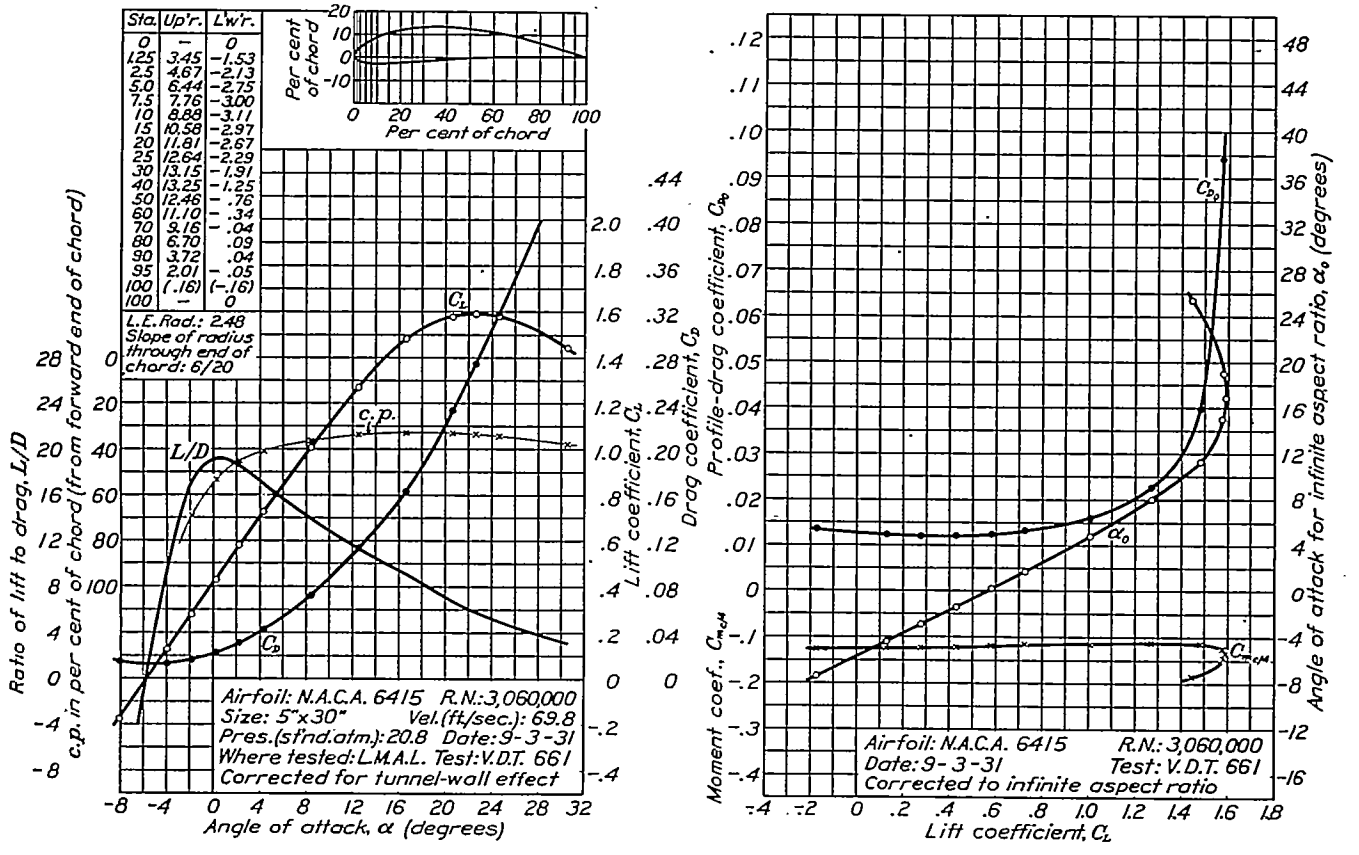

FIGURE 61.—N.A.C.A. 6415 airfoil.

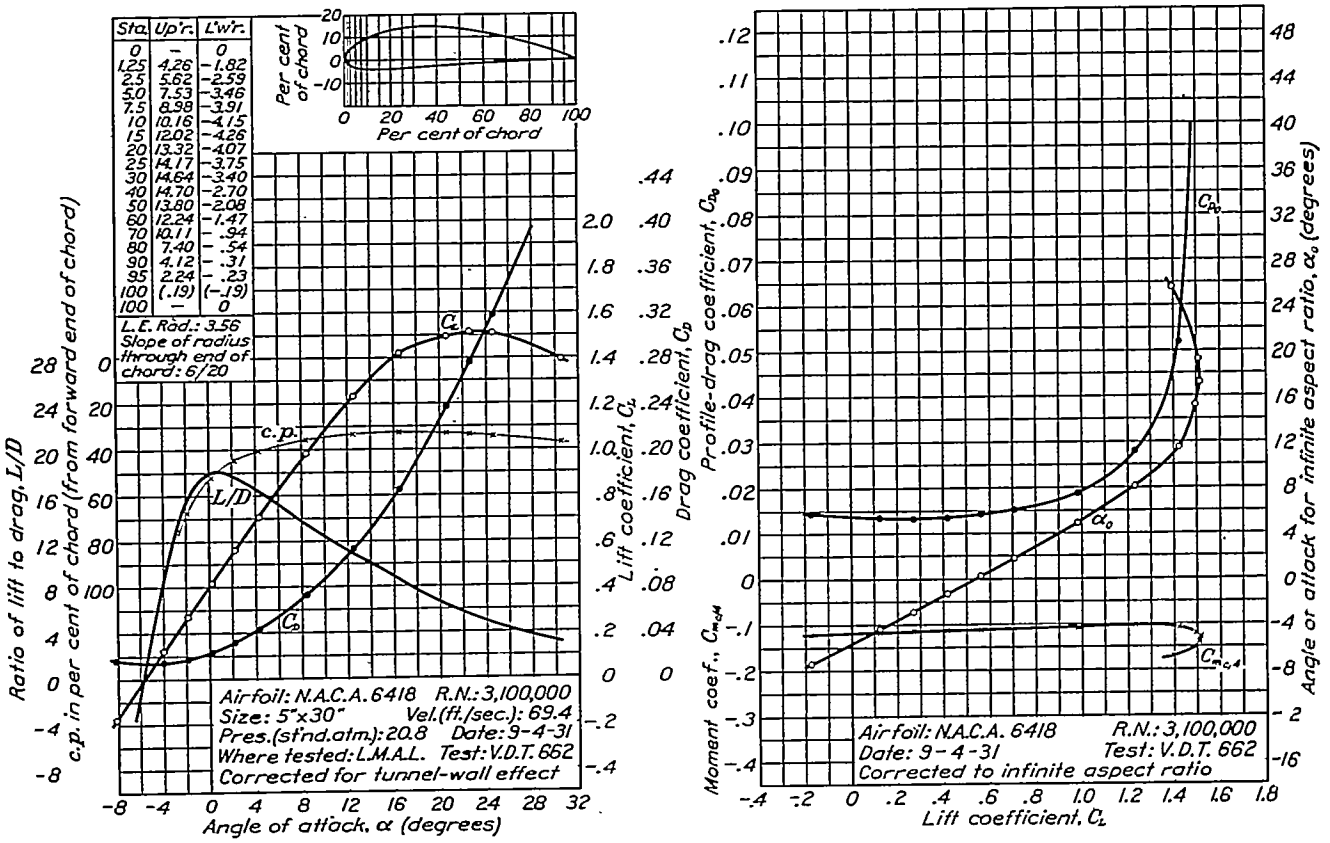

FIGURE 62.—N.A.C.A. 6418 airfoil.

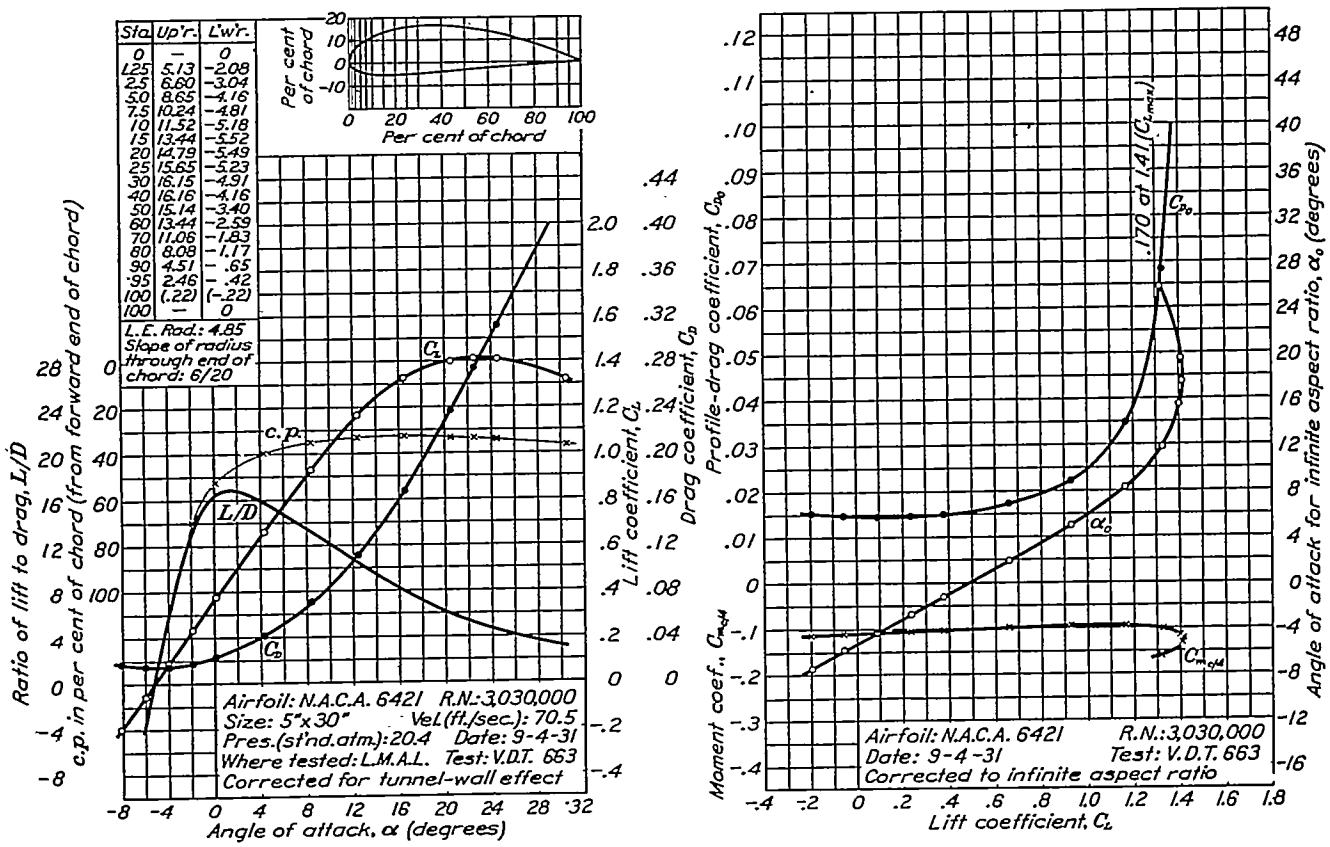

FIGURE 63.—N.A.C.A. 6421 airfoil.

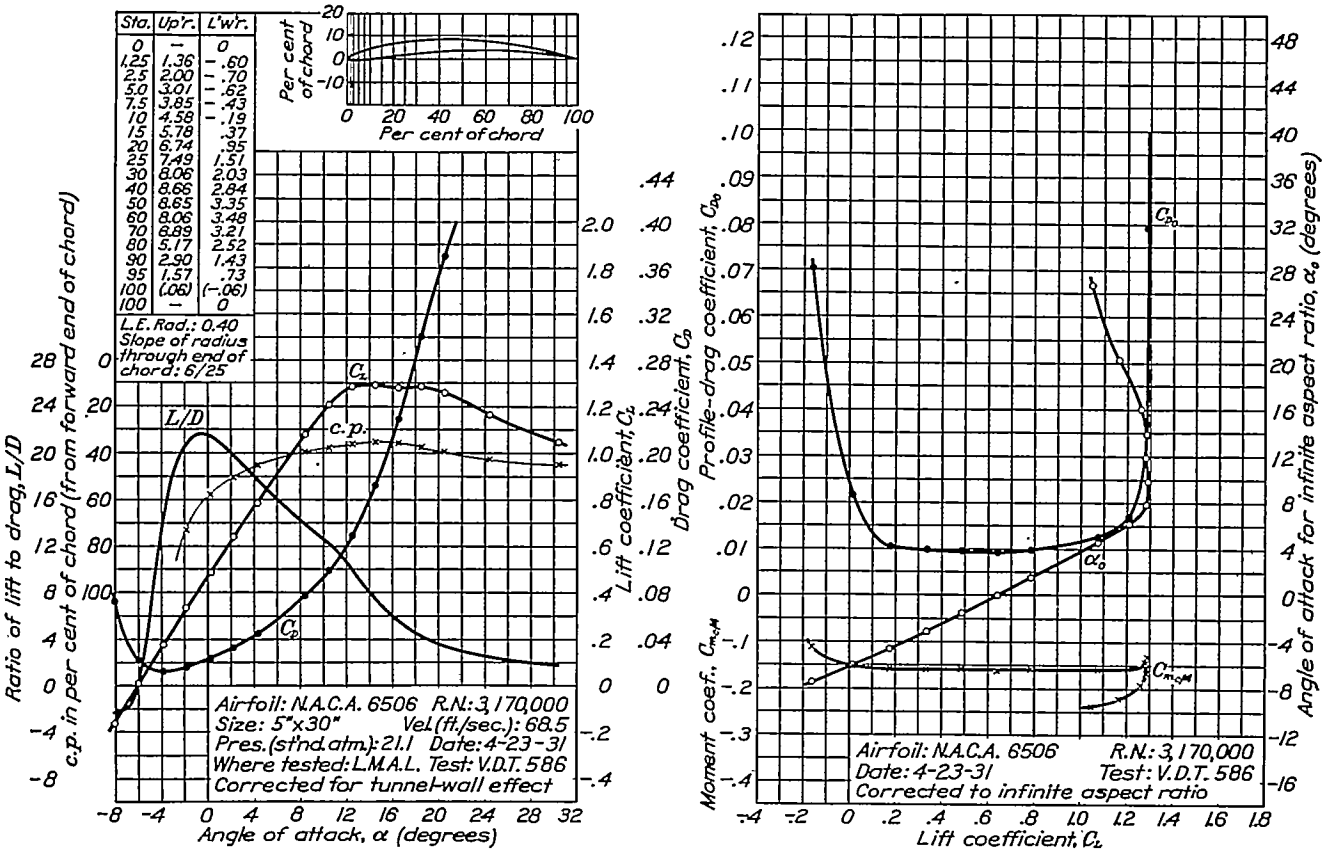

FIGURE 64.—N.A.C.A. 6506 airfoil.

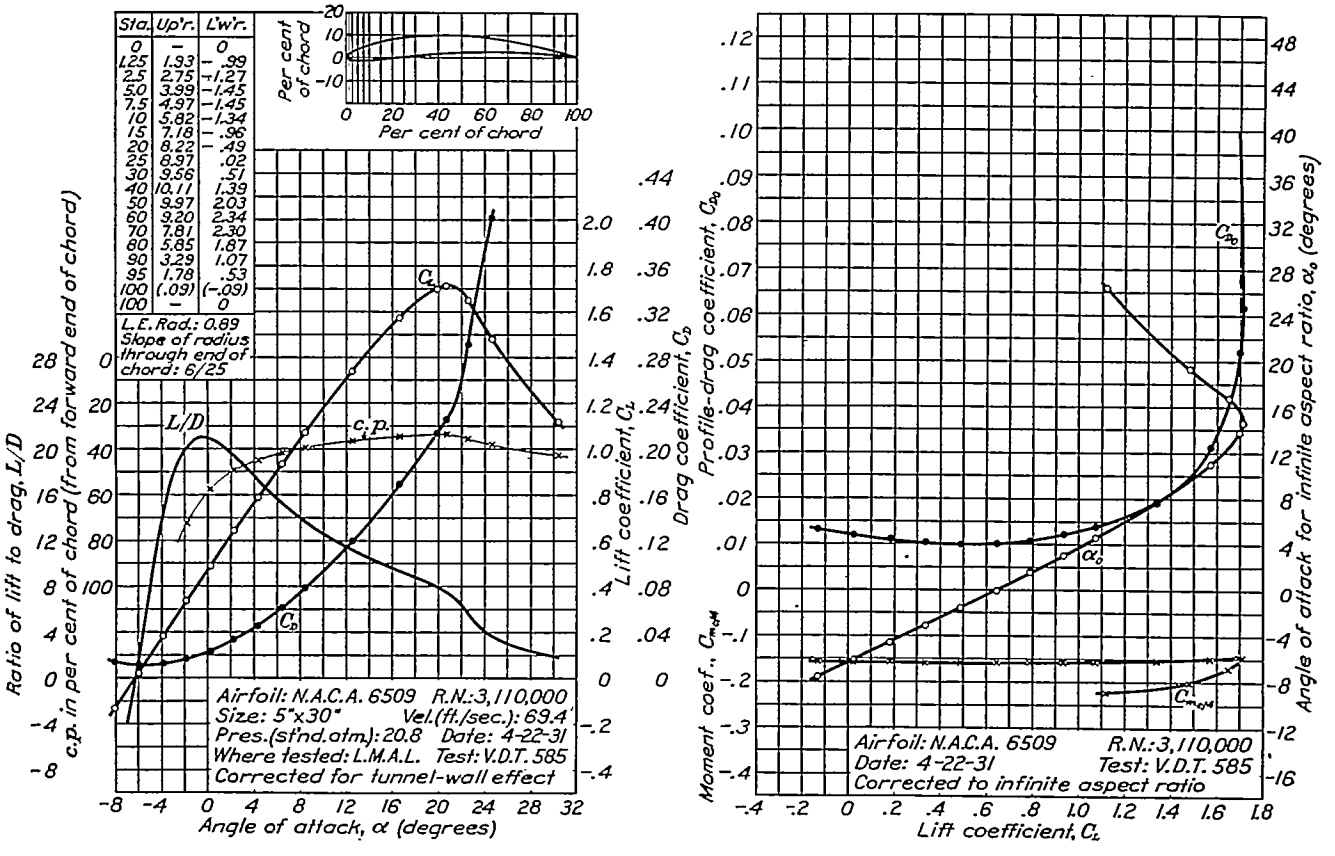

FIGURE 65.—N.A.C.A. 6509 airfoil.

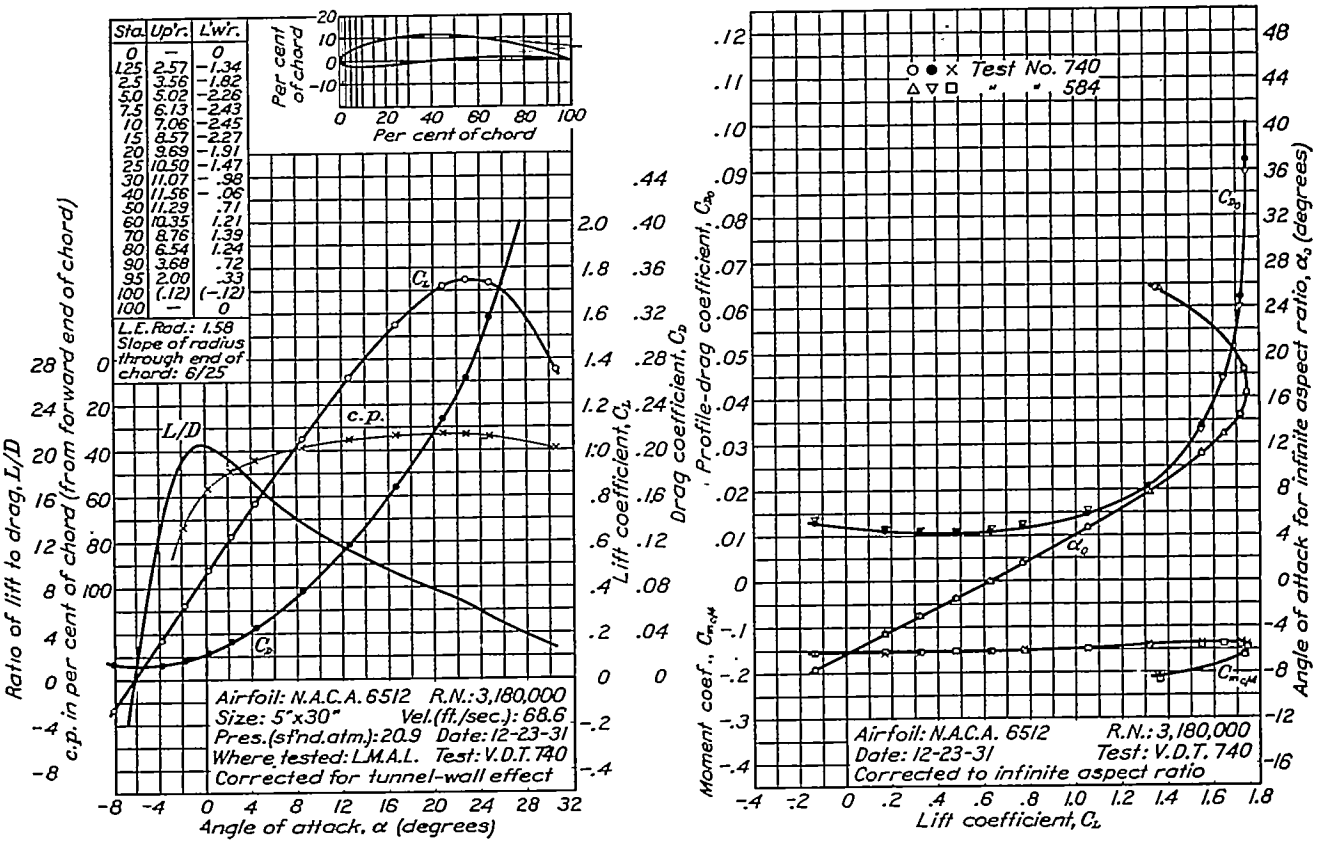

FIGURE 66.—N.A.C.A. 6512 airfoil.

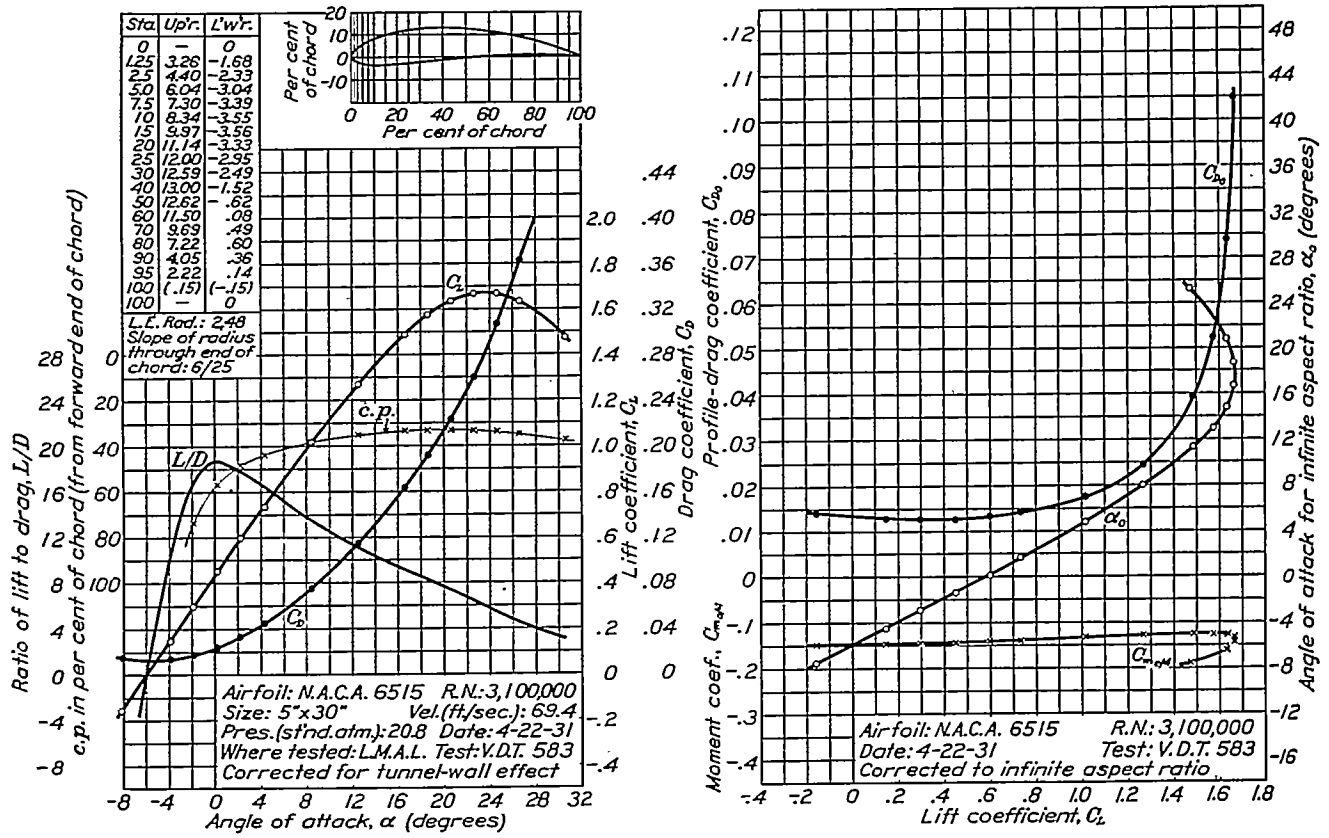

FIGURE 67.—N.A.C.A. 6515 airfoil.

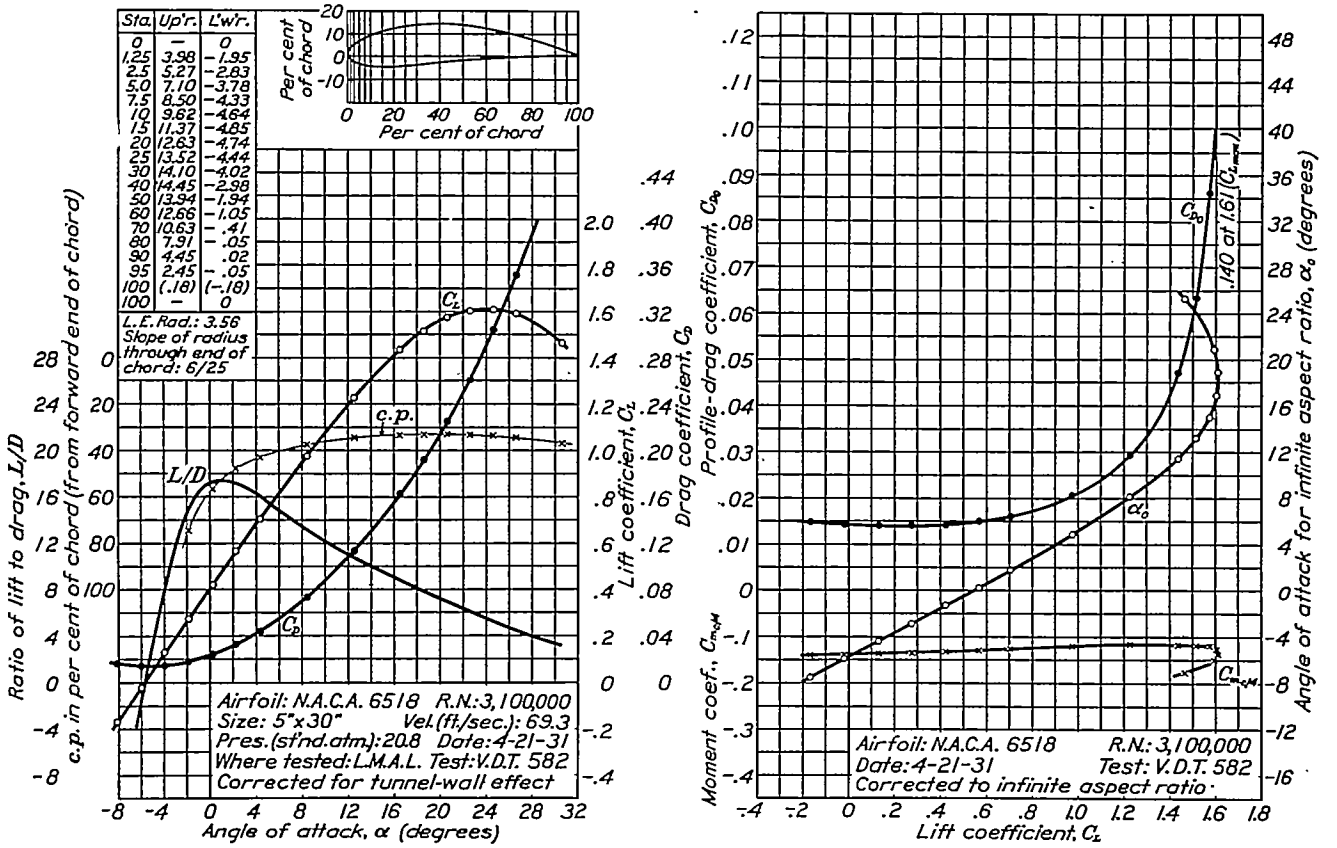

FIGURE 68.—N.A.C.A. 6518 airfoil.

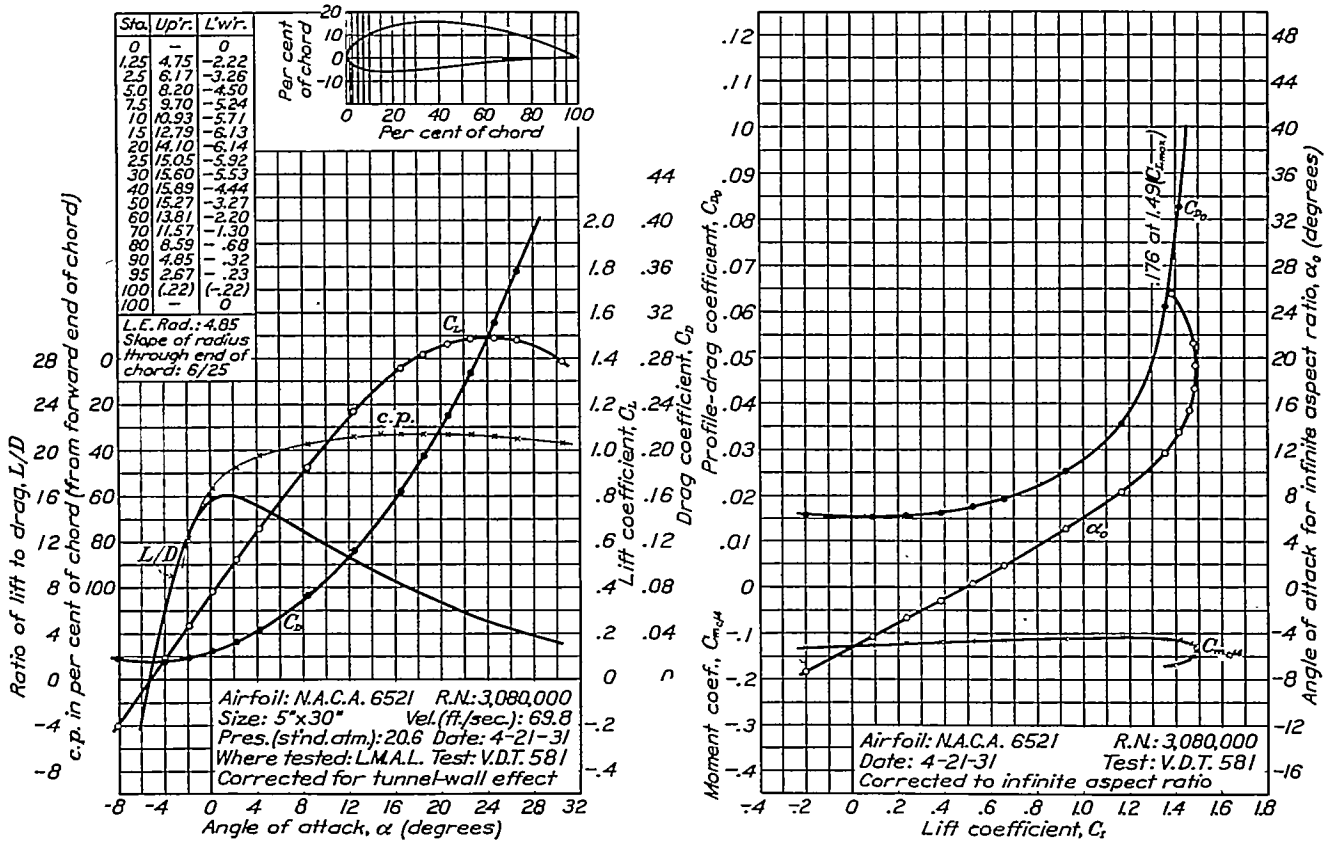

FIGURE 69.—N.A.C.A. 6521 airfoil.

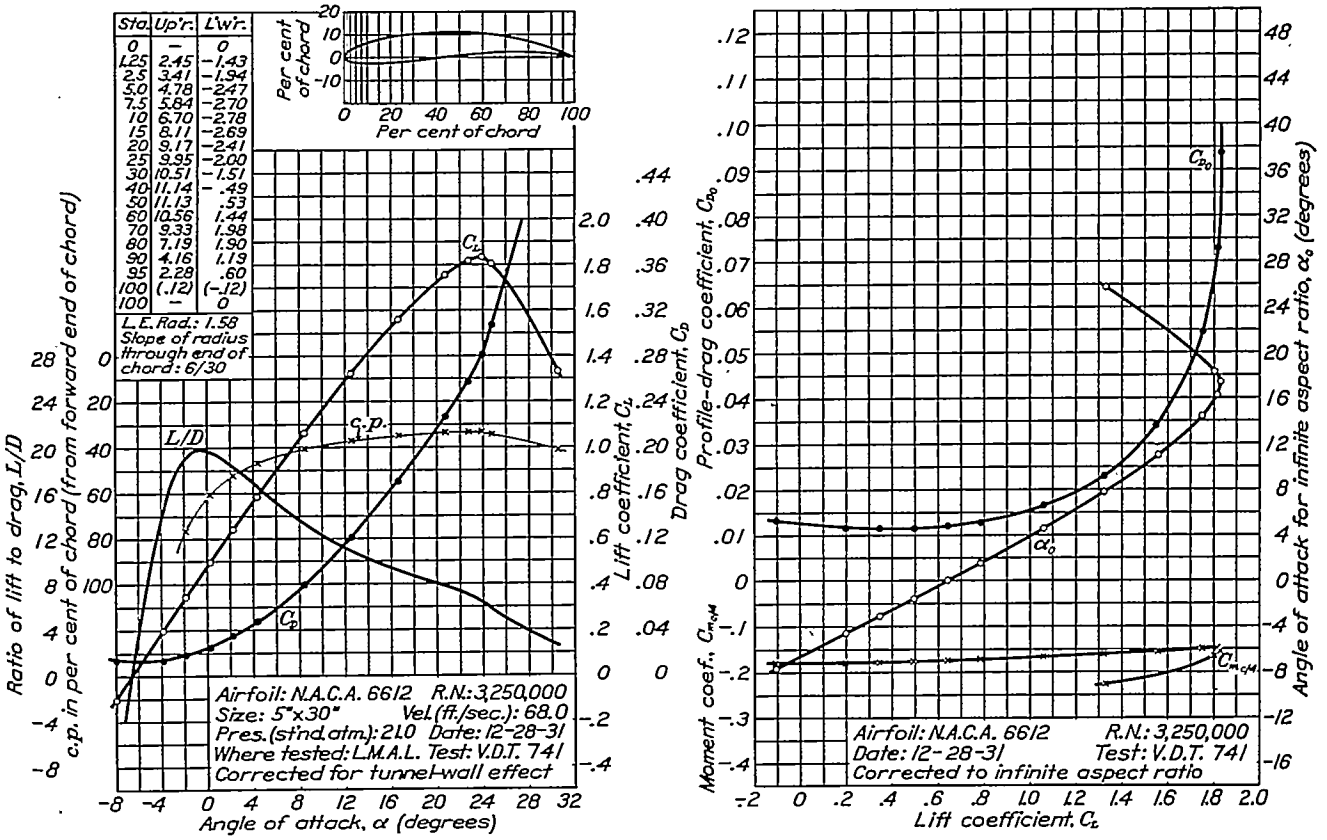

FIGURE 70.—N.A.C.A. 6612 airfoil.

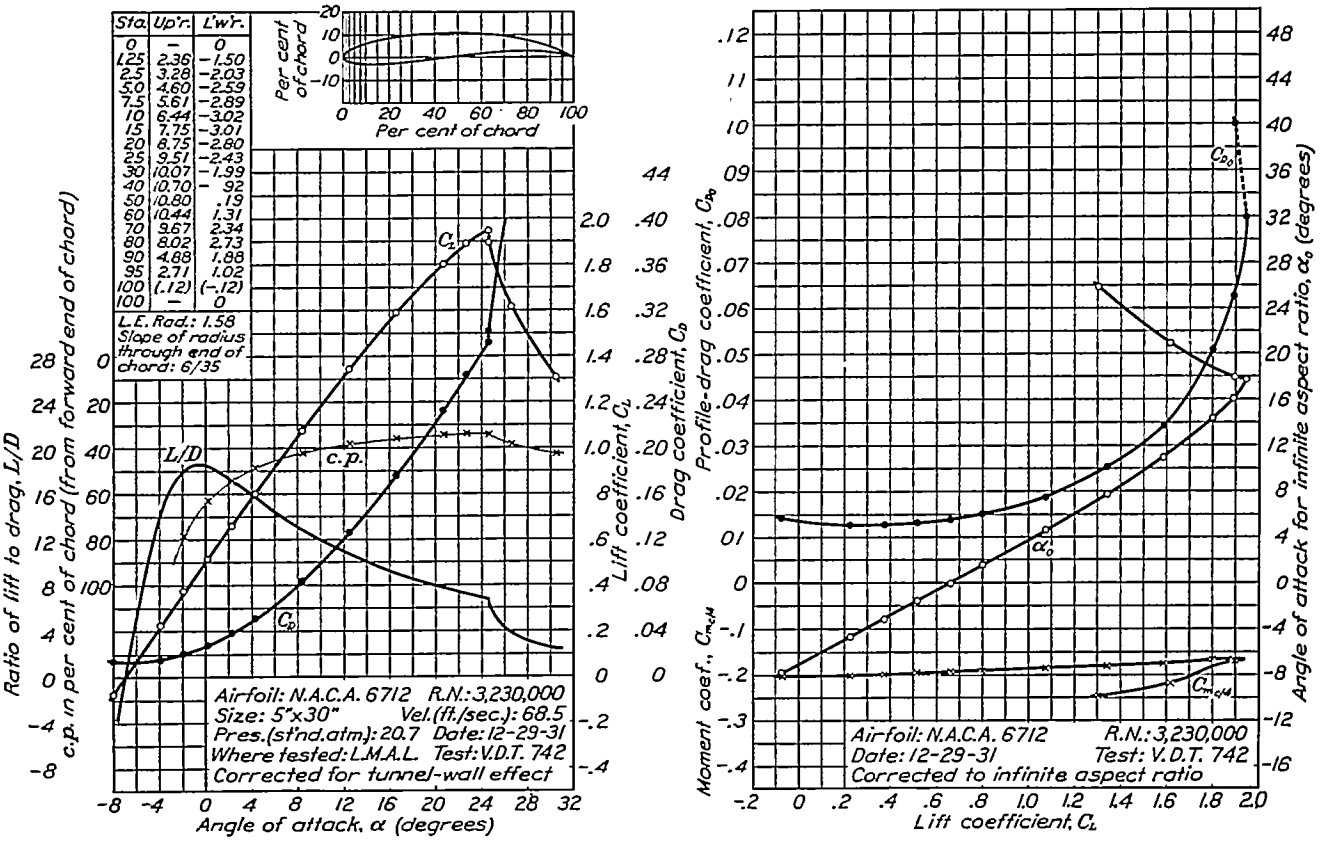

FIGURE 71.—N.A.C.A. 6712 airfoil.

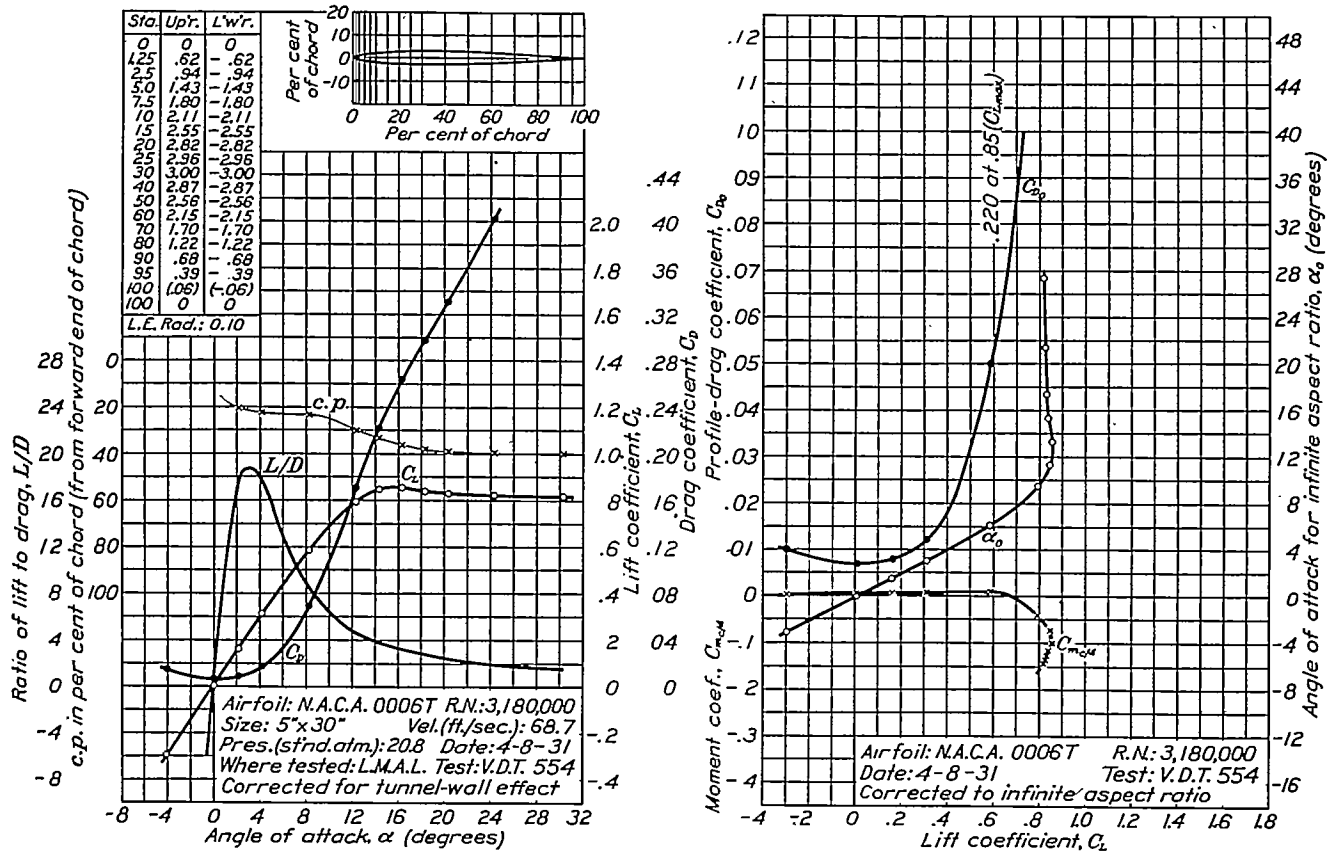

FIGURE 72.—N.A.C.A. 0006T airfoil.

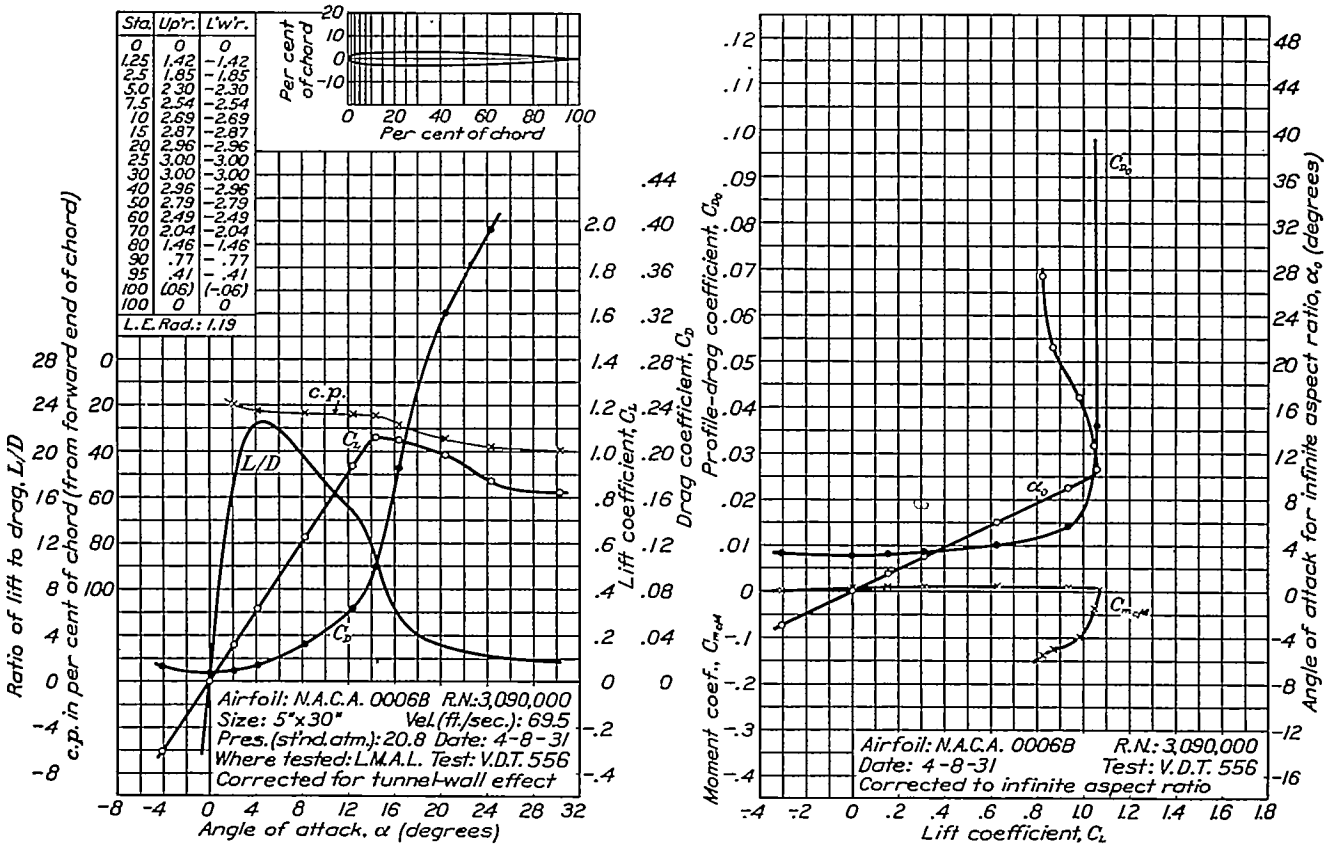

FIGURE 73.—N.A.C.A. 0006B airfoil.

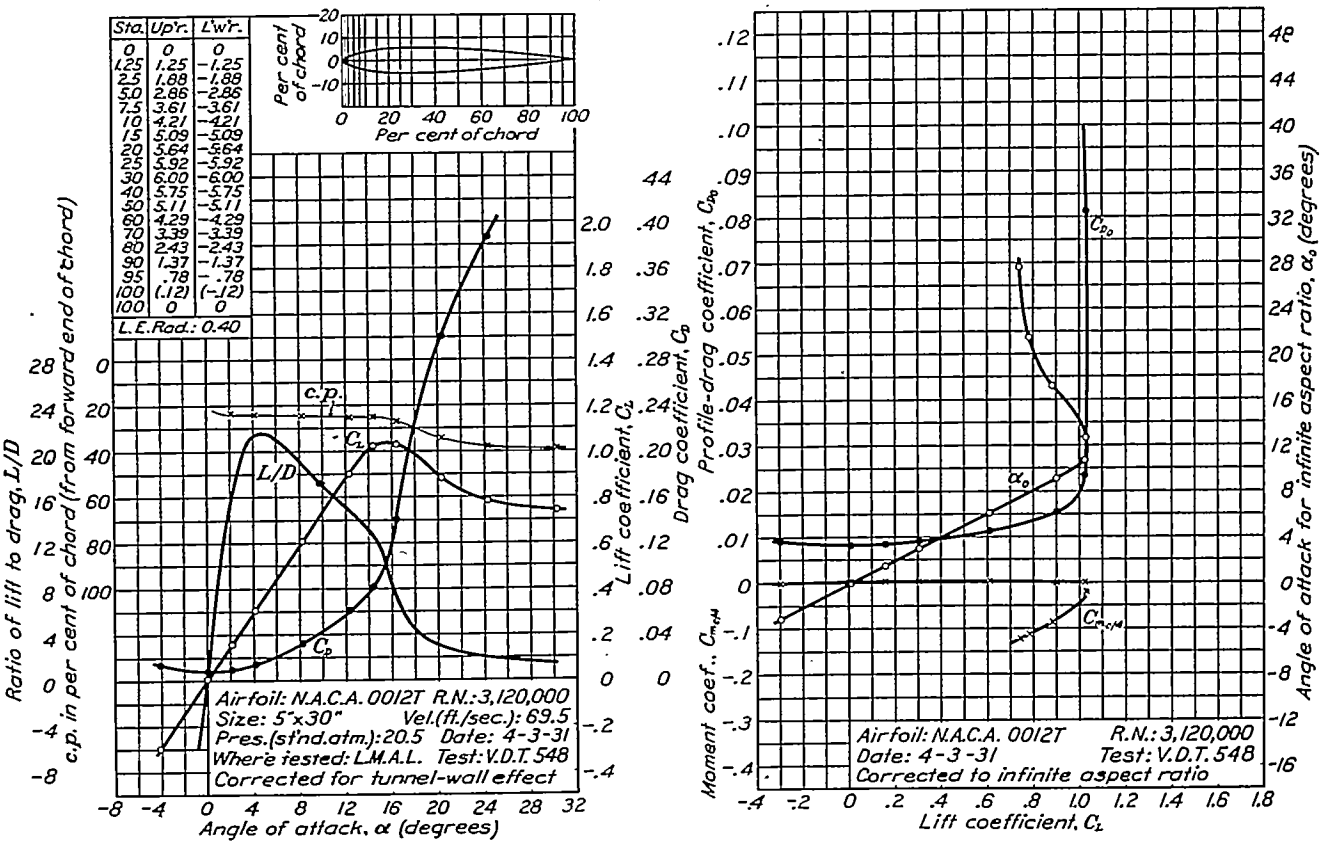

FIGURE 74.—N.A.C.A. 0012T airfoil.

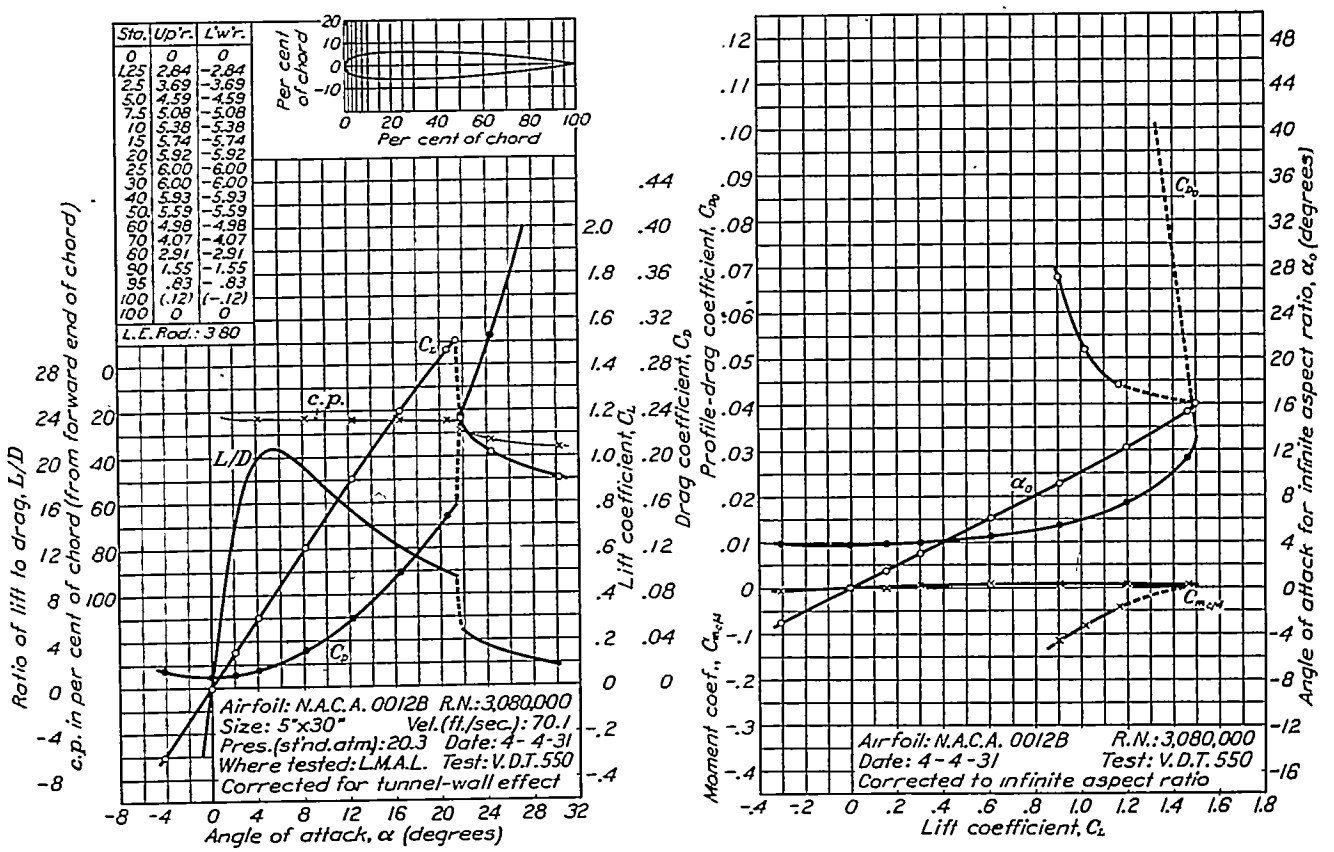

FIGURE 75.—N.A.C.A. 0012B airfoil.

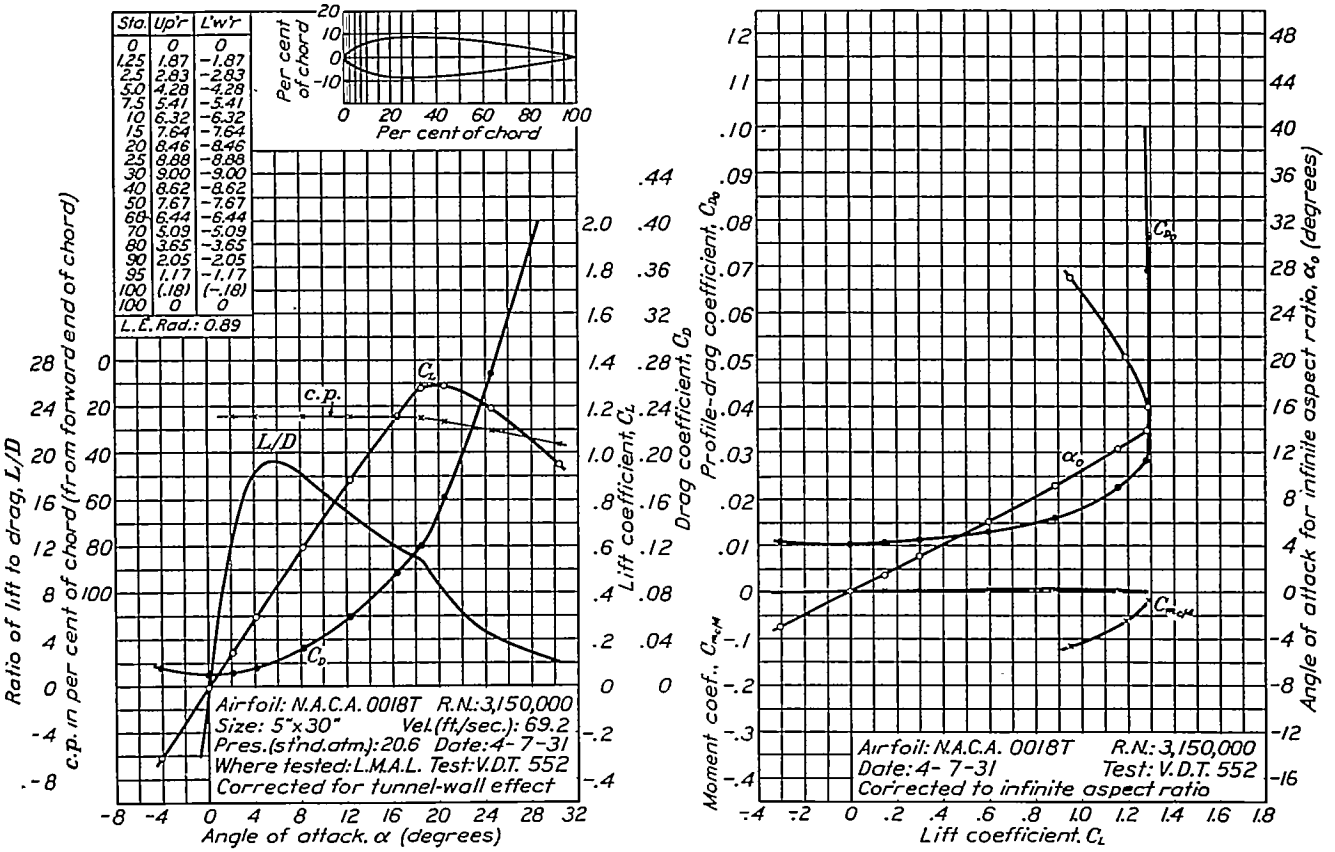

FIGURE 76.—N.A.C.A. 0018T airfoil.

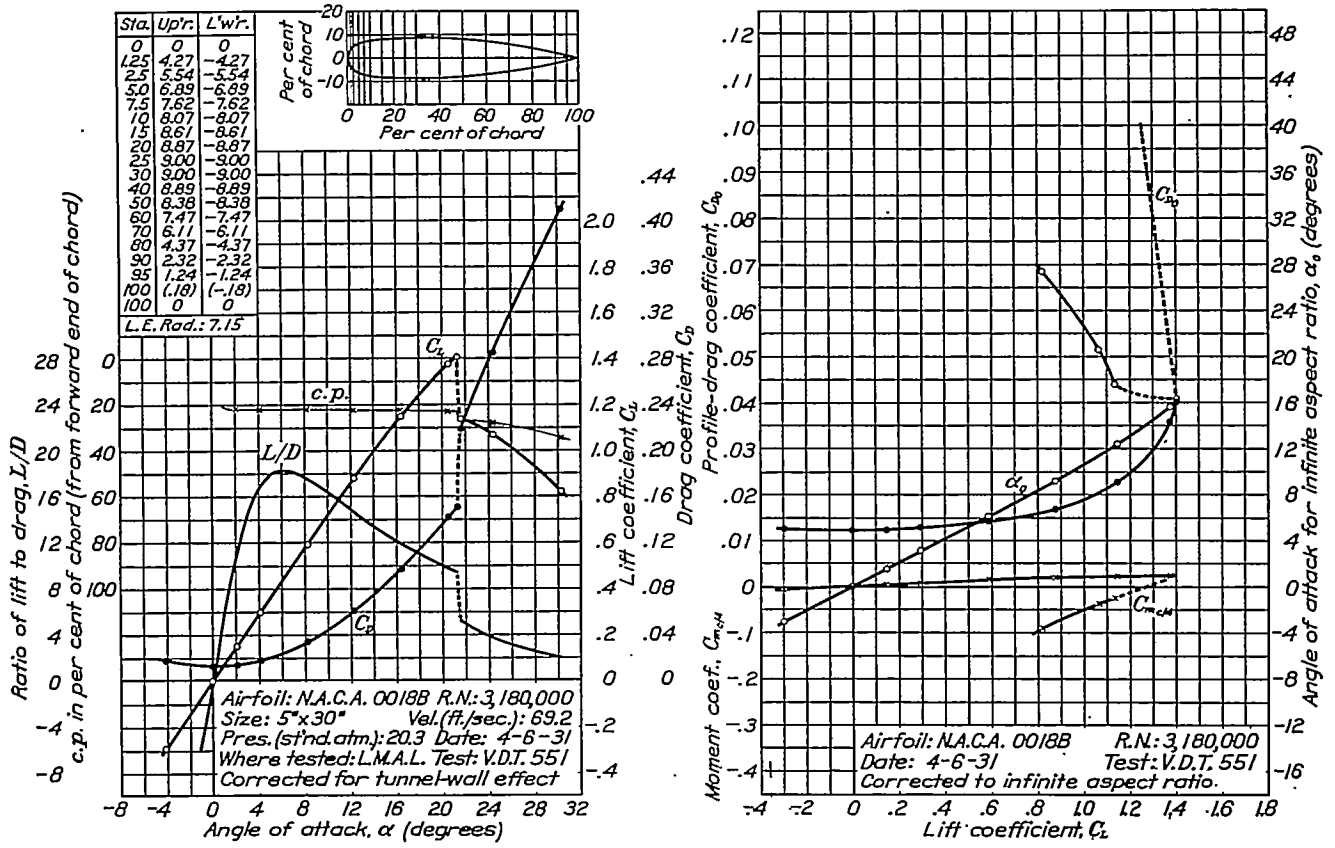

FIGURE 77.—N.A.C.A. 0018B airfoil.

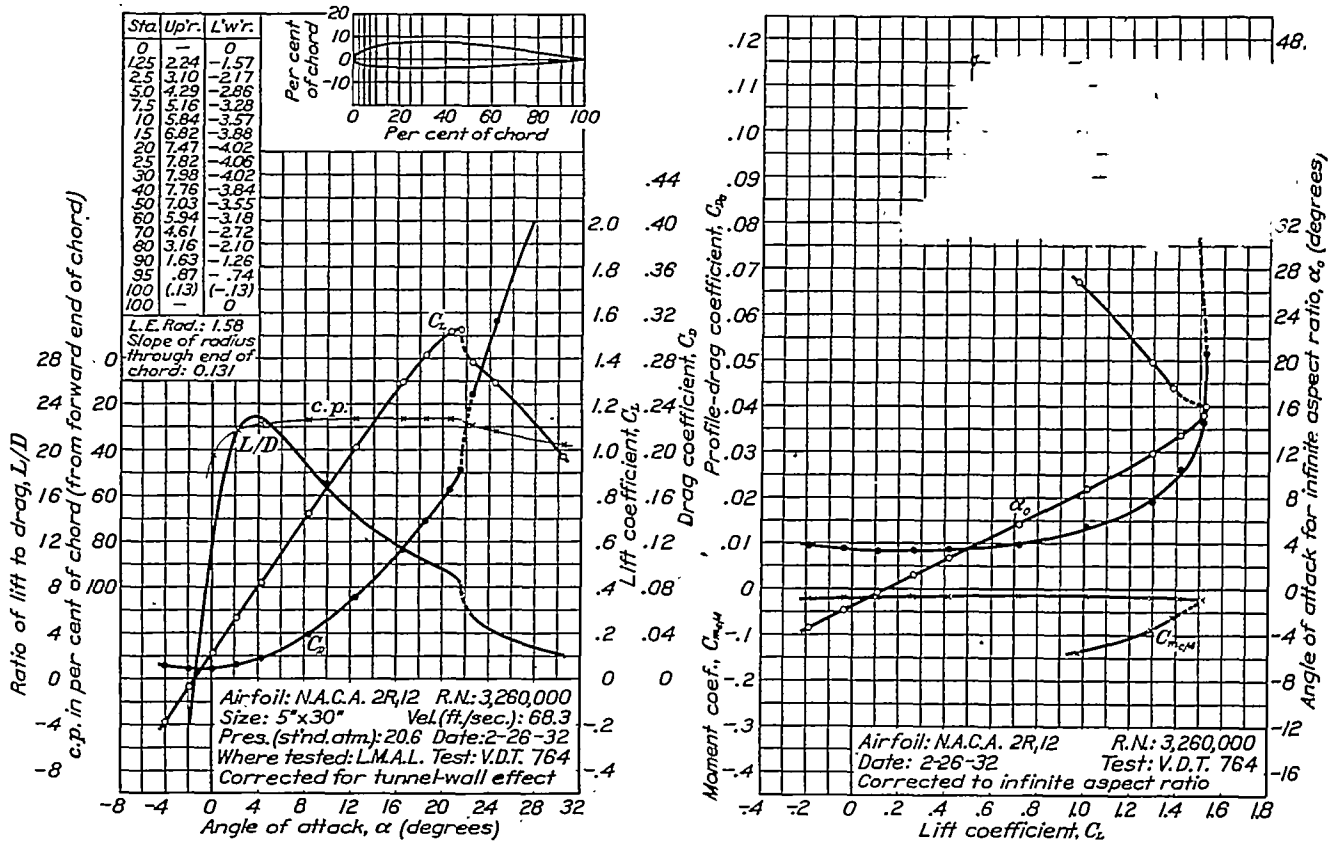

FIGURE 78.—N.A.C.A. $2R_112$ airfoil.

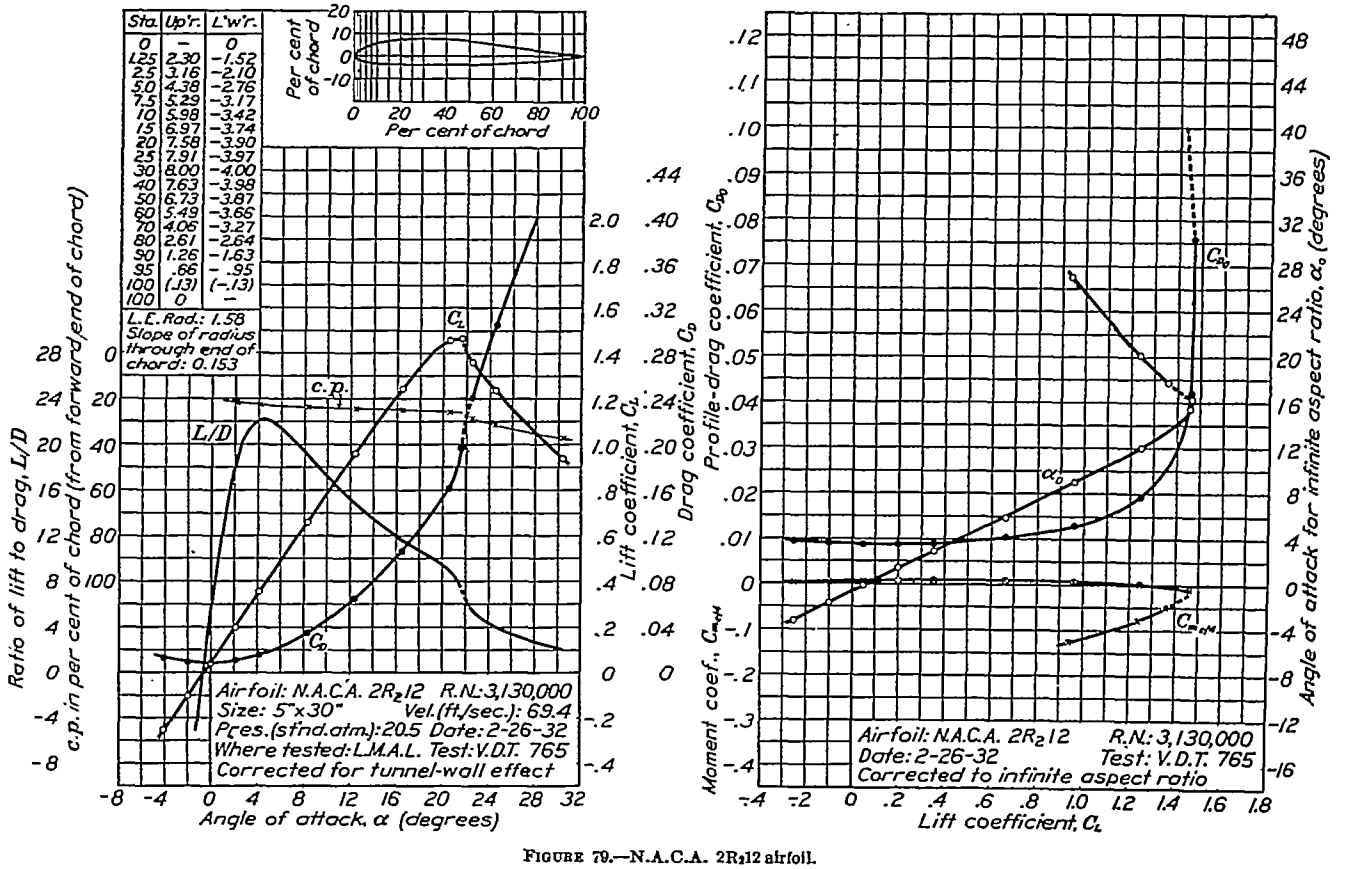

FIGURE 79.—N.A.C.A. $2R_112$ airfoil.

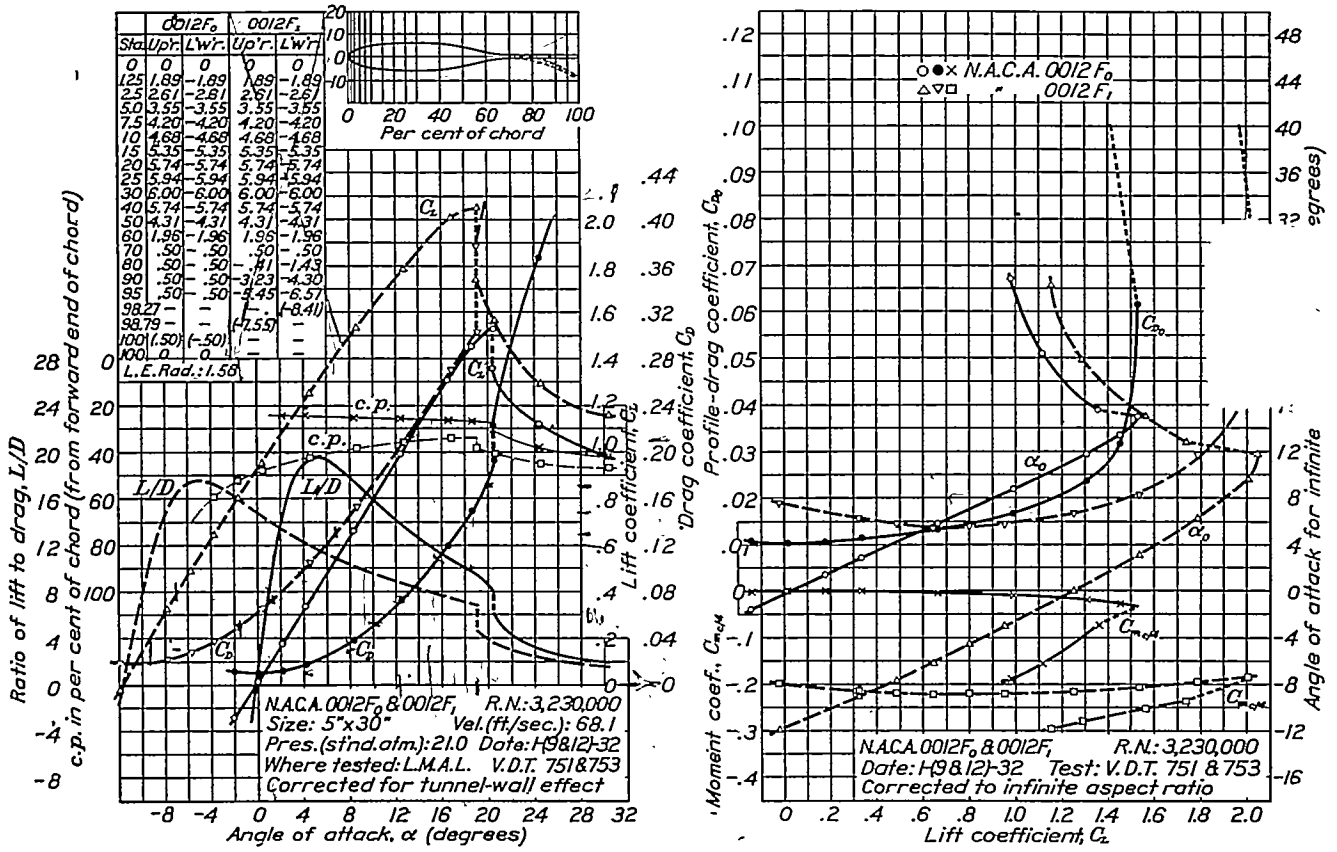

FIGURE 80.—N.A.C.A. 0012F$_0$ and 0012F$_1$ airfoils.

PRECISION

A general discussion of the errors and corrections involved in airfoil testing in the variable-density tunnel is included in reference 8. In connection with this report, it was hoped that a more specific discussion of the various sources of error and separate estimates of the various errors might be given. However, after a careful study of all the measurements it became apparent that practically all the errors may be regarded as accidental; that is, of the type the magnitude of which may best be estimated from the dispersion of the results of independent repeat measurements. The major portion of these errors is caused by insufficient sensitivity of the balance and manometers, by the personal error involved in reading mean values of slightly fluctuating quantities, and by the error due to slight surface imperfections in the model. The last is perhaps the most serious source of error. The models were carefully finished before each test, but the presence of particles of hard foreign matter in the air stream tended to cause a slight pitting of the leading edge of the model during each test. This pitting was probably the major source of error in connection with the earlier tests, but it was reduced for the later tests when the necessity of a more careful inspection of each model was appreciated. After a considerable period of running the particles in the tunnel were found to become lodged, permitting this source of error to be largely eliminated during the later tests. For this report, however, the effect of the error from this source has been minimized by repeating the tests of many of the airfoils, including all of the symmetrical series originally reported in reference 2.

The magnitude of all such accidental errors was judged from the results of repeat tests of many airfoils, and from the results of approximately 25 tests of one airfoil that were made periodically throughout the investigation to check the consistency of the measurements. The accidental errors in the results presented in this report are believed to be within the limits indicated in the following table:

α	$\pm 0.15°$
$C_{L_{max}}$	$\begin{cases} 0.01 \\ -0.03 \end{cases}$
$C_{m_{c/4}}$	± 0.003
$C_{D_0}(C_L=0)$	$\begin{cases} 0.0006 \\ -0.0002 \end{cases}$
$C_{D_0}(C_L=1)$	$\begin{cases} 0.0015 \\ -0.0008 \end{cases}$

In addition to the consideration of the accidental errors, all measurements were carefully analyzed to consider possible sources of errors of the type that would not be apparent from the dispersion of the results of repeat tests. A rather large (approximately 1.5 percent) error of this type is present in all the air-

velocity measurements resulting from a reduction in the apparent weight of the manometer liquid when the density of the air in the tunnel is raised to that corresponding to a pressure of 20 atmospheres. The effects of this error, however, are reduced by the presence of another error in the air-velocity measurements due to the blocking effects of the model in the tunnel. The measured coefficients, obtained by dividing the measured forces by $\frac{1}{2}\rho V^2$, as well as the derived coefficients are, of course, affected by errors in the air-velocity measurement. Aside from this source of error, it is believed that only two other sources need be considered: first, the deflection of the model and supports under the air load; and second, the interference of the airfoil supports on the airfoil. The angle of attack and the moment coefficient are affected by the deflection of the airfoil and supports. The error in angle of attack, which is proportional to $C_{m_{c/4}}$, was found to be approximately $-0.1°$ for an

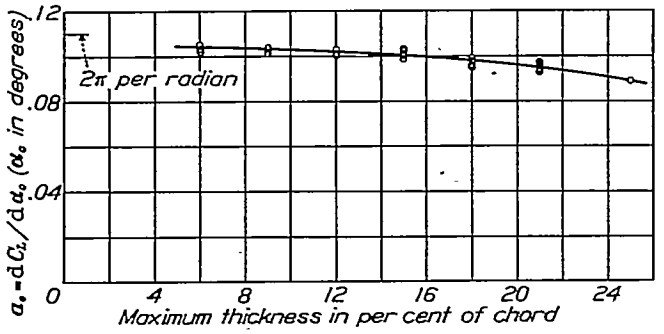

FIGURE 81.—Variation of lift-curve slope with thickness.

airfoil having a moment coefficient of -0.075. The error from this source in the moment coefficient is inappreciable at zero lift, but at a lift coefficient of 1 may amount to -0.001. The errors resulting from the support interference are more difficult to evaluate, but tests of airfoils with different support arrangements lead to the belief that they are within the limits indicated in the following table:

α	$\pm 0.05°$
$C_{L_{max}}$	$\begin{cases} 0.00 \\ -0.02 \end{cases}$
$C_{m_{c/4}}$	± 0.001
$C_{D_0}(C_L=0)$	$\begin{cases} 0.0002 \\ 0.0000 \end{cases}$
$C_{D_0}(C_L=1)$	± 0.0010

The tunnel-wall and induced-drag corrections applied to obtain the airfoil section characteristics might also be treated as sources of systematic errors. Such errors need not be considered, however, if the section characteristics are defined as the measured characteristics with certain calculated corrections applied. Errors in the tunnel-wall corrections, however, should be considered when the results from different wind tunnels are compared. For consideration of these errors, the reader is referred to references 9 and 10.

For the purpose of comparing the results from different wind tunnels and of applying these results to airplanes in flight, it is also necessary to consider the effects of air-stream turbulence. In air streams having different degrees of turbulence, the value of the Reynolds Number cannot be considered as a sufficient measure of the effective dynamic scale of the flow. The airfoil characteristics presented in this report were obtained at a value of the Reynolds Number of approximately 3,000,000, which corresponds roughly to the Reynolds Number attained in flight by a medium-sized airplane flying near its stalling speed. Consideration of the effects of the turbulence present in the variable-density tunnel (see references 11 and 12) leads, however, to the belief that these results are more nearly directly applicable to the characteristics that would be obtained in flight at larger values of the Reynolds Number.

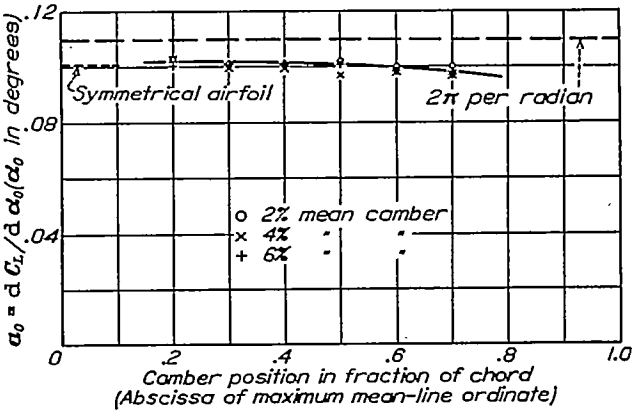

FIGURE 82.—Variation of lift-curve slope with camber. Results for 12 percent thick airfoils.

DISCUSSION

The results of this investigation are here discussed and analyzed to indicate the variation of the aerodynamic characteristics with variations in thickness and in mean-line form. For the analysis of the effect of thickness, test data from consecutive tests of airfoils having different thicknesses and the same mean-line form are used. The analysis of the effect of the mean-line form is made with respect to consecutive tests of airfoils of the same thickness (12 percent of the chord) and related mean-line forms. The results are compared, where possible, with the results predicted by thin-airfoil theory, a summary of which is presented in the appendix.

LIFT

Lift curve.—In the usual working range of an airfoil section the lift coefficient may be expressed as a linear function of the angle of attack

$$C_L = a_0 (\alpha_0 - \alpha_{L_0})$$

where a_0 is the slope of the lift curve for the wing of infinite aspect ratio and α_{L_0} is the angle of attack at zero lift.

The variation of the lift-curve slope with thickness is shown in figure 81. The points on the figure represent the deduced slopes as measured in the angular range of low profile drag. These results confirm previous results (reference 1) in that they show the lift-curve slope to decrease with increasing thickness. The camber has very little effect on the slope, as indicated in figure 82, although a rearward movement of the position of the camber tends to decrease the slope slightly. Table II gives the numerical values of the slope in convenient form for noting the general trends with respect to variations in thickness and in camber. It will be noted that all values of the slope lie below the approximate theoretical value for thin wings, 2π per radian; the measured values lie between 95 and 81 percent, approximately, of the theoretical.

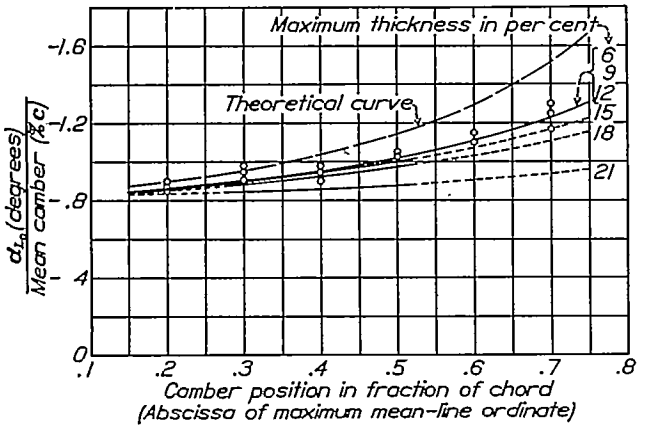

FIGURE 83.—Variation of angle of zero lift with camber. Points shown are for 12 percent thick airfoils. Curves indicate general trends for the different thicknesses.

The angle of zero lift is best analyzed by means of a comparison with that predicted by the theory. Thin-airfoil theory states that the angle of zero lift is proportional to the camber if the camber is varied, as with these related airfoils, by scaling the ordinates of a given mean line without altering the camber position. The theory also predicts an increased negative angle as the position of the camber moves back along the chord. The experimental values are compared with the theoretical values in figures 83 and 84. The experimental values lie between 100 and 75 percent, approximately, of the theoretical values, the departure becoming greater with a rearward movement of the position of the camber and with increased thickness (above 9 to 12 percent of the chord). Numerical values of the angle of zero lift are given in table III.

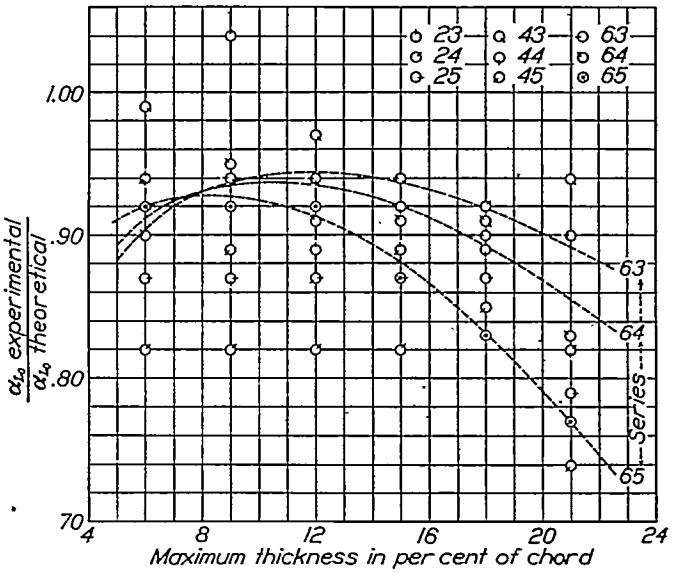

FIGURE 84.—Variation of angle of zero lift with thickness. Numbers refer to mean-camber designation.

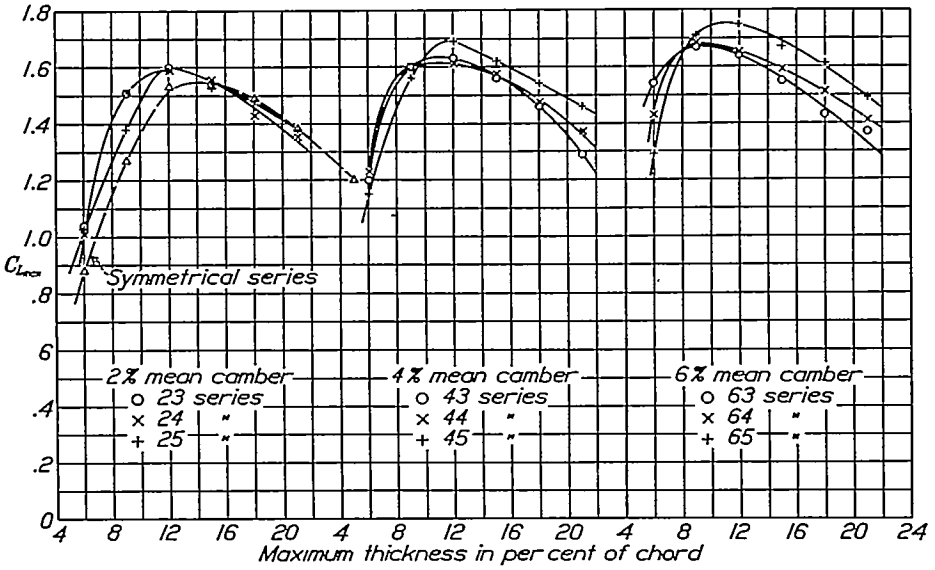

FIGURE 85.—Variation of maximum lift with thickness.

Maximum lift.—The variation of the maximum lift coefficient with thickness is shown in figure 85. It will be noted that the highest values are obtained with moderately thick sections (9 to 12 percent of the chord thick, except for the symmetrical sections for which the highest values are obtained with somewhat thicker

sections). The variation with camber, shown in figure 86, confirms the expected increase in maximum lift with camber. The gain is small, however, for the normal positions of the camber, but becomes larger as the camber moves either rearward or forward. It will be seen by reference to figure 85 that the camber becomes less effective as the thickness is increased. This reduced effectiveness of the camber is in agreement with a conclusion reached in reference 13 that for airfoils having a thickness ratio of approximately 20 percent of the chord, camber is of questionable value. Numerical values of the maximum lift coefficient are given in table IV.

Air-flow discontinuities.—These and other wind-tunnel tests indicate that at the attitude of maximum

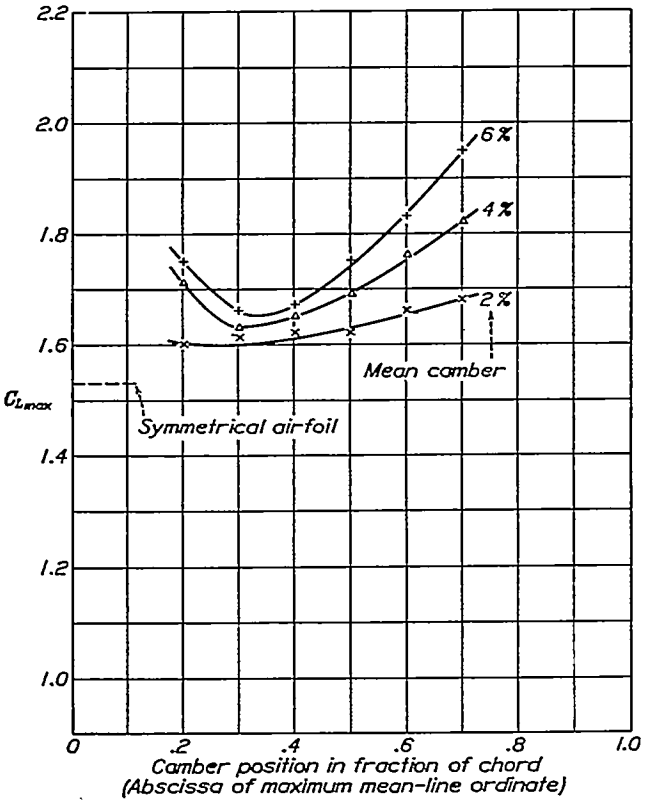

FIGURE 86.—Variation of maximum lift with camber. Results for 12 percent thick airfoils.

lift the air forces on certain airfoils exhibit sudden changes which in many instances result in a serious loss of lift. The probable cause of these air-flow discontinuities is discussed briefly in reference 13. The stability or instability of the air flow at maximum lift may be judged by the character of the lift-curve peaks indicated for the various airfoils. The curves are classified into three general types as noted in table IV, but the degree of stability is difficult to judge. It may be generally concluded that improved stability may be obtained by (1) having a small leading-edge radius, which causes an early breakdown of the flow with a consequent low value of the maximum lift, (2) increasing the thickness (beyond the normal thickness ratios), or (3) increasing the camber (for airfoils having normal camber positions; i.e., 0.3c to 0.5c).

MOMENT

Thin-airfoil theory separates the air forces acting on any airfoil into two parts: First, the forces that produce a couple but no lift (they are dependent only on the shape of the mean line); second, the forces that produce the lift only, the resultant of which acts at

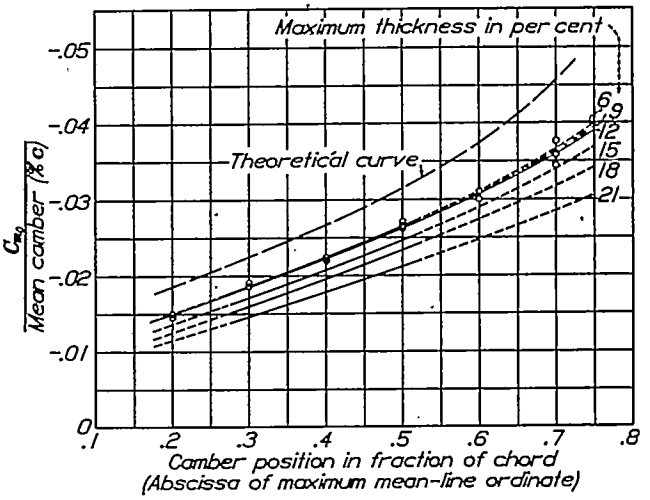

FIGURE 87.—Variation of moment at zero lift with camber. Points shown are for 12 percent thick airfoils. Curves indicate general trends for the different thicknesses.

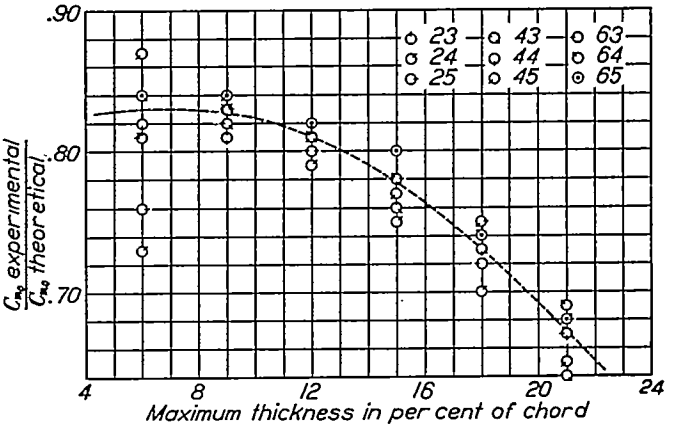

FIGURE 88.—Variation of moment at zero lift with thickness. Numbers refer to mean-camber designation.

a fixed point. We then have in the working range an expression for the total moment taken about any point

$$C_m = C_{m_0} + nC_L$$

where C_{m_0} is the moment coefficient at zero lift and nC_L is the additional moment due to lift.

As with the angle of zero lift, the theory states that the moment at zero lift is proportional to the camber and predicts an increase in the magnitude of the moment as the camber moves back along the chord. Figures 87 and 88 show the values of the moment coefficient as affected by variations of camber and thickness compared with the theoretical values. Referring to figure 87, the plotted data indicate that the

moment coefficients are nearly proportional to the camber. It will also be noted that the curves representing the ratios of the experimental coefficients to the camber are nearly parallel to the equivalent curve representing the theoretical ratios except that the curves tend to diverge for positions of the camber well back. Figure 88 shows that the experimental values lie between 87 and 64 percent, approximately, of the theoretical. Numerical values of the moment coefficient at zero lift are given in table V.

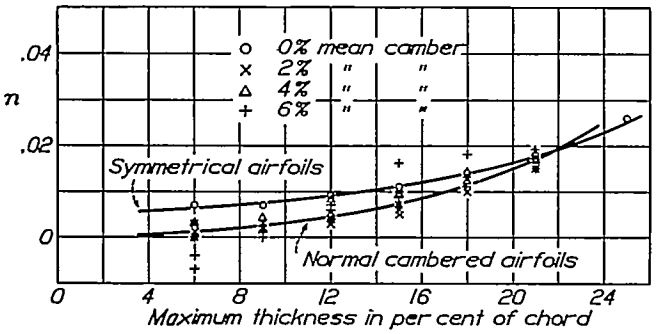

FIGURE 89.—Variation of position of constant moment with thickness. Values of n for equation $C_{m_{c/4}}=C_{m_0}+nC_L$. Results for airfoils having normal camber positions (0.3c to 0.5c).

If the resultant of the lift forces acted exactly through the quarter-chord point, as predicted by the theory of thin airfoils, there would be no additional moment due to the lift when the moments are taken about this point. The curves of $C_{m_{c/4}}$ against C_L, however, show a slope in the working range which indicates that the axis of constant moment is displaced somewhat from the quarter-chord point. The factor n represents the amount of this displacement as obtained from the deduced slopes of the moment curves in the

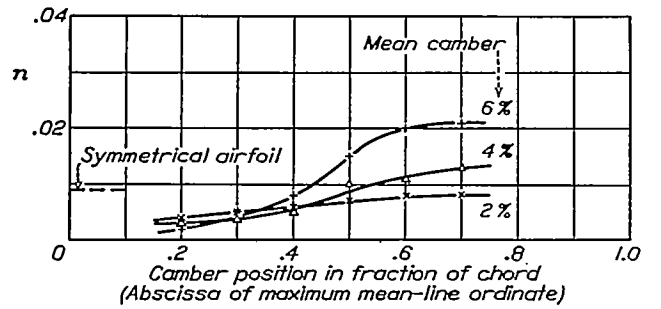

FIGURE 90.—Variation of position of constant moment with camber. Values of n for equation $C_{m_{c/4}}=C_{m_0}+nC_L$. Results for 12 percent thick airfoils.

normal working range. The variation of this displacement with thickness and with camber is shown in figures 89 and 90. Table VI gives the numerical values. Beyond the stall all the airfoils show a sharp increase in the magnitude of the pitching moment. The suddenness of this increase follows the degree of stability at the stall as indicated by the type of the lift-curve peak.

DRAG

The total drag of an airfoil is considered as made up of the induced drag and the profile drag. Considering the profile drag as the minimum value plus an additional drag dependent upon the attitude of the airfoil, we have in coefficient form

$$C_D=C_{D_i}+(C_{D_{0min}}+\Delta C_{D_0})$$

The induced-drag coefficient C_{D_i}, which is computed by means of the formula given in reference 8, is considered to be independent of the airfoil section. The variation of the profile-drag coefficient with the shape variables of the airfoil section is analyzed with respect

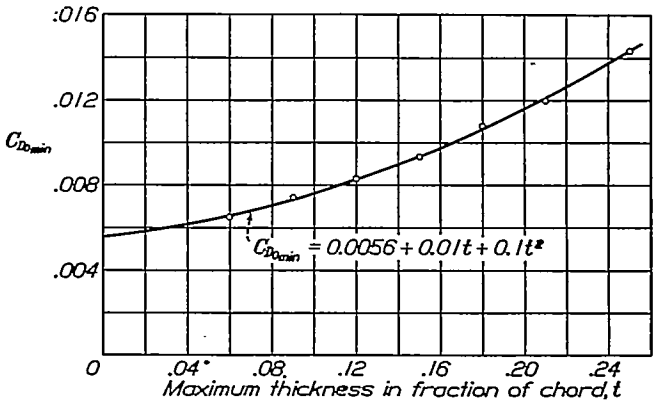

FIGURE 91.—Variation of minimum profile drag with thickness for the symmetrical airfoils.

to the variations of the two components of the profile drag.

Minimum profile drag.—The variation of the minimum profile-drag coefficient with thickness for the symmetrical sections is shown in figure 91. The cambered sections show the same general variation with thickness but, to avoid confusion, the results are not plotted. The variation of the minimum profile-drag

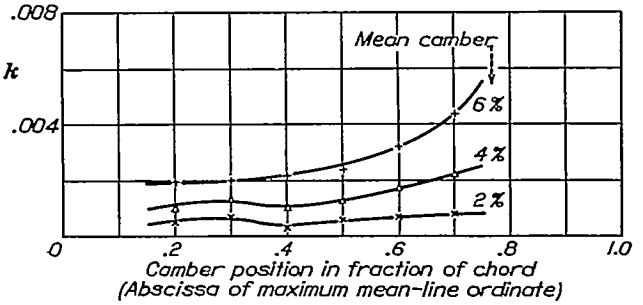

FIGURE 92.—Increase in minimum profile drag due to camber. Results for 12 percent thick airfoils. Values of k for equation $C_{D_{0min}}=k+0.0056+0.01\,t+0.1\,t^2$, where k is the increase in $C_{D_{0min}}$ due to camber and t is the maximum thickness in fraction of chord.

coefficient with the profile thickness may be expressed by the empirical relation

$$C_{D_{0min}}=k+0.0056+0.01t+0.1t^2$$

where t is the thickness ratio and k (which is approximately constant for sections having the same mean line) represents the increase in $C_{D_{0min}}$ above that computed for the symmetrical section of corresponding thickness. The variation of $C_{D_{0min}}$ with camber is indicated by the variation of k as shown in figure 92.

The effect of camber is small except for the highly cambered sections having the maximum camber well back. Numerical values of $C_{D_{0min}}$ are given in table VII.

Additional profile drag.—The additional profile drag, which is dependent upon the attitude of the airfoil, has previously been expressed as a function of the lift (reference 4) by the equation

$$\Delta C_{D_0} = C_{D_0} - C_{D_{0min}} = 0.0062(C_L - C_{L_{opt}})^2$$

where $C_{L_{opt}}$ may be called the optimum lift coefficient; that is, the lift coefficient corresponding to the minimum profile-drag coefficient. This equation holds reasonably well for the normally shaped airfoils at values of the lift coefficient below unity.

A convenient practical method of allowing for the increased values of C_{D_0} at moderately high values of the lift coefficient is to include the additional profile drag with the induced drag, as suggested in reference 2. For the symmetrical airfoils of moderate thickness the term to be added to the induced-drag coefficient was given as $0.0062\ C_L^2$. The relative importance of this term may be better appreciated by considering that it represents 11.7 percent of the induced drag of an elliptical airfoil of aspect ratio 6. The same method may also be applied to other airfoils if the value of the optimum lift is not too large.

Andrews (reference 14), using the part of these data published in references 2, 4, and 5, suggests for the additional profile drag the form

$$\Delta C_{D_0} = \mathrm{f}\left(\frac{C_L - C_{L_{opt}}}{C_{L_{max}} - C_{L_{opt}}}\right)$$

This function is represented in figure 93 as the curve determined from the results for the symmetrical airfoils and for the airfoils having a camber of 2 percent of the chord. As the camber is increased, the dispersion of the plotted points from the curve becomes greater. In general the points above the curve correspond to thick sections and sections in which the maximum camber is well back. The departure from the curve becomes greater with increased thickness and with a rearward movement of the maximum-camber position. The points well below the curve correspond to the thin airfoils.

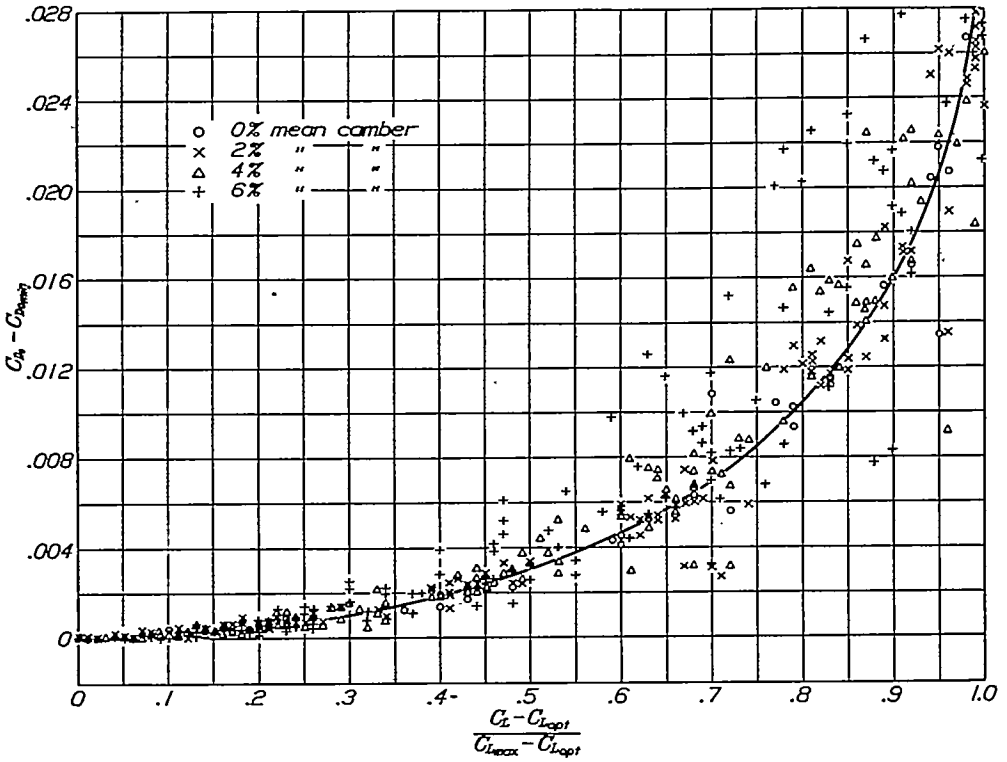

FIGURE 93.—Additional profile drag.

Because the additional profile drag is not a simple function of the lift, and also because the results as presented in figure 93 are difficult to follow, generalized curves for the relation

$$\Delta C_{D_0} = \mathrm{f}(C_L - C_{L_{opt}})$$

are given in figure 94. These curves are given to represent more accurately the additional profile drag for the normally shaped sections.

Optimum lift.—The optimum lift, as defined above, is the value of the lift corresponding to the minimum profile drag. As the determination of this value of the lift is largely dependent upon the fairing of the profile-drag curves, special curves were faired for this purpose on enlarged-scale plots corresponding to certain related airfoils grouped together. The values of the optimum lift coefficients obtained in this manner are given in table VIII. It may be noted by reference to this table that the optimum lift coefficient increases with camber

and for the highly cambered sections a definite increase accompanies a forward movement of the camber.

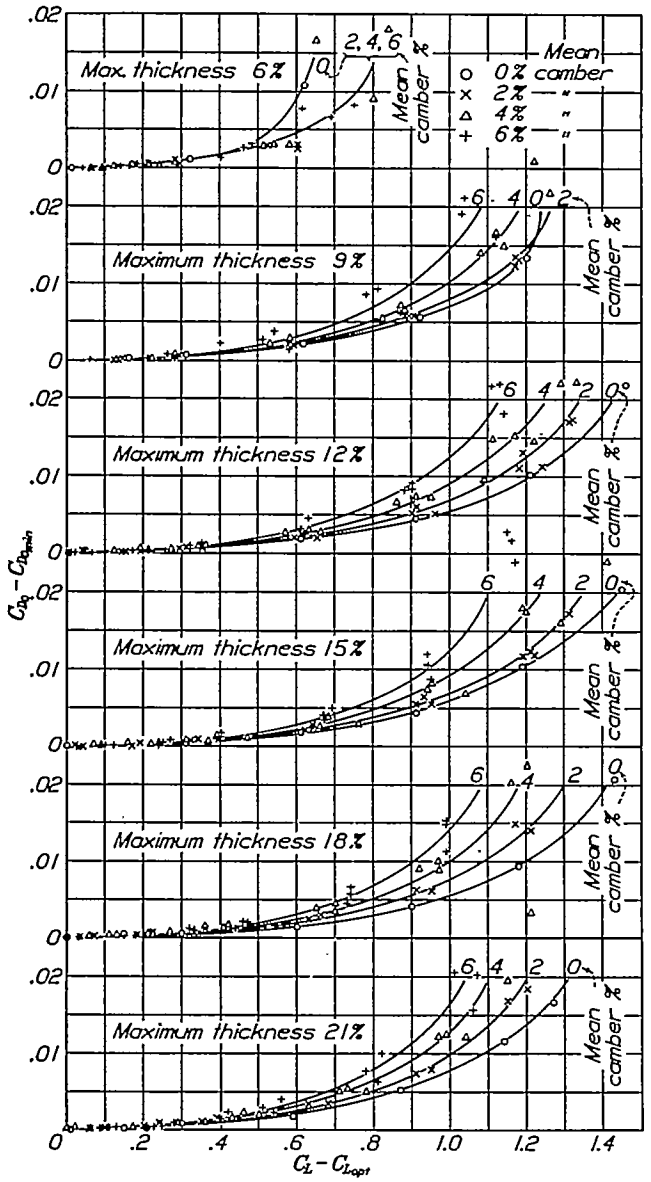

FIGURE 94.—Additional profile drag as a function of $C_L - C_{L_{opt}}$. Results are for airfoils having normal camber positions (0.3c to 0.5c).

it is not primarily dependent upon the shape of the mean line. Nevertheless it is interesting to compare the optimum lift coefficients with the values included in table VIII representing the theoretical lift coefficients at the "ideal" angle of attack for the mean line; i.e., the angle of attack for which the thin-airfoil theory gives a finite velocity at the nose. (See the appendix.)

GENERAL EFFICIENCY

The general efficiency of an airfoil cannot be expressed by means of a single number. The ratio of

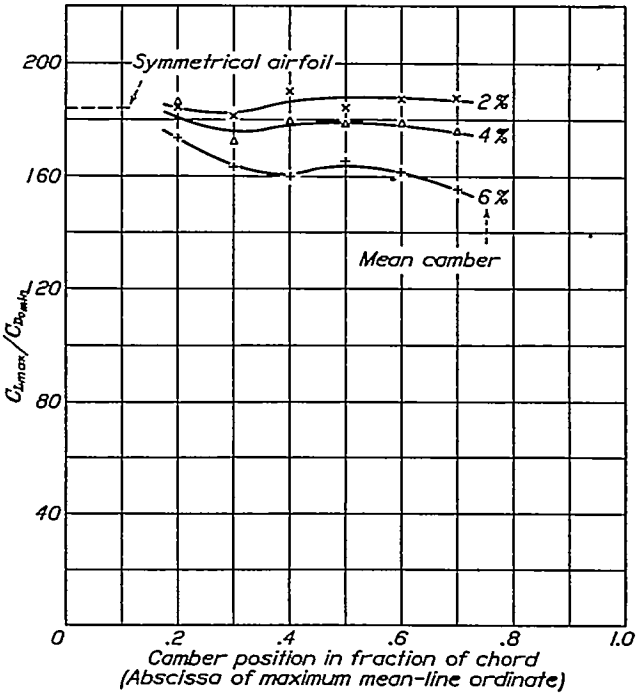

FIGURE 96.—Variation of $C_{L_{max}}/C_{D_{min}}$ with camber. Results are for 12 percent thick airfoils.

the maximum lift to the minimum profile drag is, however, of some value as the measure of the efficiency of an airfoil section. The variation of this ratio with thickness is shown in figure 95. The curves of this figure indicate that the highest values of the ratio are

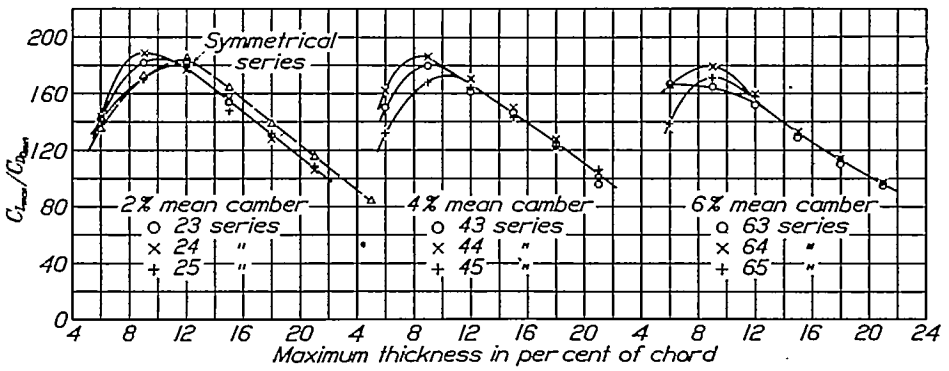

FIGURE 95.—Variation of $C_{L_{max}}/C_{D_{min}}$ with thickness.

More important than these variations, however, is the variation with thickness. The rapid decrease in the optimum lift with increased thickness indicates that given by the sections between 9 and 12 percent of the chord thick. The variation with camber, shown in figure 96, is less important. An increase in the camber

above 2 percent of the chord and a rearward movement of the camber (for the highly cambered sections) tend to decrease the value of $C_{L_{max}}/C_{D_{0min}}$. The numerical values of the ratio are given in table IX.

SUPPLEMENTARY AIRFOILS

For the purpose of investigating briefly the effects of certain shape variables other than those discussed in the main body of the report, 10 supplementary airfoils were tested. The airfoil sections were as follows: 6 symmetrical sections with modified nose shapes, 2 sections with reflexed mean lines, and 2 sections simulating those of a wing having a flexible trailing edge.

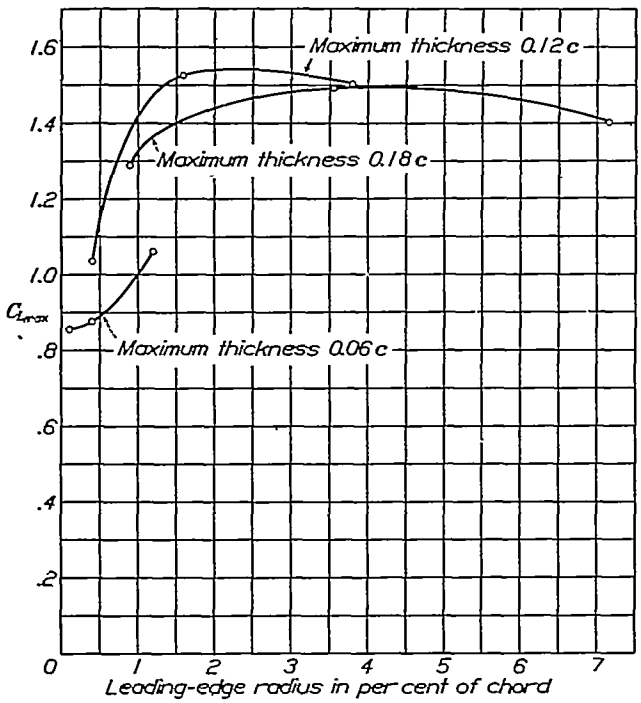

FIGURE 97.—Variation of maximum lift with nose radius.

Airfoils with modified nose shapes.—The airfoils of the first supplementary group investigated were developed from three of the symmetrical N.A.C.A. family airfoils: The N.A.C.A. 0006, the N.A.C.A. 0012, and the N.A.C.A. 0018. For each of these basic (or normal) sections one thinner-nosed section, denoted by the suffix T, and one blunter-nosed section, denoted by the suffix B, were developed and tested. The derivation of each modified section was similar to that of the normal section and was accomplished by a systematic change in the equation that defines the normal section. This change is principally a change in the nose radius, but it also results in modifications to the profile throughout its length, except at the maximum ordinate and at the trailing edge. The nose radii of the sections in percent of the chord are as follows:

Section	T series	Normal	B series
0006	0.10	0.40	1.19
0012	.40	1.58	3.80
0018	.89	3.56	7.15

The aerodynamic characteristics of the modified sections are given in figures 72 to 77. These may be compared with the characteristics of the normal sections given in figures 4, 6, and 8. The maximum lift coefficients of the modified and the normal sections are plotted against the leading-edge radii in figure 97. It is interesting to note that the leading-edge radius is very critical in its effect on the maximum lift when the radius is small. This critical effect is also indicated by the rapid increase in the maximum lift with increasing thickness for the thin sections as shown in figure 85.

Airfoils with reflexed mean lines.—Previous investigations have shown that the pitching moment of cambered airfoils can be reduced by altering the form of the mean line toward the trailing edge, with a consequent loss of maximum lift but only a small reduction in drag. In order to compare the characteristics of sections of this type with those of the related sections of normal form, two airfoils were developed with the basic thickness distribution of the N.A.C.A. 0012 disposed about certain mean lines of the form given in reference 15

$$y_c = hx(1-x)\ (1-\lambda x)$$

The values of h in this equation were chosen to give a camber of 0.02 and the values of λ were chosen to give the airfoil designated the N.A.C.A. $2R_112$ a small negative moment and the airfoil designated the N.A.C.A. $2R_212$ a small positive moment. Characteristic curves for the two airfoils are given in figures 78 and 79. The principal characteristics of the sections may be conveniently compared with those of the related symmetrical section, the N.A.C.A. 0012, and a related normal section having a camber of 2 percent of the chord, the N.A.C.A. 2412, by means of the following table arranged in the order of increasing pitching-moment coefficients.

Section	$C_{L_{max}}$	$C_{D_{0min}}$	$\frac{C_{L_{max}}}{C_{D_{0min}}}$	C_{m_0}
$2R_212$	1.47	0.0086	171	0.004
0012	1.53	.0083	184	−.002
$2R_112$	1.53	.0083	184	−.020
2412	1.62	.0085	190	−.044

These results indicate that airfoils having reflexed mean lines may be of questionable value because of the adverse effect of this mean-line shape on the maximum lift coefficient.

Thickness and camber modifications near the trailing edge.—Two airfoils were developed to simulate an airfoil having a flexible trailing edge in a straight and in a given deflected position. The thickness distribution is composed of three parts: the forward portion (0 to 0.3c) having the same distribution as the N.A.C.A. 0012, the rear portion (from 0.7c to the trailing edge) having a thin, uniform value, and the central portion joining these two with fair curves. As shown in figure 80, the two airfoils differ only in the rear portion, the section designated N.A.C.A. 0012F_0 simulating that of a wing having the trailing edge deformed for the high-speed condition, and the section designated N.A.C.A. 0012F_1 simulating that of the same wing with the trailing edge bent down in a circular arc. Curves of the aerodynamic characteristics for both conditions are compared in figure 80. Considering the results given by both airfoils as two conditions for one airfoil, a very high maximum lift with a reasonably low minimum drag is obtained. On this assumption the ratio $\frac{C_{L_{max}}}{C_{D_{0min}}}$ is 197, slightly higher than the value of this ratio given by the N.A.C.A. 2412.

In order to study the effects of an extreme change in the thickness distribution, the principal characteristics of the two sections may be compared with those of the related normal sections, the N.A.C.A. 0012 and the N.A.C.A. 6712. The maximum lift coefficient is little affected by the change in the thickness distribution, but it is of interest to note (table I) that the slope of the lift curve of the N.A.C.A. 0012F_0 is slightly greater than 2π per radian, as compared with an appreciably lower slope for the N.A.C.A. 0012. The profile drag is also affected by the change in the thickness distribution. Of the two symmetrical sections, the profile drag of the N.A.C.A. 0012F_0 is much higher than that of the N.A.C.A. 0012 over the entire lift range. This is not true, however, for the two cambered sections. Comparing the characteristics of the N.A.C.A. 0012F_1 with those of the N.A.C.A. 6712, we find that at low values of the lift the profile drag of the former is much higher, but as the lift increases this difference becomes less, and in the high-lift range the profile drag of the N.A.C.A. 0012F_1 is considerably less than that of the N.A.C.A. 6712.

CONCLUSIONS

The variation of the aerodynamic characteristics of the related airfoils with the geometric characteristics investigated may be summarized as follows:

Variation with thickness ratio:

1. The slope of the lift curve in the normal working range decreases with increased thickness, varying from 95 to 81 percent, approximately, of the theoretical slope for thin airfoils (2π per radian).

2. The angle of zero lift moves toward zero with increased thickness (above 9 to 12 percent of the chord thickness ratios).

3. The highest values of the maximum lift are obtained with sections of normal thickness ratios (9 to 15 percent).

4. The greatest instability of the air flow at maximum lift is encountered with the moderately thick, low-cambered sections.

5. The magnitude of the moment at zero lift decreases with increased thickness, varying from 87 to 64 percent, approximately (for normally shaped airfoils), of the values obtained by thin-airfoil theory.

6. The axis of constant moment usually passes slightly forward of the quarter-chord point, the displacement increasing with increased thickness.

7. The minimum profile drag varies with thickness approximately in accordance with the expression

$$C_{D_{0min}} = k + 0.0056 + 0.01t + 0.1t^2$$

where the value of k depends upon the camber and t is the ratio of the maximum thickness to the chord.

8. The optimum lift coefficient (the lift coefficient corresponding to the minimum profile-drag coefficient) approaches zero as the thickness is increased.

9. The ratio of the maximum lift to the minimum profile drag is highest for airfoils of medium thickness ratios (9 to 12 percent).

Variation with camber:

1. The slope of the lift curve in the normal working range is little affected by the camber; a slight decrease in the slope is indicated as the position of the camber moves back.

2. The angle of zero lift is between 100 and 75 percent, approximately, of the value given by thin-airfoil theory, the smaller departures being for airfoils with the normal camber positions.

3. The maximum lift increases with increased camber, the increase being more rapid as the camber moves forward or back from a point near the 0.3c position.

4. Greater stability of the air flow at maximum lift is obtained with increased camber if the camber is in the normal positions (0.3c to 0.5c).

5. The moment at zero lift is nearly proportional to the camber. For any given thickness, the difference between the experimental value of the constant of proportionality and the value predicted by thin-airfoil theory is not appreciably affected by the position of the camber except for the sections having the maximum camber well back, where the difference becomes slightly greater.

6. The axis of constant moment moves forward as the camber moves back.

7. The minimum profile drag increases with increased camber, and also with a rearward movement of the camber.

8. The optimum lift cofficient increases with the camber and for the highly cambered sections a definite increase accompanies a forward movement of the camber.

9. The ratio of the maximum lift to the minimum profile drag tends to decrease with increased camber (above 2 percent of the chord) and with a rearward movement of the camber (for the highly cambered sections).

LANGLEY MEMORIAL AERONAUTICAL LABRATORY,
NATIONAL ADVISORY COMMITTEE FOR AERONAUTICS,
LANGLEY FIELD, VA., *December 20, 1932.*

APPENDIX

It is proposed in this section of the report to present, briefly, a summary of the results of the existing thin-airfoil theory (based on the section mean line) as applied to the prediction of certain section characteristics. Such a summary is desirable because at present the results must be obtained from several different sources which give them in a form not easily applied. Three characteristics are considered; namely, (1) the angle of zero lift α_{L_0}, (2) the pitching-moment coefficient $C_{m_{c/4}}$, and (3) the "ideal" angle of attack α_I, or the corresponding lift coefficient C_{L_I}, that is, values corresponding to the unique condition for which the theory gives a finite velocity at the nose of the airfoil. (See reference 16.)

Expressions for lift and moment coefficients may be written as follows if the angles are measured in radians:

$$C_L = 2\pi(\alpha - \alpha_{L_0}) \tag{1}$$

$$C_{L_I} = 2\pi(\alpha_I - \alpha_{L_0}) \tag{2}$$

$$C_{m_{c/4}} = \frac{\pi}{2}(\beta + \alpha_{L_0}) \tag{3}$$

If the leading end of the mean line is chosen as the origin of coordinates and the trailing end is taken on the x axis at $x=1$, then the parameters α_{L_0}, α_I, and β are given by the following integrals

$$\alpha_{L_0} = \int_0^1 y\, f_1(x)\, dx \tag{4}$$

$$\alpha_I = \int_0^1 y\, f_2(x)\, dx \tag{5}$$

$$\beta = \int_0^1 y\, f_3(x)\, dx \tag{6}$$

where

$$f_1(x) = \frac{-1}{\pi(1-x)\,[x(1-x)]^{\frac{1}{2}}} \tag{7}$$

$$f_2(x) = \frac{(1-2x)}{2\pi[x(1-x)]^{\frac{1}{2}}} \tag{8}$$

$$f_3(x) = \frac{4(1-2x)}{\pi[x(1-x)]^{\frac{1}{2}}} \tag{9}$$

and y is the ordinate of the mean line at a given abscissa x. The integrals (4) and (6) may be shown to be identical with the corresponding integrals given by Glauert (reference 15) and by Munk (reference 17), and integral (5) is given by Theodorsen (reference 16).

The evaluation of these integrals for the N.A.C.A. airfoil sections given in this report was accomplished analytically. The values of α_{L_0} (changed from radians to degrees), $C_{m_{c/4}}$ and C_{L_I}, so computed, are given in tables III, V, and VIII, respectively, in the main body of the report. This method of evaluation, however, cannot be applied to many of the commonly used sections because they do not have analytically defined mean lines; hence, an approximate method must be used. A graphical determination gives good results and for convenience the values of the three functions, (7), (8), and (9), at several values of x, are given in the following table:

x	$f_1(x)$	$f_2(x)$	$f_3(x)$	x	$f_1(x)$	$f_2(x)$	$f_3(x)$
0	$-\infty$	∞	∞	0.30	−0.992	0.662	1.111
0.0125	−2.901	113.15	11.17	.40	−1.088	.271	.520
.0250	−2.091	39.73	7.747	.50	−1.273	0	0
.0500	−1.537	13.84	5.258	.60	−1.624	−.271	−.520
.0750	−1.306	7.403	4.109	.70	−2.315	−.662	−1.111
.1000	−1.179	4.716	3.395	.80	−3.979	−1.492	−1.910
.15	−1.049	2.447	2.496	.90	−10.61	−4.716	−3.395
.20	−.995	1.492	1.910	.95	−29.21	−13.84	−5.258
.25	−.980	.980	1.470	1.00	$-\infty$	$-\infty$	$-\infty$

In general, some difficulty would be expected with the graphical method because the values of the above functions tend to infinity at the leading and trailing edges. Actually, because the ordinates of the mean-line extremities are zero, the integrand may approach zero, and does at the leading edge for the integral (4), and at the leading and trailing edges for the integral (6). Difficulty, however, is encountered at the trailing edge for the integral (4) and at the leading and trailing edges for the integral (5). In order to avoid this difficulty, integral (4) is evaluated graphically from $x=0$ to $x=0.95$, and the increment contributed by the portion from $x=0.95$ to $x=1$ is determined analytically. Likewise, integral (5) is evaluated graphically from $x=0.05$ to $x=0.95$ and analytically for the extremities. The analytical determination of the increments is accomplished by assuming the mean line near the ends to be of the form

$$y = a + bx + cx^2$$

Evaluating the integrals gives

$$\Delta\alpha_{L_0} = -0.964y_{0.95} + 0.0954y_1' \qquad (x=0.95 \text{ to } x=1)$$

$$\Delta\alpha_I = \begin{cases} +0.467y_{0.05} + 0.0472y_0' & (x=0 \text{ to } x=0.05) \\ -0.467y_{0.95} + 0.0472y_1' & (x=0.95 \text{ to } x=1) \end{cases}$$

where y_0 and y_1' are the mean-line slopes at the leading and trailing edges, respectively.

REFERENCES

1. Jacobs, Eastman N., and Anderson, Raymond F.: Large-Scale Aerodynamic Characteristics of Airfoils as Tested in the Variable-Density Wind Tunnel. T.R. No. 352, N.A.C.A., 1930.
2. Jacobs, Eastman N.: Tests of Six Symmetrical Airfoils in the Variable-Density Wind Tunnel. T.N. No. 385, N.A.C.A., 1931.
3. Pinkerton, Robert M.: Effect of Nose Shape on the Characteristics of Symmetrical Airfoils. T.N. No. 386, N.A.C.A., 1931.
4. Jacobs, Eastman N., and Pinkerton, Robert M.: Tests of N.A.C.A. Airfoils in the Variable-Density Wind Tunnel. Series 43 and 63. T.N. No. 391, N.A.C.A., 1931.
5. Jacobs, Eastman N., and Pinkerton, Robert M.: Tests of N.A.C.A. Airfoils in the Variable-Density Wind Tunnel. Series 45 and 65. T.N. No. 392, N.A.C.A., 1931.
6. Jacobs, Eastman N., and Pinkerton, Robert M.: Tests of N.A.C.A. Airfoils in the Variable-Density Wind Tunnel. Series 44 and 64. T.N. No. 401, N.A.C.A., 1931.
7. Jacobs, Eastman N., and Ward, Kenneth E.: Tests of N.A.C.A. Airfoils in the Variable-Density Wind Tunnel. Series 24. T.N. No. 404, N.A.C.A., 1932.
8. Jacobs, Eastman N., and Abbott, Ira H.: The N.A.C.A. Variable-Density Wind Tunnel. T.R. No. 416, N.A.C.A., 1932.
9. Higgins, George J.: The Prediction of Airfoil Characteristics. T.R. No. 312, N.A.C.A., 1929.
10. Knight, Montgomery, and Harris, Thomas A.: Experimental Determination of Jet Boundary Corrections for Airfoil Tests in Four Open Wind Tunnel Jets of Different Shapes. T.R. No. 361, N.A.C.A., 1930.
11. Stack, John: Tests in the Variable-Density Wind Tunnel to Investigate the Effects of Scale and Turbulence on Airfoil Characteristics. T.N. No. 364, N.A.C.A., 1931.
12. Dryden, H. L., and Kuethe, A. M.: Effect of Turbulence in Wind Tunnel Measurements. T.R. No. 342, N.A.C.A., 1930.
13. Jacobs, Eastman N.: The Aerodynamic Characteristics of Eight Very Thick Airfoils from Tests in the Variable-Density Wind Tunnel. T.R. No. 391, N.A.C.A., 1931.
14. Andrews, W. R.: The Estimation of Profile Drag. Flight, vol. XXIV, no. 25, pp. 530a–530d, 1932 and no. 31, pp. 710a–710c, 1932.
15. Glauert, H.: The Elements of Aerofoil and Aircrew Theory. Cambridge University Press (London), 1926.
16. Theodorsen, Theodore: On the Theory of Wing Sections with Particular Reference to the Lift Distribution. T.R. No. 383, N.A.C.A., 1931.
17. Munk, Max M.: Elements of the Wing Section Theory and of the Wing Theory. T.R. No. 191, N.A.C.A., 1924.

TABLE I.—IMPORTANT CHARACTERISTICS

Airfoil	Page	Section characteristics							Wing characteristics A.R. 6			Thickness at		c.p. at		[4](C/B)$_0$
		$C_{L_{max}}$	α_0 at $C_{L_{max}}$ (deg.)	α_{L_0} (deg.)	$a_0=\frac{dC_L}{d\alpha_0}$ (per deg.)	$C_{D_{0min}}$	$\frac{C_{L_{max}}}{C_{D_{0min}}}$	C_{m_0}	$C_{D_{min}}$	$(L/D)_{max}$	C_L at $(L/D)_{max}$	0.15 chord	0.65 chord	Maximum forward position	¾ $C_{L_{max}}$	
												Percent chord		Percent chord		
0006	303	0.88	13	−0.1	0.102	0.0065	135	−0.002	0.0065	23.8	0.31	5.35	4.13	25	25	−0.082
0009	303	1.27	14	.0	.101	.0074	172	−.003	.0074	22.9	.36	8.02	6.20	25	25	−.213
0012	304	1.53	17	.0	.101	.0083	184	−.002	.0083	22.2	.37	10.69	8.27	[1] 25	25	−.285
0015	304	1.53	17	.0	.100	.0093	164	.000	.0093	21.2	.40	13.36	10.33	[1] 25	24	−.270
0018	305	1.49	17	.0	.098	.0108	138	−.002	.0108	19.8	.40	16.04	12.40	24	24	−.295
0021	305	1.38	17	−.1	.094	.0120	115	−.001	.0120	18.5	.44	18.71	14.46	23	23	−.270
0025	306	1.20	16	.0	.089	.0143	84	−.003	.0143	16.5	.47	22.27	17.22	23	23	−.233
2212	306	1.60	16	−1.8	.103	.0087	184	−.029	.0088	22.4	.40	10.69	8.25	27	32	−.262
2306	307	1.04	11	−1.8	.104	.0073	142	−.036	.0075	23.9	.33	5.36	4.14	29	38	−.130
2309	307	1.51	15	−2.0	.103	.0083	182	−.036	.0085	22.9	.39	8.04	6.21	28	34	−.230
2312	308	1.61	16	−1.9	.101	.0089	181	−.038	.0090	22.1	.39	10.71	8.27	27	34	−.208
2315	308	1.64	15	−1.7	.102	.0100	164	−.034	.0100	20.5	.41	13.38	10.36	27	34	−.251
2406	309	1.01	13	−1.7	.103	.0070	144	−.039	.0074	24.9	.32	5.34	4.14	29	40	−.103
2409	309	1.51	14	−1.7	.103	.0080	189	−.044	.0082	23.1	.36	8.02	6.20	28	36	−.242
2412	310	1.62	17	−1.8	.101	.0085	190	−.044	.0087	22.5	.39	10.71	8.27	28	35	−.274
2415	310	1.55	16	−1.7	.101	.0099	156	−.040	.0100	20.8	.40	13.39	10.34	28	35	−.262
2418	311	1.43	15	−1.9	.098	.0112	128	−.037	.0113	19.4	.42	16.08	12.39	27	34	−.238
2421	311	1.35	16	−1.7	.097	.0127	106	−.036	.0128	17.9	.43	18.75	14.46	27	34	−.229
2506	312	1.03	15	−2.0	.103	.0073	141	−.048	.0076	24.2	.36	5.36	4.13	30	44	−.116
2509	312	1.38	13	−2.0	.102	.0081	170	−.052	.0083	22.9	.37	8.04	6.21	29	40	−.207
2512	313	1.62	17	−2.1	.102	.0088	184	−.054	.0091	22.3	.39	10.70	8.27	28	37	−.270
2515	313	1.53	16	−2.0	.099	.0103	148	−.049	.0104	20.4	.41	13.38	10.33	28	37	−.255
2518	314	1.48	16	−2.0	.096	.0112	132	−.047	.0113	19.1	.42	16.07	12.41	28	36	−.255
2521	314	1.38	16	−1.8	.095	.0126	109	−.043	.0126	17.7	.44	18.72	14.47	28	36	−.233
2612	315	1.66	17	−2.3	.100	.0089	187	−.060	.0091	22.1	.38	10.70	8.26	28	38	−.274
2712	315	1.68	17	−2.6	.100	.0090	187	−.075	.0093	22.0	.38	10.69	8.25	29	41	−.272
4212	316	1.71	16	−3.4	.102	.0092	186	−.059	.0100	22.1	.40	10.70	8.27	29	38	−.260
4306	316	1.20	10	−3.8	.103	.0080	150	−.075	.0094	23.7	.38	5.40	4.14	31	49	−.141
4309	317	1.60	15	−3.6	.103	.0089	180	−.073	.0094	22.3	.39	8.09	6.21	29	43	−.236
4312	317	1.63	16	−3.9	.100	.0095	172	−.075	.0100	21.7	.40	10.77	8.27	30	43	−.230
4315	318	1.56	15	−3.6	.103	.0107	146	−.068	.0108	20.2	.42	13.47	10.34	29	42	−.233
4318	318	1.46	14	−3.5	.099	.0119	123	−.065	.0121	19.0	.43	16.14	12.41	29	41	−.225
4321	319	1.29	15	−3.6	.095	.0134	96	−.057	.0134	17.4	.45	18.81	14.46	29	41	−.196
4406	319	1.23	10	−3.9	.104	.0076	162	−.087	.0089	24.2	.38	5.40	4.16	32	53	−.144
4409	320	1.60	15	−3.6	.103	.0086	186	−.086	.0092	22.9	.40	8.07	6.21	31	46	−.242
4412	320	1.65	16	−3.9	.100	.0092	179	−.089	.0096	22.1	.40	10.77	8.28	31	45	−.253
4415	321	1.57	15	−3.8	.101	.0105	150	−.083	.0108	20.5	.42	13.45	10.34	30	45	−.242
4418	321	1.47	17	−3.7	.096	.0116	127	−.078	.0120	19.2	.43	16.15	12.40	30	44	−.231
4421	322	1.37	19	−3.4	.093	.0132	104	−.071	.0133	17.7	.44	18.79	14.48	30	44	−.222
4506	322	1.15	13	−4.3	.104	.0087	132	−.109	.0098	22.7	.40	5.38	4.14	33	63	−.103
4509	323	1.56	13	−4.1	.103	.0093	168	−.106	.0099	22.0	.40	8.08	6.21	32	52	−.229
4512	323	1.69	17	−4.2	.097	.0095	178	−.105	.0099	21.7	.40	10.74	8.28	31	49	−.262
4515	324	1.62	17	−4.1	.101	.0113	143	−.097	.0116	19.6	.43	13.44	10.35	31	48	−.253
4518	324	1.54	17	−3.9	.096	.0125	123	−.094	.0126	18.4	.43	16.14	12.41	31	48	−.244
4521	325	1.46	19	−3.4	.095	.0138	106	−.082	.0138	17.2	.45	18.80	14.47	30	46	−.244
4612	325	1.76	17	−4.6	.098	.0099	178	−.124	.0105	21.1	.41	10.73	8.27	31	52	−.275
4712	326	1.82	18	−5.0	.097	.0104	175	−.143	.0110	20.7	.41	10.74	8.26	32	55	−.290
6212	326	1.75	14	−5.2	.100	.0101	173	[3]−.087	.0117	20.9	.44	10.78	8.29	30	44	−.240
6306	327	1.54	12	[2]−5.2	.105	.0092	167	[3]−.109	.0177	21.6	.42	5.47	4.15	32	54	−.187
6309	327	1.67	13	−5.4	.104	.0101	165	−.110	.0116	21.1	.42	8.18	6.23	32	51	−.213
6312	328	1.66	14	−5.5	.101	.0102	163	−.110	.0115	20.9	.44	10.86	8.29	31	51	−.218
6315	328	1.55	13	−5.4	.101	.0120	129	−.105	.0125	19.3	.45	13.58	10.37	32	52	−.214
6318	329	1.43	13	−5.2	.098	.0130	110	−.097	.0133	18.4	.45	16.27	12.44	32	50	−.209
6321	329	1.37	17	−5.2	.096	.0144	95	−.090	.0145	17.0	.47	18.92	14.51	31	50	−.214
6406	330	1.43	9	−5.6	.104	.0086	166	[3]−.129	.0139	22.6	.42	5.42	4.15	34	62	−.157
6409	330	1.63	15	−5.9	.101	.0094	179	−.133	.0113	21.6	.42	8.14	6.21	33	57	−.225
6412	331	1.67	15	−5.7	.101	.0104	160	−.132	.0117	20.8	.42	10.85	8.29	33	56	−.242
6415	331	1.59	17	−5.7	.099	.0120	133	−.125	.0127	19.2	.45	13.55	10.36	33	56	−.238
6418	332	1.51	18	−5.7	.099	.0132	114	−.118	.0137	18.1	.45	16.28	12.43	33	55	−.231
6421	332	1.41	18	−5.2	.096	.0146	97	−.110	.0148	16.9	.46	18.96	14.50	33	54	−.224
6506	333	1.29	10	[2]−6.3	.101	.0093	139	[3]−.159	.0122	21.6	.42	5.41	4.14	35	74	−.121
6509	333	1.71	15	−6.3	.103	.0100	171	−.158	.0119	21.0	.43	8.14	6.21	34	62	−.236
6512	334	1.75	17	−6.2	.101	.0106	165	[3]−.159	.0119	20.6	.42	10.84	8.30	33	60	−.257
6515	334	1.67	18	−6.0	.099	.0127	132	[3]−.150	.0134	18.7	.44	13.53	10.36	33	59	−.253
6518	335	1.61	18	−5.7	.095	.0141	114	−.139	.0142	17.4	.46	16.22	12.44	33	58	−.251
6521	335	1.49	19	−5.3	.094	.0154	97	−.129	.0155	16.0	.47	18.92	14.49	33	57	−.233
6612	336	1.83	17	−6.6	.099	.0114	161	[3]−.186	.0124	19.8	.43	10.80	8.28	33	64	−.270
6712	336	1.95	18	−7.0	.097	.0126	155	[3]−.206	.0135	18.6	.45	10.76	8.27	34	65	−.289
0006T	337	.85	13	−.1	.100	.0069	123	.005	.0069	18.7	.23	5.09	3.84	[1] 24	21	−.028
0006B	337	1.06	11	.0	.104	.0076	139	.005	.0076	22.5	.34	5.74	4.57	[1] 24	22	−.102
0012T	338	1.03	12	−.1	.099	.0082	126	.001	.0082	21.5	.36	10.19	7.63	[1] 25	24	−.178
0012B	338	1.50	16	.0	.101	.0095	158	.000	.0095	20.8	.40	11.48	9.13	[1] 24	23	−.275
0018T	339	1.29	15	.1	.098	.0102	127	.000	.0102	19.3	.41	15.28	11.52	[1] 25	24	−.238
0018B	339	1.40	16	.0	.097	.0122	115	.001	.0122	18.2	.44	17.23	13.70	[1] 23	22	−.272
$2R_112$	340	1.53	16	−1.5	.101	.0083	184	−.020	.0086	22.8	.38	10.70	8.26	26	29	−.264
$2R_212$	340	1.47	16	−.6	.102	.0086	171	.004	.0087	22.2	.38	10.71	8.25	[1] 25	23	−.257
$0012F_0$	341	1.53	15	−.2	.111	.0104	147	.000	.0104	19.5	.42	10.70	--------	[1] 26	25	−.238
$0012F_1$	341	2.05	12	−11.7	.099	.0139	147	−.199	.0184	17.6	.55	10.70	--------	34	68	−.189

[1] Based on ¾ $C_{L_{max}}$.
[2] Based on straight portion of lift curve extended. See curve for actual value.
[3] Based on straight portion of moment curve extended. See curve for actual value.
[4] Ratio of the chord component to the beam component of the air forces to be used for the high angle of attack condition if the plane of the drag truss is parallel to the airfoil chord. C/B should be calculated when the plane of the drag truss is not parallel to the chord.

$$C/B=\tan\left[\tan^{-1}(C/B)_0-i_t\right] \quad \text{or} \quad C/B=\frac{(C/B)_0+k}{1-k\,(C/B)_0}$$

where i_t is the angle of incidence of the drag truss with respect to the airfoil chord.

where k is the slope of the drag truss with respect to the airfoil chord.

TABLE II.—SLOPE OF LIFT CURVE, $a_0=\frac{dC_L}{d\alpha_0}$ (PER DEG.)

Camber designation \ Thickness designation	06	09	12	15	18	21	25	[1]12
00	0.102	0.101	0.101	0.100	0.098	0.094	0.089	0.101
22								.103
23	.104	.103	.102	.102				.101
24	.103	.103	.103	.101	.098	.097		.101
25	.103	.102	.102	.099	.096	.095		.102
26								.100
27								.100
42								.102
43	.103	.103	.102	.103	.099	.095		.100
44	.104	.103	.100	.101	.096	.093		.100
45	.104	.103	.101	.101	.096	.095		.097
46								.098
47								.097
62								.100
63	.105	.104	.102	.101	.098	.096		.101
64	.104	.101	.102	.099	.099	.096		.101
65	.101	.103	.101	.099	.095	.094		.101
66								.099
67								.097

[1] Additional tests to determine variation with camber.

TABLE III.—ANGLE OF ZERO LIFT, α_{L_0} (DEGREES)

Camber designation \ Thickness designation	06	09	12	15	18	21	25	12	Theor.
00	−0.1	0.0	0.0	0.0	0.0	−0.1	0.0	0.0	0
22								−1.8	−1.80
23	−1.8	−2.0	−1.7	−1.7				−1.9	−1.92
24	−1.7	−1.7	−1.7	−1.7	−1.9	−1.7		−1.8	−2.08
25	−2.0	−2.0	−2.0	−2.0	−2.0	−1.8		−2.1	−2.29
26								−2.3	−2.59
27								−2.6	−3.04
42								−3.4	−3.60
43	−3.8	−3.6	−3.7	−3.6	−3.5	−3.6		−3.9	−3.84
44	−3.9	−3.6	−3.9	−3.8	−3.7	−3.4		−3.9	−4.15
45	−4.3	−4.1	−4.0	−4.1	−3.9	−3.4		−4.2	−4.58
46								−4.6	−5.18
47								−5.0	−6.09
62								−5.2	−5.40
63	[1]−5.2	−5.4	−5.4	−5.4	−5.2	−5.2		−5.5	−5.75
64	−5.6	−5.9	−5.7	−5.7	−5.7	−5.2		−5.7	−6.23
65	[1]−6.3	−6.3	−6.3	−6.0	−5.7	−5.3		−6.2	−6.88
66								−6.6	−7.78
67								−7.0	−9.13

[1] Based on straight portion of lift curve extended. See curve for actual value.

TABLE IV.—MAXIMUM LIFT COEFFICIENT, $C_{L_{max}}$

Camber designation \ Thickness designation	06	09	12	15	18	21	25	12
00	[a]0.88	[b]1.27	[a]1.53	[b]1.53	[b]1.49	[a]1.38	[b]1.20	[a]1.53
22								[b]1.60
23	[c]1.04	[a]1.51	[b]1.60	[b]1.54				[b]1.61
24	[a]1.01	[b]1.51	[b]1.59	[b]1.55	[b]1.43	[a]1.35		[b]1.62
25	[a]1.03	[a]1.38	[b]1.60	[b]1.53	[a]1.48	[b]1.38		[b]1.62
26								[b]1.66
27								[b]1.68
42								[c]1.71
43	[a]1.20	[b]1.60	[b]1.63	[b]1.56	[b]1.46	[a]1.29		[b]1.63
44	[a]1.23	[b]1.60	[a]1.61	[a]1.57	[a]1.47	[a]1.37		[c]1.65
45	[a]1.15	[a]1.56	[b]1.69	[a]1.62	[a]1.54	[a]1.46		[b]1.69
46								[b]1.76
47								[a]1.82
62								[b]1.75
63	[c]1.54	[b]1.67	[b]1.64	[b]1.55	[a]1.43	[a]1.37		[b]1.66
64	[c]1.43	[a]1.68	[a]1.65	[a]1.59	[a]1.51	[a]1.41		[a]1.67
65	[a]1.29	[a]1.71	[c]1.75	[a]1.67	[a]1.61	[a]1.49		[c]1.75
66								[c]1.83
67								[a]1.95

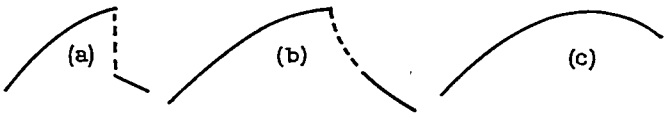

NOTE.—Letter indicates type of lift curve peak.

TABLE V.—MOMENT COEFFICIENT AT ZERO LIFT, C_{m_0}

Camber designation \ Thickness designation	06	09	12	15	18	21	25	12	Theor.
00	−0.002	−0.003	−0.002	0.000	−0.002	−0.001	−0.003	−0.002	0
22								−0.029	−0.0370
23	−.036	−.036	−.036	−.034				−.038	−.0447
24	−.039	−.044	−.042	−.040	−.037	−.036		−.044	−.0531
25	−.048	−.052	−.050	−.049	−.047	−.043		−.054	−.0628
26								−.060	−.0749
27								−.075	−.0912
42								−.059	−.0739
43	−.075	−.073	−.072	−.068	−.065	−.057		−.075	−.0894
44	−.087	−.086	−.087	−.083	−.078	−.071		−.089	−.1062
45	−.109	−.106	−.102	−.097	−.094	−.082		−.105	−.1257
46								−.124	−.1497
47								−.143	−.1825
62								[1] −.087	−.1109
63	[1] −.109	−.110	−.108	−.105	−.097	−.090		−.110	−.1342
64	[1] −.129	−.133	−.129	−.125	−.118	−.110		−.132	−.1594
65	[1] −.159	−.158	−.154	[1]−.150	−.139	−.129		[1] −.159	−.1835
66								[1] −.186	−.2246
67								[1] −.206	−.2737

[1] Based on straight portion of moment curve extended. See curve for actual value.

TABLE VI.—DISPLACEMENT OF CONSTANT MOMENT POSITION IN PERCENT CHORD AHEAD OF QUARTER-CHORD POINT (100 TIMES VALUES OF n FOR EQUATION $C_{m_{c/4}}=C_{m_0}+nC_L$)

Camber designation \ Thickness designation	06	09	12	15	18	21	25	12
00	0.7	0.7	0.9	1.1	1.4	1.8	2.6	0.9
22								.4
23	.3	.3	.3	.5				.5
24	.1	.3	.4	.7	1.0	1.5		.6
25	.0	.2	.3	.6	1.0	1.7		.7
26								.8
27								.8
42								.3
43	.3	.4	.5	.7	1.2	1.6		.4
44	.3	.3	.5	1.0	1.4	1.7		.5
45	.3	.3	.8	.9	1.4	1.7		1.0
46								1.1
47								1.3
62								.2
63	−.4	.1	.4	.9	1.1	1.5		.5
64	−.7	.0	.6	.9	1.3	1.7		.8
65	.0	.0	.7	1.6	1.8	1.9		1.5
66								2.0
67								2.1

TABLE VII.—MINIMUM PROFILE-DRAG COEFFICIENT, $C_{D_{0min}}$

Camber designation \ Thickness designation	06	09	12	15	18	21	25	12
00	0.0065	0.0074	0.0083	0.0093	0.0103	0.0120	0.0143	0.0083
22								.0087
23	.0073	.0083	.0088	.0100				.0089
24	.0070	.0080	.0090	.0099	.0112	.0127		.0085
25	.0073	.0081	.0089	.0103	.0112	.0126		.0088
26								.0089
27								.0090
42								.0092
43	.0080	.0089	.0101	.0107	.0119	.0134		.0095
44	.0076	.0086	.0095	.0105	.0116	.0132		.0092
45	.0087	.0093	.0103	.0113	.0125	.0138		.0095
46								.0099
47								.0104
62								.0101
63	.0092	.0101	.0108	.0120	.0130	.0144		.0102
64	.0086	.0094	.0104	.0120	.0132	.0146		.0104
65	.0093	.0100	.0111	.0127	.0141	.0154		.0106
66								.0114
67								.0126

TABLE VIII.—OPTIMUM LIFT COEFFICIENT, $C_{L_{opt}}$

Camber designation \ Thickness designation	06	09	12	15	18	21	25	12	[1]C_{L_I}
00	0.00	0.00	0.00	0.00	0.00	0.00	0.00	0.00	0
22								.17	0.303
23	.17	.18	.10	.10				.15	.272
24	.23	.17	.15	.12	.11	.07		.20	.256
25	.18	.16	.15	.11	.08	.03		.23	.251
26								.20	.256
27								.20	.272
42								.35	.016
43	.35	.30	.23	.12	.20	.05		.34	.544
44	.40	.36	.33	.22	.16	.10		.32	.512
45	.40	.34	.27	.22	.16	.08		.30	.502
46								.30	.512
47								.33	.544
62								.55	.923
63	.63	.45	.40	.33	.24	.13		.47	.816
64	.60	.55	.42	.33	.24	.15		.45	.707
65	.60	.53	.42	.33	.24	.10		.45	.754
66								.38	.767
67								.30	.816

[1] Theoretical lift coefficient at "ideal" angle of attack.

TABLE IX.—RATIO OF MAXIMUM LIFT COEFFICIENT TO MINIMUM PROFILE-DRAG COEFFICIENT, $C_{L_{max}}/C_{D_{0min}}$

Camber designation \ Thickness designation	06	09	12	15	18	21	25	12
00	135	172	184	164	138	115	84	184
22								184
23	142	182	182	154				181
24	144	189	177	156	128	106		190
25	141	170	180	148	132	109		184
26								187
27								187
42								186
43	150	180	161	146	123	96		172
44	162	186	170	150	127	104		179
45	132	188	164	143	123	106		178
46								178
47								175
62								173
63	167	165	152	129	110	95		163
64	166	179	159	133	114	97		160
65	139	171	153	132	114	97		165
66								161
67								155